Dissertation

Non-Local Effective SU(2) Polyakov-Loop Models from Inverse Monte-Carlo Methods

---

Bardiya Bahrampour

July 2017

JUSTUS-LIEBIG-UNIVERSITÄT GIESSEN

FACHBEREICH 07

INSTITUT FÜR THEORETISCHE PHYSIK

Dekan:	**Prof. Dr. Bernhard Mühlherr**
Betreuer:	**Prof. Dr. Lorenz von Smekal,** **Dr. Björn Wellegehausen**
Erstgutachter:	**Prof. Dr. Lorenz von Smekal**
Zweitgutachter:	**Prof. Dr. Christian Fischer**

Zusammenfassung

Die starke Kopplungsentwicklung von Gittereichtheorien führt zu Polyakov-Loop Modellen, welche eine effektive Beschreibung der Gluodynamik bei niedrigen Temperaturen liefern. Zusammen mit der Hopping-Expansion der Fermion-Determinante erlaubt dies Einsichten in das QCD-Phasendiagramm bei endlicher Dichte und niedrigen Temperaturen, auch wenn die erreicharen Pionmassen vergleichsweise groß sind. Bei hohen Temperaturen bricht die starke Kopplungsentwicklung jedoch schließlich zusammen und es wird erwartet, dass die Wechselwirkungsterme von Polyakov-Loops zunehmend nicht-lokal werden. Daher verwenden wir die inverse Monto-Carlo Methode, um eine reine SU(2) Yang-Mills Theorie auf verschiedene nicht-lokale Polyakov-Loop Modelle abzubilden. Wir beziehen dabei Polyakov-Loops in höheren Darstellungen mit ein und fügen schrittweise Wechselwirkungsterme bei höheren Abständen hinzu, um herauszufinden, wie gut wir die volle Theorie beschreiben können, und das konvergente Verhalten gegen die volle Theorie zu untersuchen. Wir untersuchen dabei verschiedene Observablen und sind insbesondere an der Qualität unserer Modelle bei zunehmender Gittergröße interessiert. Des Weiteren versuchen wir ein möglicherweise analytisches Verhalten des Abfalls der Kopplungen der nicht-lokalen Terme (mit dem Wechselwirkungsabstand) zu bestimmen. Wir testen verschiedene Möglichkeiten für solch ein Verhalten, vergleichen unsere Resultate mit existierenden Aussagen, und versuchen einen Zusammenhang zur Korrelationslänge der vollen Theorie herzustellen.

Abstract

The strong coupling expansion of the lattice gauge action leads to a Polyakov loop model that effectively describes the gluodynamic at low temperatures and together with the hopping expansion of the fermion determinant allows for insights into the QCD phase diagram at finite density and low temperatures, although the accessible pion masses are rather large. At high temperatures the strong coupling expansion breaks down and it is expected that the interaction of Polyakov loops becomes non-local. Therefore we use inverse Monte-Carlo methods to map SU(2) gluodynamic to different non-local Polyakov loop models . We take into account Polyakov loops in higher representations and gradually add interaction terms at larger distances to find out how well we can describe the full theory and to investigate the convergent behavior towards the full theory. We investigate thereby different kind of observables and are particularly interested in the quality of our models in the large volume limit. Furthermore we try to determine a possibly analytical behavior for the fall-off of the couplings of the non-local terms (with respect to the interaction distance). We test different possibilities for such a behavior, compare our results to existing statements and try to find connections to the correlation length of the full theory.

Contents

Introduction

The standard model of particle physics describes the fundamental forces between particles. Its mathematical framework is quantum field theory, which yields a quantization procedure of classical field equations, whose description relie on gauge symmetries, i.e. local symmetries of the system. The first prototype of a quantum field theory was realized by quantum electrodynamics (QED), the quantized theory of the electromagnetic field [1–3]. Local invariance under the abelian gauge group U(1) was built into the corresponding classical equations almost by accident and only later was the importance of gauge invariance understood; especially in context of quantum field theories, where the gauge principle ensures the avoidance of divergences that cannot be dealt with and makes the theories renormalizable [4, 5]. The gauge principle was extended to non-abelian gauge groups later and the framework of quantum field theory was successfully applied to describe the weak force, which was unified with the electromagnetic force into a single electroweak force based on the gauge group $U(1) \times SU(2)$ [6–8], and the strong force, based on the gauge group SU(3) [9, 10] . This has lead to an almost complete description of nature in terms of quantum field theories. Today the standard model of particle physics describes with the electrodynamic, the weak and the strong force, 3 of the 4 fundamental forces (with only the gravitational force persistently resisting a quantum field theoretical description), making the standard model the most successful theory ever written. Among some of its successes are the calculation of the anomalous magnetic moment of the electron within the QED sector, with an unmatched accuracy to an order beyond of 10^{-9} [11–14], the correct prediction of various particles, such as the top quark, the W and Z bosons [15] and the most recently discovered Higgs boson [16, 17]. Even the prediction of completely new interactions between particles, such as the interaction between particles based on neutral currents within the electroweak sector [18–22], can be accounted to the successes of the standard model.

However, in spite of the overwhelming success of the standard model there are still many open questions to answer and problems to solve. Some of those problems are of very theoretical nature and are for example dealing with rigorous mathematical formulations of the theory itself or proofs of mechanisms that seem to be correctly implemented into the standard model but not fully understood, such as the mechanism behind mass generation, the realization of a mass gap or the confinement mechanism in quantum chromodynamics (QCD), the sector of the standard model which describes the strong force between quarks, the constituents of protons, neutrons and other hadrons. Other

problems deal with the many hints that point towards different possible extensions of the standard model, in order to make sense of features realized in nature but not fully explained or not implemented at all by the standard model. Examples for not explained features are the different constants of the standard model and their values [23], the hierarchy problem [24], which deals with the differences in strengths of the fundamental forces, or the non-breaking of CP invariance within the QCD sector (known as the strong CP problem) [25,26]. Examples of features that have not been implemented by the standard model correctly or even at all are the non-vanishing neutrino masses observed in nature [27], the existence of dark matter and the value of dark energy [28, 29]. Also, in order to get a consistent picture of all interactions down to the Planck scale, and be able to describe situations that occur in black holes or in the early stages of the universe, one has to find a way in order to incorporate gravity into the same framework with the other 3 forces, which might require the development of a drastic new mathematical description [30].

Apart from such very theoretical problems, there are also more straight forward, practical problems one has to deal with in the standard model, regarding the highly non-trivial nature of the equations, which makes performing actual calculations a challenging task. The QCD sector of the standard model is especially puzzling. The interaction between quarks is described in the QCD sector by complex rotations in the 3-dimensional complex space, corresponding to the 3 different charges, referred to as the colors red, green and blue. It is based on the non-abelian symmetry group SU(3) and the classical equations of QCD are a straight forward generalization of electrodynamic equations, obtained by generalizing the local gauge invariance based on the abelian group U(1), to non-abelian symmetry groups. The non-abelian nature of QCD yields a direct self-interaction of the gluon field, i.e. the QCD gauge field, by exchange of gluons and leads in addition to the expectation that bound states consisting purely of gluons, called glueballs, must exist, to several other profound implications, which are in good agreement with experimental observations. One of those implications is asymptotic freedom [31,32], the feature that the strong interaction becomes increasingly weak and particles therefore become asymptotically free at short distances (or equivalently at large energies). On larger scales on the other hand, the non-abelian structure leads to confinement, the observation that the interaction strength becomes large enough to force quarks and gluons into colorless bound states, such that color-charged particles have never been observed directly by themselves in nature. With rising energy of the system, QCD therefore possesses a deconfinement phase transition, which describes the transition from a phase, where color-charged particles are confined, into a phase of almost freely moving quarks and gluons, called quark-gluon plasma (QGP) [33]. The QGP was experimentally verified in heavy ion collisions as preformed at RHIC and LHC [34–36]. One believes that the confining behavior of QCD is due to the self-interaction of the gluon field, which leads to some sort of anti-screening effect of the vacuum, forcing the field lines between quark anti-quark pairs into a flux tube, giving at large separation distances rise to a linearly rising potential between quarks and anti-quarks [37, 38]. However. the situa-

tion is to this day not fully understood and there is no analytical proof of a mechanism for confinement. Furthermore, also abelian systems in appropriate dimensions [39–41] or non-abelian systems with gauge groups with trivial center [42–44] can exhibit such behaviors. The fact that quarks interact strongly in large regions of the theory and therefore are bound into hadrons, makes it challenging on the experimental side to investigate the theory, creating demand for larger and larger particle colliders in order to reach the energy levels needed for an investigation of the theory. On the theoretical side it makes perturbative approaches to calculations impossible in many regions of interest, creating a demand for non-perturbative approaches. The most straight forward non-perturbative approach to deal with the theory is lattice field theory, which we are also using in this thesis, in which the spacetime continuum is taken to be closed and replaced by a lattice of discrete points. However the notorious sign problem [45, 46], which we will talk about later, makes it impossible to apply lattice methods easily to calculations with non-zero chemical potential, restricting us essentially to the $\mu = 0$ line in the phase diagram. The problem arises from the fact that lattice calculations rely on Monte-Carlo methods, in which integrals are evaluated numerically by approximation with finite sums over sets of randomly chosen supporting points. The method breaks down if applied to integrals of functions that are highly oscillating, with a near-cancellation of their oscillations, which would require a computational precision far beyond achievable in order to obtain useful results. Unfortunately this is exactly the case in QCD with fermions at non-zero chemical potential and the severity of the problem increases exponentially with the lattice volume, meaning that the problem, which is already hard to handle on very small lattices, gets quickly impossible to deal with on larger ones and therefore makes an extrapolation to the continuum or even just calculations on lattices large enough to give some meaningful results impossible. This leads to an only very crude understanding of the QCD phase diagram and in order to obtain insight into the phase diagram away from the line of zero chemical potential a combination of different theoretical and experimental approaches, as discussed in greater detail in [47–49], must be applied. A rough sketch of of the resulting idea about the QCD phase diagramm is shown in Fig. 1 in the μ-T-plane (chemical potential vs. temperature plane).

From the experimental side input for the phase diagram is coming from heavy ion collisions performed at particles colliders such as RHIC, LHC, ALICE, FAIR and others, of which a few have been depicted in the phase diagram in Fig. 1 at the range at which they operate.

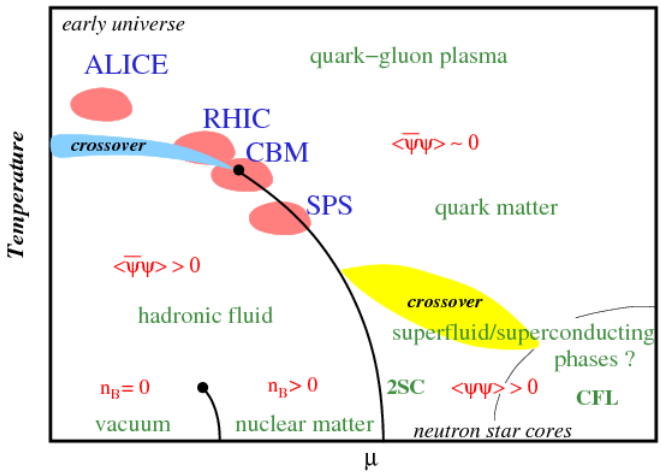

Figure 1: Hypothetical QCD phase diagram as obtained by different model calculations taken from [50]

From the theoretical side there are many approaches and attempts to get insight into the QCD phase diagram away from the line of zero chemical potential one has to either use methods that deal with the sign problem, such as as the Taylor expansion in terms of μ/T [51, 52], the analytical continuation of imaginary chemical potential to real values [53, 54], complex Langevin methods [55–58], density of states methods [59] or simulations on Lefschetz-Thimbles [60]; or one has to apply completely different non-perturbative techniques, as provided by the functional renormalization group (FRG) [61] and by methods based on Dyson-Schwinger equations (DSE) [62–64]. Another way to circumvent the sign problem is to resort to the use of simpler effective models, such as provided by the Nambu-Jona-Lasinio (NJL) [65,66] model, quark-meson models [67], Polyakov-NJL models [68–72] and Polyakov-quark-meson models [73–75]. A similar approach is given by the investigation of models referred to as QCD-like theories [76, 77], which preserve important features of QCD, such as a deconfinement and chiral restoration phase transition, while at the same time avoiding the sign problem in lattice calculations by modifying the gauge action. Examples of QCD-like theories are adjoint QCD [78], where the SU(3) gauge group acts in the adjoint representation on fermions, and QCD-like theories based on other non-abelian gauge groups, such as SU(2) or G_2 [79–85]. All these techniques come with their own issues or predictive restrictions and collaborate effort has to be made in order to get an insight into the phase diagram which is as accurate as possible.

As depicted in the phase diagram in Fig. 1, this collaborate effort of theoretical and experimental efforts has left us with an idea of what to expect, over a large region of the phase diagram. Chiral symmetry (whose order parameter is given by the chiral condensate $\langle\psi\bar{\psi}\rangle$) is explicitly broken by the non-zero quark masses. But even in the

chiral limit, where the quark masses are taken to be zero, at low values for T and μ the ground state of QCD breaks chiral symmetry spontaneously. With increasing values for T and μ this symmetry is restored. At small values of the chemical potential this restoration comes with an analytical cross over around 155 MeV, which is confirmed by lattice results [86–88]. At larger values for μ results the picture becomes less clear, as the sign problem prevents straight forward lattice calculations of QCD. However, model and DSE calculations suggest that the transition of chiral symmetry restoration becomes a true phase transition of the order 1, which ends at a critical point [48, 89, 90]. At small temperatures and chemical potential quarks are confined into hadrons, which break up at larges values for T and μ, leading to the deconfined phase of the quark gluon plasma, where quarks and gluons move almost freely. The phase transition of chiral symmetry restoration is accompanied at zero chemical potential by the deconfinement phase transition. Within the confined hadronic phase there is another 2nd order liquid-gas phase transition [91] ending in a critical point as well and within the deconfined phase at moderate temperatures and large baryon chemical potential one expects from large-N_c calculations that the deconfined phase is reached without a restoration of chiral symmetry at the same time, leading to a quarkyonic phase [92], with quark matter in many different phases similar to the many different phases of ice. At even larger values of μ, color superconducting phases are expected, where residual quark-quark interactions lead to their condensation, similar to what is described by the BCS theory for superconductivity. It seems to lead at large values of the chemical potential to a condensation of quark pairs with only certain flavor-color-combinations possible, referred to as color flavor locked (CFL) phase [93, 94].

To get an even better understanding of the phase diagram techniques and models are constantly developed and improved. Another method of interest, which leads to a sign problem weak enough to be dealt with [95–100], is to reduce the gauge degrees of freedom of QCD to Polyakov loop variables, leading to effective Polyakov loop models, while applying a hopping expansion for quarks at large masses at the same time. However, to derive such effective models analytically from a given theory can be challenging already for a pure gauge theory, and can be usually done only in small areas of the phase diagram and up to a few orders in a given expansion, which is usually not enough to accurately describe the dynamics of the system, especially near the deconfinement phase transition. In this work, where we will discuss such effective Polyakov loop models, our main interest therefore lies in the mapping of SU(2) Yang-Mills theories onto different highly non-local Polyakov models by the use of inverse Monte-Carlo methods [101–103] and the investigation of the so obtained effective SU(2) models. SU(2) gauge theories pose an excellent starting point to investigate the construction of non-local Polyakov loop models via inverse Monte-Carlo methods, as the group structure is much simpler compared to SU(3) and other gauge groups of interest, while still possessing a rich enough structure to be worth investigated (in fact as we will see the confinement character of a theory is determined by its pure gauge part and yields a deconfinement phase transition already for the pure SU(2) Yang-Mill theory). Furthermore for SU(2) based theories the fermionic sign problem can be avoided, which makes future extension of our

research by inclusion of dynamical fermions easier compared to SU(3) theories. Also the inverse Monte-Carlo method itself turns out to be less problematic for SU(2) theories and appears to very stable in contrast to the SU(3) case. In order to derive different effective models, we will show how to construct ansatzes for Polyakov loop models by strong coupling expansion and how to numerically map full gauge theories onto to given ansatzes via inverse Monte-Carlo methods. In this way we will obtain mappings for different competing models, which we will systematically improve and compare to each other. We will investigate those models on lattices of different sizes in order to obtain insight regarding their convergence towards the full theory in the limit of an increasing number of terms taken into account on fixed lattices sizes and in the continuum limit. We will also search for analytical forms of the numerically obtained mappings.

This work is structured as follows: The first part is devoted to the theoretical framework used. In the first chapter we will give a review of the theoretical foundations of quantum field theory and QCD in the continuum and on the lattice. In chapter 2 we will then summarize the mathematical concepts of Lie groups and Lie algebras, which we will be using when deriving the ansatzes for different effective Polyakov loop models and in the discussions of the inverse Monte-Carlo method. The reader already familiar with the mathematical theory of Lie groups and Lie algebras is invited to skip that chapter. In the third chapter we will then talk about different SU(2) Polyakov loop models and their motivation by the strong coupling expansion. In the fourth chapter we will then derive the so called inverse Monte-Carlo method, which we will use to map the full SU(2) Yang-Mills theory to different ansatzes for effective Polyakov loops models, before we turn to the investigation of those models in the remaining result chapters in the second part of this work. The final chapter will consist of a conclusion and a summary of open question, as well as an outline of possible future ways in order to progress this work.

Part I

Theoretical Framework

Chapter 1

Non-Abelian Gauge Theories in the Continuum and on the Lattice

Let us start in this chapter the discussion of our theoretical framework with a short summary of non-abelian gauge theories. We will begin with introduction of the Lagrange Density, talk about its quantization in the continuum and the Euclidean formulation of quantum field theories, which allows us to interpret the equations in terms of a statistical quantum system and investigate its phase structure. We will then turn our discussion to confinement, especially in pure gauge theories, as we will be later on in this work concerned with SU(2) gauge theories only. In the last sections, we will then give a short introduction into the lattice formulation of quantum field theories, talk about their advantages and disadvantages to continuum formulations, as well as about Monte-Carlo methods used in lattice calculations and the resulting numerical sign problem. This chapter is mainly based on [104–106] and partly on other material, which we will explicitly reference, when used.

1.1 Lagrange Density

The Lagrange density of a non-abelian gauge theory is a straight forward generalization of the electrodynamical Lagrange density, obtained by demanding the gauge invariance $\psi \to \psi' = \Omega\psi$, $\Omega \in G$, with a non-abelian Lie group G, of the kinetic term for fermions ψ, which are now elements of an n-dimensional vector space on which the gauge group G is acting. The gauge field A_μ is then an element of the tangent space, hence the Lie algebra and can be expanded in form of a basis $\{T_1, \ldots, T_r\}$ of the Lie algebra. Writing all gauge-field dependent variables in terms of the covariant derivate D_μ, and allowing different fermions flavors ψ_j, labeled by the index j. the Lagrange density takes the (to

the electrodynamical density analogous) form

$$\begin{aligned}\mathcal{L} &= -\frac{1}{4}F^a_{\mu\nu}F^{a\mu\nu} + \bar{\psi}_i\left(i(\gamma_\mu D^\mu) - m_i\right)\psi_i,\\ D_\mu &= (\partial_\mu - igA^a_\mu T^a),\\ F_{\mu\nu} &= \frac{i}{g}[D_\mu, D_\nu],\end{aligned}$$

with the gauge transformations

$$\begin{aligned}\psi &\to \Omega\psi,\\ A^a_\mu T^a &\to \Omega A^a_\mu T^a \Omega^{-1} + \frac{i}{g}\Omega(\partial_\mu\Omega^{-1}),\\ D_\mu &\to \Omega D_\mu \Omega^{-1},\\ F_{\mu\nu} &\to \Omega F_{\mu\nu}\Omega^{-1},\end{aligned} \tag{1.1}$$

$\Omega \in G$, where the gauge transformation of the gluon field (and hence the field strength tensor $F_{\mu\nu}$ and the covariant derivative D_μ) are set by demanding gauge invariance of the term containing the fermionic part of the action and the additional trace for the Yang-Mills (pure gauge theory) part is needed in order to guarantee gauge invariance for the pure gauge theory by itself. The gamma matrices used in eq. (1.1) satisfy the Clifford algebra and often used choices for the representation are given by the the Dirac representation and the chiral representation (see A.1).

1.2 Geometric Interpretation of Gauge Theories

As the term "covariant derivative", which we are familiar with from general relativity, already suggests, the Lagrange density (1.1) yields a geometric interpretation of gauge theories. In analogy to general relativity, where one has to deal with fibre bundles[1] with curved manifolds as the base space, the tangent space as the fibre, and the affine connection in the covariant derivative takes into account the change of the fibre as one moves along the base space, the covariant derivative of gauge theories,

$$D_\mu\psi = \mathbb{1} + iA_\mu\psi(x), \tag{1.2}$$

takes into account the change of the fibre space, which is given by the gauge group manifold, as one moves along the base space, which is the ordinary space-time. The gauge field A_μ takes the role of the connection in this interpretation and the field strength

[1] A fibre bundle E is a manifold that can be locally written as a product manifold $B \times F$, where B is referred to as the base space and F the fibre, which in general exhibits a topology, i.e. global geometry, different from the product manifold. The local isomorphy is understood by the existence of a surjective projection $\pi : E \mapsto B$, such that the inverse $\pi^{-1}(p) \simeq F$ for all $p \in B$. For the precise mathematical definition we refer to the appropriate mathematical literature, e.g. [107]. The simplest example of a non-trivial fibre bundle is the Möbius strip.

tensor is the analog of the curvature term. The parallel transport from a point x to point a y along the path C_{yx} is then obtained by

$$\begin{aligned} &\psi(y) = U(C_{yx})\psi(x), \\ &U(C_{yx}) = \mathcal{P}\left(\exp\left(i\int_{C_{yx}} A_\mu dx^\mu\right)\right) \in G, \end{aligned} \tag{1.3}$$

where U is called parallel transporter, and $\mathcal{P}$ is the path ordering operator, which yields in an expansion of the exponential function an ordering of the product of operators with respect to the path and is necessary due to the non-abelian nature and the related non-commutativity of the connection operators in the expansion. The parallel transporter then transforms under the action of the gauge group according to

$$U(C_{yx}) \to \Omega(y)U(C_{yx})\Omega(x)^{-1}. \tag{1.4}$$

We will use this interpretation later to motivate the lattice formulation of quantum field theories.

1.3 Functional Integral Quantization

After having discussed the Lagrange density of non-abelian gauge theories, let us now introduce quickly the quantization scheme used in this thesis. There are different possible ways to quantize a field theory. In hindsight of the rest of this work, we will here discuss the functional integral quantization (also referred to as path integral quantization) of field theories, which is the most suitable one for lattice formulations. Here the quantization is obtained by calculating expectation values for observables $\mathcal{O}$ over field configurations that are weighted with the exponential of the classical action, i.e.

$$\begin{aligned} &Z = \int D[\psi, \bar{\psi}, A] \exp(iS), \qquad S = \int d^3x\, dt\, \mathcal{L} \\ &\langle \mathcal{O} \rangle = \frac{1}{Z}\int D[\psi, \bar{\psi}, A]\mathcal{O} \exp(iS). \end{aligned} \tag{1.5}$$

Note that this integral is, although from a physical point of view intuitive, from a mathematical point of view very problematic. First of all, it contains integrals of variables, defined at every point of space-time. Hence we are dealing with uncountably-infinite dimensional integrals, with the integration variables being labeled by continuous parameters $(\vec{x}, t) \in \mathbb{R}^4$ (or in the more general case of an arbitrary dimensional spacetime $\mathbb{R}^d$). It is in general unclear how to define such an integration, i.e. how to construct an appropriate measure. Even in the 1-dimensional case of ordinary quantum mechanics, where integral (1.5) can be interpreted as a true path integral, a measure on the space on continuous paths can only be constructed in the Euclidean version (introduced in the next section), where the oscillating complex weight factor $\exp(iS)$ is changed into

a Boltzmann-like real weight factor $\exp(-S_E)$,. This leads to the construction of the Wiener measure connected to stochastic processes. In the case of quantum field theory however, where quantum fields are distributions, a measure is only applicable for non-interacting quantum fields. For interacting quantum field theories on the other hand, we would have to deal with products of distributions which are mathematically ill-defined. This makes the situation from a rigorous mathematical point of view quite unclear. No measure can be defined in general and one has to regularize the theory in some way in order to make sense of the integral (1.5) at all. However in lattice formulations, which we will introduce in the end of this chapter, the spacetime is taken to be of finite volume and is then discretized. Therefore problems arising from having to deal with distributions are avoided, a rigorous formulation of the theory is applicable and a regularization of infrared and ultraviolet divergences is implemented automatically, due to the finite volume of the spacetime and the finite value of the lattice spacing a (the minimal lattice distance of two neighboring lattice points). Apart from regularization issues in the continuum, another problem one has to deal with arises from the gauge invariance of the action. Gauge invariance implies that the action is constant on configurations connected by gauge transformation and leads to a redundant integration over gauge orbits of gauge equivalent configurations. This redundant integration leads at every point of spacetime to an additional factor $vol(G)$, which is the volume of the gauge group and therefore introduces another kind of divergence into the equations of quantum field theory. This makes gauge fixing, where one restricts the system to one configurations per gauge orbit, in continuum theories necessary and leads to the introduction of Faddeev-Popov operators and additional auxiliary and ghost fields, which can be done systematically via the BRST formalism (see [108]). However such a gauge fixing procedure is also problematic in the non-perturbative regime, since the closed topology of the gauge groups prevents the possibility of imposing gauge conditions with a unique solution. Instead, one obtains several solutions, known as Gribov copies, which cancel each other on a non-perturbative level. However, the problem of gauge invariance is also automatically taken care of in lattice formulations, as the additional volume factor for every space time point leads to an overall factor $vol(G)^{\#\text{sites}}$. Due to the finite number of lattice sites, this factor is finite and the uniform over-counting in integrals cancels for expectation values of observables, due to the factor Z^{-1}, making a gauge fixing procedure unnecessary in lattice formulations (although gauge fixing is often done anyways to simplify calculations or compare results of gauge dependent objects, such as n-point functions, with other formulations).

1.4 Euclidean Quantum Field Theory and Statistical Physics

In order to take care of the oscillating complex weight factor in (1.5), which spoils convergent behavior in the sum over all field configurations, one usually adds a small imaginary term into the action, which acts as dampening factor for the oscillation. The problem of a purely imaginary argument in the weight factor also shows itself in explicit calculations of n-point functions, such as propagators, for which real poles occur, which need to be shifted slightly into the complex plane by adding small imaginary terms, which can be sent to zero after evaluating the occurring integrals. An equivalent way, which avoids the adding of small imaginary parts, is to apply a Wick rotation, which involves a rotation of the real time variable onto the imaginary axis by applying the complex rotation $x_0 \to ix_4$. As we switch from a real to an imaginary time variable, the metric for the time component switches signs, and in our signature of the metric, this results in a negative Euclidean metric. In order to avoid doing a Wick rotation by hand, one can equivalently just replace the Minkowski metric by an Eudclidean metric

$$(g^{\mu\nu}_{Minkowski}) \to (\delta^{\mu\nu}), \tag{1.6}$$

which will also result in a redefinition of related quantities, such as gamma matrices, gauge fields and integrals (see [109]). The so obtained quantum field theory is referred to as Euclidean quantum field theory, with the resulting equations given by

$$\begin{aligned} Z &= \int D[\psi, \bar{\psi}, A] \exp(-S_E), \\ S_E &= \int d^D x \left(\frac{1}{4} F^a_{\mu\nu} F^{a\mu\nu} + \bar{\psi}_i \left((\gamma_\mu D^\mu)_{ij} + m_i \delta_{ij} \right) \psi_j \right), \\ D_\mu &= (\partial_\mu + igA^a_\mu T^a). \end{aligned} \tag{1.7}$$

In a strict mathematical formulation the quantum field theory defined on the Minkowski space does not exist due to the ill-defined integrals and in an axiomatic approach one starts with the formulation of a Euclidean field theory (see [110]). The n-point function of the real time variables are then obtained by again rotating the time variable in the complex plane, for which one has to construct analytical continuations of those n-point function. On the lattice such analytical continuations are problematic and a straight forward analytical continuation is in general not possible due to the finite set of lattice data.

An interesting feature of the equations (1.7) is its analogous form to the equations of statistical system. Putting the Euclidean field theory on a finite volume with temporal extend β_T and applying periodic boundary conditions to the bosonic gauge fields and anti-periodic boundary conditions to the fermionic fields, we obtain the partition function

$$Z = \int_{\text{anti-periodic}} D[\psi, \bar{\psi}] \int_{\text{periodic}} D[A] \exp\left(- \int_0^\beta dt \int d^{D-1} x \; S_E \right). \tag{1.8}$$

In analogy to statistical mechanics, we can identify this partition function with the partition function of a statistical system, where the temporal extend is identified with the inverse Temperature, i.e. $\beta_T = 1/T$, yielding the possibility to calculate statistical observables for the quantum field theory. Having made the transition from usual quantum field theory of interacting particles to a statistical quantum field system, it is only natural to add a quark density to the Lagrange density in order to model the thermodynamical behavior of systems away from the vacuum. With statistical physics familiar, we introduce the chemical potential term μN_q, where the quark number operator N_q is the integral over the time component of the conserved Dirac current $\bar{\psi}\gamma_\mu\psi$. This leads in the continuum to adding for each quark flavor a term $\bar{\psi}\mu\gamma_4\psi$ to the Lagrange density, hence

$$\mathcal{L}_E = \frac{1}{4}F^a_{\mu\nu}F^{a\mu\nu} + \bar{\psi}_i\left((\gamma_\mu D^\mu)_{ij} + (m + \mu\gamma_4)\delta_{ij}\right)\psi_j, \tag{1.9}$$

where μ is refered to as baryon chemical potential.

1.5 Confinement in Pure Gauge Theories

As already mentioned confinement is the feature that color-charged particles in nature are never observed by themselves but always in color-neutral bound states. Yet the requirement of color-neutrality is not strong enough to make up for the lack of observation of free quarks in nature, as a color-neutral hadronic state could (from group theoretical arguments only) in principle consist of color-charged quarks, which are spatially far apart. The potential energy between quarks in a bound state has to rise with the distance in a way that confines the different quarks into a small area. A precise definition of the confinement is difficult but can be given in the quenched theory, where the quark masses are taken to infinity, i.e. in a pure gauge theory.

Now it might be counter intuitive that the concept of confinement of quarks can be described in the most easiest way in a theory without fermions at all. However in a theory with fermions that are infinitely heavy confinement can be explained by a linear rising of the potential at large separation distances of a quark anti-quark pair. In an unquenched theory this rising would eventually stop, since the energy would become large enough to produce another quark anti-quark pair within the flux tube, screening the former particles and resulting in two separated quark anti-quark pairs, which is known as string-breaking. As we will see, the observable related to potential can be formulated and interpreted in terms of a pure gauge theory. Furthermore in pure gauge theory, with non-trivial center subgroup, we can connect the deconfinement phase transition to the spontaneous breaking of center symmetry and define an order parameter via the Polyakov loop variable, which we will show in the next section. In a fermionic theory center symmetry is explicitly broken by the fermion fields and the Polyakov loop can only be regarded as an approximate order parameter, which makes a precise definition

of confinement and a description in terms of symmetries problematic.

1.5.1 Wilson Line and Static Quark Potential

In a gauge theory with quarks we can define a quark anti-quark creation operator $Q(t)$, which creates at a time t a gauge invariant quark anti-quark pair (coupled by the gauge field, i.e. connected by parallel transport) with spatial separation distance R. In a quenched theory with infinite large fermion masses, where string breaking effects can be neglected, the potential between the quark anti-quark pair rises linearly for large separations R. In fact, in the infinite mass limit, we can integrate out the fermionic fields, which yields for the expectation value of a quark anti-quark pair at spatial seperation R, created at the time $t = 0$ and annihilated at $t = T$, the expression

$$\left\langle Q(T)^\dagger Q(0) \right\rangle \sim \langle \mathrm{Tr}[U(R,T)] \rangle =: W(R,T), \tag{1.10}$$

where the Wilson loop operator $W(R,T) := \mathrm{Tr}[U(R,T)]$ is the trace of the parallel transporter around a closed rectangular loop of spatial size R and temporal size T. Inserting a unity in the operator formalism we obtain the form

$$\begin{aligned} W(R,T) \sim \left\langle Q(T)^\dagger Q(0) \right\rangle &= \frac{\sum_{n,m} \left\langle 0|Q(0)^\dagger|n\right\rangle \langle n| \exp(-HT)|m\rangle \langle m|Q(0)|0\rangle}{\langle 0| \exp(-HT)|0\rangle} \\ &= \sum_n |c_n|^2 \exp(-\Delta E_n T). \end{aligned} \tag{1.11}$$

Now the requirement of a linear rising quark-anti quark potential at large distances R means that the Wilson loop operator around the closed rectangular loop must take the form

$$W(R,T) \sim \exp[\sigma RT - 2V_0 T] \tag{1.12}$$

or for a general closed loop the form

$$W(C) \sim \exp[\sigma A(C) - V_0 P(C)], \tag{1.13}$$

where $A(C)$ is the area enclosed by the loop and $P(C)$ is the perimeter, yielding an area law fall-off for large spatial extends. The distance depended term of the potential $V(R)$ is obtained in the limit $T \to \infty$ by

$$V(R) = -\lim_{T\to\infty} \log\left[\frac{W[R,T+1]}{W[R,T]}\right], \tag{1.14}$$

which must yield for a rectangular loop in the limit of large R the linear form

$$V(R) \sim \sigma R. \tag{1.15}$$

We see that the confinement character of a gauge theory, which is defined in a straight forward manner only in a quenched theory, is determined by the fall-off of the Wilson loop operator, due to its relation to the propagation of a static quark anti-quark pair through time. However in the end the Wilson line is the trace of a product of gauge variables around a closed loop and only depending on the gauge degrees of freedom. It is perfectly defined in pure gauge theories, being a measure for the vacuum fluctuations of the gauge field. Hence the confining character of a theory is determined by the vacuum fluctuations of the pure gauge theory and we can observe deconfinement phase transitions in pure gauge theories, including (as we will see later) the SU(2) Yang-Mill theory, and also in the corresponding effective Polyakov loop models. It is known that the SU(2) Yang-Mill theory exhibits a 2nd order deconfinement phase transition [79–82], in contrast to SU(3) Yang Mills theory, which shows a 1st order phase transition.

1.5.2 Center Symmtery and Polyakov Loops

The effect of the gauge group of a gauge theory on its confining character (or lack of it), suggests that the symmetry corresponding to the deconfinement phase transition is somehow connected to the gauge group. However, as known by Elitzur's theorem, local (gauge) symmetries cannot be broken. Also a breaking of remnant symmetries seems not to give the right results. As it turns out for gauge groups with non-trivial center, the phase transition can be related to the breaking of center symmetry, a global symmetry related to the center of the corresponding gauge group. Looking at the Yang-Mills part of the action defined in (1.8), one can actually see that it possesses a larger symmetry than just given by the gauge group and the extended transformations, leaving the action invariant, are given by the non-periodic gauge transformations

$$\Omega(\vec{x}, x_4 + \beta) = zU(\vec{x}, x_4), \qquad \Omega \in G,\ z \in Z(G), \tag{1.16}$$

where the element $z \in Z(G)$ of the center of the gauge group G introduces the additonal center symmetry of the action. In contrast to gauge transformations, there is an observable which is non-invariant under a global center transformation. The non-invariant observable is given by the Polyakov loop

$$P(\vec{x}) = \mathrm{Tr}\ \mathcal{P}\left(\exp\left(\int_0^{\beta_T} dx_4 A_4(\vec{x}, x_4)\right)\right), \tag{1.17}$$

which is gauge-invariant but transforms non-trivially under center transformations according to

$$P(\vec{x}) \to P(\vec{x})' = zP(\vec{x}),\ z \in Z(G). \tag{1.18}$$

hence making the expectation value

$$\langle P(\vec{x})\rangle = \begin{cases} 0 & \text{in the unbroken phase,} \\ \text{non-zero} & \text{in the broken phase,} \end{cases} \tag{1.19}$$

of the Polyakov loop into an order parameter for center symmetry.

It can be shown that the Polyakov correlator is related via $\langle P(\vec{x})P(\vec{y})\rangle \propto \exp(-F_{q\bar{q}})$ to the free energy in a quark anti-quark pair. For large separation distances asymptotic independence of the Polyakov loop variables implies $\langle P(\vec{x})P(\vec{y})\rangle \approx \langle P(\vec{x})\rangle\langle P(\vec{y})\rangle$ and we can write the expectation value of the Polyakov loop as

$$\langle P(\vec{x})\rangle \propto \exp(-\beta F_q), \tag{1.20}$$

where F_q can be interpreted as the free energy of a quark, in an quark anti-quark pair, with its anti-quark taken to infinity. Hence a vanishing expectations value of the Polyakov loop yields an infinite free energy and therefore confinement, connecting preservation of center symmetry to confinement and its breaking to deconfinement. We want to stress again that this is only true for gauge theories with non-trivial center and cannot explain the full picture, since non-abelian gauge theories with trivial center (such as gauge theories based on the exceptional Lie group G_2) exist, which also exhibit a confinement-deconfinement phase transition [42–44].

1.6 Lattice Field Theory

Let us now introduce the lattice formulation of quantum field theories. In lattice formulations the continuous spacetime of Euclidean field theories, given by a torus, is replaces with a discrete, usually hyper-cubic lattice. With the spatial extend N_s and temporal extend N_t the discrete spacetime is given by

$$(\vec{x}, x_4) \in [1, N_s]^3 \times [1, N_t] \simeq \{1, \ldots, L\}, \qquad L = N_s^3 N_t. \tag{1.21}$$

As we saw ealier, the temporal extend of the euclidean theory can be identified with the inverse temperature of a statistical system, which yields for the lattice theory

$$\frac{1}{T} = aN_{\mathrm{t}}, \tag{1.22}$$

where a is the lattice spacing, the physical distance between two neighboring lattice sites. Lattice field theories provide a natural non-perturbative approach to perform numerical calculations and have several advantages compared to continuum formulations regarding regularization.

In order to obtain a discretization of the equations of quantum field theory and an appropriate formulation on the lattice on has to realize that the derivatives involved in the fermionic part of the action will become finite difference quotients on the lattice. The differences involved at spacetime points of finite distance will demand, just like in general relativity, a parallel transport of the fermionic degrees of freedom, in order to preserve gauge invariance. Therefore in a lattice field theory, the gauge degrees of freedom are formulated in terms of the parallel transporter (1.3) between neighboring lattice points. The finite lattice version of such a parallel transporter between a lattice

point x and its neighboring lattice point in direction $\mu \in \{1, \ldots, d\}$ is given by the link variables

$$U_\mu = \exp\left(iaA_\mu\left(x\right)\right) \in G, \tag{1.23}$$

which are elements of the compact gauge group G (in contrast to the vector potential A_μ, which lives in the unbound algebra) and thereby also avoids a numerical integration over an unbound space. The link variables transform under gauge transformations in the adjoint representation and satisfy the condition

$$U_{-\mu}(x) = U_\mu^{-1}(x - \hat{\mu}). \tag{1.24}$$

Using the link variables as the fundamental degrees of freedom, it can be shown that Yang mills action can be approximated up to higher orders $\mathcal{O}(a^2)$ by the Wilson action [40]

$$S_G[U] = \beta \sum_{n\in\Lambda} \sum_{\mu<\nu} \mathrm{Re}\ \mathrm{tr}\left(1 - U_{\mu\nu}(n)\right), \qquad \beta = \frac{2N_\mathrm{c}}{g^2}, \tag{1.25}$$

where N_c is the number of colors, i.e. the dimension of the vector space, the gauge group is acting on, and the plaquette variables $U_{\mu\nu}$ are defined by

$$U_{\mu\nu}(x) = U_{+\mu}(x)U_{+\nu}(x + \hat{\mu})U_{-\mu}(x + \hat{\mu} + \hat{\nu})U_{-\nu}(x + \hat{\nu}). \tag{1.26}$$

Note that the lattice action is only determined by its continuum limit, and the Wilson action is only one possibility to obtain the desired continuum limit but also leaves the possibility to apply improved actions, which contain terms of higher order in the lattice spacing a.

In order to discretise the fermionic part of the interaction, the occuring derivatives are replaces with discrete difference quotients,

$$\partial_\mu \psi(x) \to \frac{1}{2a}(\psi(x + \hat{\mu}) - \psi(x - \hat{\mu})). \tag{1.27}$$

Since the fermionic fields transform under the gauge action according to

$$\psi(x) \to \Omega(x)\psi(x), \qquad \bar{\psi}(x) \to \bar{\psi}(x)\Omega(x)^{-1}, \tag{1.28}$$

terms like $\bar{\psi}(x)\psi(x \pm \hat{\mu})$ coming from $\bar{\psi}(x)\psi\partial_\mu\psi(x)$ are not gauge invariant and the terms shifted by $\pm\hat{\mu}$ have to be parallel transported to the lattice point x in order to obtain a gauge invariant difference quotient. This yields a fermionic action of the form

$$S_F[\psi, \bar{\psi}, U] = a^4 \sum_{f=1}^{N_\mathrm{f}} \sum_{n\in\Lambda} \left(\bar{\psi}^f(n) \sum_{\mu=\pm1}^{\pm4} (1 - \gamma_\mu) \frac{U_\mu(n)\psi^f(n + \hat{\mu})}{2a} + m^f \bar{\psi}^f(n)\psi^f(n) \right). \tag{1.29}$$

However it can be shown that this naive discretization leads to a description of 2^d fermions instead of just one, which is known as the doubler problem. This problem can be circumvented or reduced in different ways, for example by making use of different lattice versions of fermions, such as Wilson fermions or staggered fermions, where either option comes with a trade off. For example it can be shown that Wilson fermions, which avoid the occurrence of doublers in the continuum limit by introducing an extra mass term for the unphysical doubler modes, which vanishes in the continuum limit with $1/a$, break chiral symmetry. On the other hand one could use staggered fermions, which respect a lattice version of chiral symmetry, but only reduce the doubler problem, on a 4-dimensional spacetime by a factor of 4, which still leaves 4 different flavors of fermions, which have to be reduced by the controversial rooting procedure. In fact the Nielsen-Ninomiya theorem states there is no discrete version of a Dirac operator which is free of doublers, local, translational invariant and does not break chiral symmetry all at the same time. Hence any lattice version of fermions will cause some sort of problems.

Using Wilson fermions gives rise to the fermionic action

$$S_F[\psi,\bar{\psi},U] = a^4 \sum_{f=1}^{N_\mathrm{f}} \sum_{n\in\Lambda} \left(\bar{\psi}^f(n) \sum_{\mu=\pm1}^{\pm4} (1-\gamma_\mu) \frac{U_\mu(n)\psi^f(n+\hat{\mu})}{2a} + \left(m^f + \frac{4}{a} r \right) \bar{\psi}^f(n)\psi^f(n) \right). \tag{1.30}$$

Discretization of the chemical potential part of the action is a non-trivial task. A naive discretization yields to divergences. A way to avoid this and introduce the chemical potential into the action in a way that reproduces the continuum action correctly, is to multiply temporal links in positive and negative time-direction with the factors $\exp(\pm\mu a\delta_{\mu,4})$. For a detailed discussion of this we again refer to [104]. For our purposes it is enough to state that this can be done but will lead to the fermionic sign problem on the lattice, discussed in the upcoming sections.

Before moving on to the next section, we quickly introduce the lattice formulation of the Polyakov loop (1.17) and the center transformation introduced in (1.16), as they will be of major interest in the final results chapters of this work. The Polyakov loop on the lattice is given by

$$P(\vec{x}) = \mathrm{Tr} \prod_{t=1}^{N_t} U_0(\vec{x},t) \tag{1.31}$$

and transformations of center symmetry are given by a multiply of all temporal link variables at a fixed time slice $t = t_0$, i.e.

$$U_0(\vec{x},t_0) \to z U_0(\vec{x},t_0), \qquad z \in Z(G), \text{ for all } \vec{x} \text{ and } t_0 \text{ fixed.} \tag{1.32}$$

1.7 Lattice Regularization and Continuum Limit

In order to obtain a reasonable approximation of the continuum theory, the continuum limit $a \to 0$, where the lattice spacing is sent to zero, must eventually be taken. However, in the partition function we have control only over dimensionless parameters such as β and am, where m is the bare quark mass. (For a pure theory a is still implicitly contained in the link variables.) So the question arises how the physical value of the lattice spacing a is determined by lattice calculations and how to send it to zero. This can be done in several ways depending on the context. For a pure gauge theory we can calculate at a fixed value of β the expectation value of the Wilson loop around a rectangular loop which extends over n_s sites in spatial direction and n_t sites in timelike direction, which can be shown to have the form

$$\langle W(n_s, n_t)\rangle = C \exp(-n_t a V(n_s a)). \tag{1.33}$$

By first fixing n_s and varying n_t one can then determine (by a fit) the dimensionless parameters C and $aV(n_s a)$. This can be then done for different values of n_s to determine $aV(n_s a)$ as a function of n_s. Via the shape of the potential a certain value n_s^* can be identified with the Sommer parameter $r_0 \simeq 0.5fm$ [111]), which then determines the value of lattice spacing by

$$n_s^*(\beta)a = r_0. \tag{1.34}$$

For a theory with fermions, hadron correlators, which decay exponentially with the distance, are calculated and the hadron masses are then related to the correlation length via

$$aM_H = \xi_H(\beta). \tag{1.35}$$

This determines the value of the lattice spacing a by fixing eq. (1.35) to the experimental value of a hadron mass. Since M_H is a constant, the correlation length ξ_H must diverge in the limit $a \to 0$, which corresponds to a 2nd order phase transition. In order to have reached an approximation close enough to the the continuum limit all length scales related to physical quantities must be much larger than the lattice spacing, i.e.

$$\xi \gg a. \tag{1.36}$$

We have seen how the lattice spacing can be extracted from lattice results and also the behavior of correlation length in the continuum limit. However this still leaves the question of how to actually perform the continuum limit. Equations (1.34) and (1.35) already suggest that the lattice spacing, over whose value we have no direct control, somehow depends on the values of the other couplings such as β (or equivalently the coupling constant g) and quark mass terms of the form am. To understand this we have to realize that the finite lattice spacing a regulates the theory by introducing a cutoff in the momentum space and that the bare couplings g and m in the action do not directly correspond to physical observables. In order to obtains the physically observable

values, quantum corrections up to the corresponding scale, at which the physical values are observed, must be taken into account. Those quantum corrections depend on the lattice spacing a, due the corresponding momentum cut-off and the thereby neglected corrections at momenta beyond the cut-off. Hence the bare couplings depend on the renormalization scale, i.e. $g = g(a)$, $m = m(a)$. The requirement that any physical observable $\mathcal{O}(a, g)$ of the lattice theory does not depend on the lattice spacing, gives rise to the renormalization group equation [112–115]

$$\left[a\frac{\partial}{\partial a} - \beta(g)\frac{\partial}{\partial g}\right]\mathcal{O}(a, g), \qquad \beta(g) = -a\frac{\partial g}{\partial a}, \tag{1.37}$$

where the β-function calculates the change of the bare coupling g as a function of the lattice spacing. Near a fixed point g^* of the RG flow, which satisfies

$$\beta(g^*) = 0, \tag{1.38}$$

the beta function can by explicitly calculated by use of an expansion. Asymptotic freedom of QCD implies that a fixed point exists in the ultraviolet, i.e.

$$g^* = \lim_{a\to 0} g(a) = 0. \tag{1.39}$$

Using using perturbation theory to 1-loop order [116] one can derive the running coupling equation

$$g^2(a) = \frac{1}{\left(\frac{11}{3}N_\mathrm{c} - \frac{2}{3}N_\mathrm{f}\right)\log\left(\frac{\Lambda^2_\mathrm{QCD}}{a^2}\right)}, \tag{1.40}$$

which shows a logarithmic decrease of the quadratic coupling constant with the quadratic momentum.

We see that the continuum limit is approached by sending the bare coupling $g \to 0$ ($\beta \to \infty$), while at the same time compensating for the shrinking of the lattice, due to the implicit limit $a \to 0$, by taking the thermodynamical limit. Therefore the continuum limit is obtained by applying

$$N_s, N_t \to \infty, \quad \beta \to \infty. \tag{1.41}$$

with hadron masses fixed by (1.35) and the temperature given by

$$\frac{1}{T} = a(\beta)N_t. \tag{1.42}$$

1.8 Monte-Carlo Method

Monte-Carlo methods provide a powerful method for numerical calculation of non-trivial, high-dimensional integrals as they occur in lattice field theory. The integral over the space of field variables is replaced by a sum of configurations that are in the field space which are chosen randomly. For an 1-dimensional integral this written as

$$\int d(x)\mu(x)f(x) \to \frac{1}{|\{x_i\}|}\sum_j f(x_j), \tag{1.43}$$

where the set of configurations $\{x_i\}$ is distributed along the $\mu(x)$-part of the measure $d(x)\mu(x)$. Of course replacing the integral by a finite sum yields an approximation of the real result, which will improve when increasing the number of configurations taken into account.

For the high dimensional integral

$$\langle\mathcal{O}\rangle = \frac{1}{Z}\int D[\psi,\bar{\psi},U]\mathcal{O}[\psi,\bar{\psi},U]\exp(-S). \tag{1.44}$$

of lattice field theory, the exponential Boltzmann factor is usually viewed as part of the measure and the Monte-Carlo sum takes therefore the form

$$\langle\mathcal{O}\rangle = \frac{1}{|\{C\}|}\sum_{\{C\}}\mathcal{O}(\mathcal{C}), \tag{1.45}$$

where $\{C\}$ denotes the set of configurations, which is distributed with respect to the Boltzmann factor $\exp(-S)$. In order to ensure such a distribution, which is referred to as important sampling, appropriate update algorithms that produce from a chosen starting point in the space of configurations Markov chains with the appropriate distribution. Possible algorithms are the given by the Metropolis algorithm and the Hybrid-Monte-Carlo algorithm.

1.9 Numerical Sign Problem

When trying to apply Monte-Carlo methods to calculate the integral of a highly oscillatory function, with near-cancellation of the positive and the negative parts of the oscillations, one is faced with the issue that the near-cancellation needs to be calculate with an accuracy usually far beyond the accuracy attainable in order to have a useful approximation of the integral. Unfortunately this is exactly the case in ordinary QCD with gauge group SU(3) if one takes into account the contribution of a non-vanishing chemical potential. The Grassmann integration of the fermionic fields yields a factor in the bosonic integrals given by the complex determinant of the Dirac operator and its highly oscillatory nature prevents us from simply applying Monte-Carlo methods on

lattices of meaningful size, as the accuracy, which one needs, rises exponentially with the lattice volume. Interpreting the determinant as part of the measure is not possible either, as the complex determinant cannot be interpreted as a probability weight, and important sampling methods which are supposed yield a set of configurations distributed along the measure cannot be applied, unless the measure is real and positive.

For vanishing chemical potential the complex nature of the Dirac operator's determinant can be avoided, if the Dirac operator satisfies the γ_5-hermicity condition

$$\gamma_5 D \gamma_5 = D^\dagger, \tag{1.46}$$

which is the case for QCD with zero chemical potential. It yields for the determinant of the Dirac operator

$$det[D]^* = det[D^\dagger] = det[\gamma_5 D \gamma_5] = det[D], \tag{1.47}$$

hence the determinant is real but in general it will be still not positive. The positivity can be achieved if the masses of the two light quarks u, d are taken to be equal, which yields for the corresponding Dirac operators $D_u = D_d \equiv D$, and the overall factor

$$det[D_u] det[D_d] = det[D]^2 = det[D] det[D^\dagger] = det[D D^\dagger] \geq 0 \tag{1.48}$$

in the bosonic integrals is therefore positive, making a interpretation in terms of a probability weight possible.

However for finite chemical potential the attained factor in the bosonic integrals is due to

$$\gamma_5 D(\mu) \gamma_5 = D(-\mu^*)^\dagger, \tag{1.49}$$

$$det[D(\mu)]^* = det[D^\dagger(\mu)] = det[\gamma_5 D(-\mu^*) \gamma_5] = det[D(-\mu^*)], \tag{1.50}$$

even in the limit of two mass degenerate light quarks not real (unless the two mass degenerate quarks have a chemical potentials that differ by a reflection along the imaginary axis, i.e. $\mu_u = -\mu_d^*$, which is satisfied for example by using purely imaginary potentials and setting $\mu_u = \mu_d$, or using the (real) isospin chemical potential $\mu = \mu_u = -\mu_d$). However in the case of $SU(2)$, pseudo-reality of the gauge group yields and additional symmetry for the system, which can be used in order to show that the sign problem can be avoided.

This concludes our discussion of the basics of quantum field theories. In the next chapter we will discuss the mathematical concepts needed for the derivation of the effective Polyakov loop models and the inverse Monto-Carlo method later in this work.

Chapter 2

Basics of Lie Groups and Lie Algebras

In the upcoming chapters of this work, where we will derive effective Polyakov loop models for the SU(N) gauge theories and introduce the IMC method, we will have to make use of different concepts and features of the gauge group, which is a Lie group, and its underlying Lie algebra. Therefore in this chapter we want to give a short introduction into needed concepts and theorems. Lie groups in physics are usually first encountered in terms of the classical Lie groups, which are the real and complex rotation groups SO(N), SU(N) and U(1). Especially SU(2) plays a crucial role in quantum mechanics, describing the spin degree of freedom of fermions. The classical Lie groups consist of uncountably infinite many elements, that can be parametrized by a finite number of continuous parameters $\vec{\lambda} \in \mathbb{R}^n$ in the form of an exponential function

$$G = \left\{ \exp\left(i \sum_{j=1}^{n} \lambda_j H_j \right) \middle| \, \vec{\lambda} \in \mathbb{R}^n \right\}, \tag{2.1}$$

where the set $\{H_1, \ldots, H_n\}$ are called the generators of the group. Such a parametrization shows that Lie groups are differentiable manifolds. For SU(N) the generators are given by the N^2-1 hermitian $(N \times N)$-matrices with determinant equal to 1 and again it is well known for SU(2) that endowed with the commutator they satisfy closed algebraic relations, hence the vector spaced spanned by generators forms a Lie algebra, associated with the Lie group. From the mathematical treatment of spin-1/2 particles, we are also familiar with the concept of forming tensor products of particles, hence vector spaces, and tensor products of the group and algebra elements that act on those spaces, yielding operators that act on higher dimensional spaces and satisfy the same group theoretic and algebraic relations. Building tensor products results in higher dimensional representations of the Lie group and algebra. In a strict mathematical treatment the emphasis is put on those group theoretic and algebraic relations, where group and algebra elements are not given the explicit form of matrices. That way all possible matrix representations on vector spaces of arbitrary dimension, i.e. all possible representations of a group and its algebra are can be considered later on. As we will see, a special class of representations, called fundamental representations, can be identified and used to construct all

other representations, just like in the case of SU(2), where higher spin representations are obtained by tensor products of spin-1/2 particles. In this chapter we will give a short introduction into the mathematical theory of Lie groups and Lie algebras, based on [107,117–119], with emphasis on SU(2) and SU(3). Note that the results as presented here are in general only true for semi-simple Lie algebras and their associated Lie groups, which include the classical Lie groups, although some results might also extend to more general cases. This introduction will be a simplified heuristic discussion. For a strict mathematical discussion and proofs of the statements that are presented here we refer to the mathematical literature.

2.1 Basic Definitions

Let us first start with the mathematical definitions of Lie groups and Lie algebras and a few basic relations between them.

Lie Group: A Lie group G is a differentiable manifold, which is endowed with a group structure, such that the group operations

$$\begin{aligned} &G \times G \mapsto G, \;\; (g_1, g_2) \to g_1 \cdot g_2, \\ &G \mapsto G, \;\; g \to g^{-1}, \end{aligned} \tag{2.2}$$

are differentiable.

Lie Algebra: A Lie algebra is a vector space A over a field $\mathbb{K}$ equipped with a Lie bracket, a bilinear function $[.,.] : A \times A \mapsto A$ satisfies (for $x, y, z \in A$ and $\lambda, \beta \in \mathbb{K}$)

$$\begin{aligned} &[\alpha x + \beta y, z] = \alpha[x, z] + \beta[y, z], \\ &[x, y] = -[y, x], \\ &[x, [y, z]] + [y, [z, x]] + [z, [x, y]] = 0. \end{aligned} \tag{2.3}$$

Given a basis $\{t_1, \ldots, t_n\}$, we can expand the result of a Lie bracket between two elements according to $[t_a, t_b] = \sum_c f_{ab}^c t_c$, where the numbers $f_{b,c}^a$, with $a, b, c = 1, \ldots, n$, are called **structure constants**.

Semi-Simple Lie algebra: A semi-simple Lie algebra is a direct sum of simple Lie algebras. A simple Lie algebra $\mathfrak{g}$ is a non-abelian Lie algebra, which contains no ideal except of $\mathfrak{g}$ itself and the zero-space, where an ideal is a subspace $\mathfrak{i} \subseteq \mathfrak{g}$, such that $[\mathfrak{g}, \mathfrak{i}] \subseteq \mathfrak{i}$.

Cartan algebra and Rank: The Cartan algebra $\mathfrak{h} \subset \mathfrak{g}$ of a Lie algebra $\mathfrak{g}$ is defined as the maximal abelian sub-algebra, i.e. the maximal sub-space which satisfies

$$[a, b] = 0, \quad \forall a, b \in \mathfrak{h}. \tag{2.4}$$

The rank of a Lie algebra or Lie group is the dimension of its Cartan algebra.

Lie groups and algebras are deeply connected. Given a local parametrization of the group manifold, one can show that the tangent space at the neutral element is the lie algebra and that the algebra elements are related to the group elements by the exponential map. To generalize the concept of a directional derivative on a usual manifold to a Lie group, let us recall the directional derivate. For a manifold M with $p \in M$ one defines the derivative at point p in direction of an element v of the tangent space, by taking a path $\gamma : [-1, 1] \mapsto M$, with $\gamma(0) = p$, $\gamma'(\tau)|_{t=0} = v$ and defining the derivative as $\nabla_v f(p) = \frac{d}{d\tau} f(\gamma(\tau))|_{\tau=0}$ which, as can be shown, is independent of the specific choice of γ. The straight forward generalization to Lie groups is done by setting the path to $\gamma(t) = \exp(t \cdot a)\, g$ or $\gamma(t) = g\, \exp(t \cdot a)$, where we see that, due to the non-commutativity of the group structure, we have to be careful if we multiply the exponential map to the group element from the left or the right, which introduces the concept of right- and left-derivatives.

Exponential Map: As the tangent space of a Lie group is a Lie algebra, it can be shown that all closed and connected Lie groups can be given in terms of the exponential map $\exp : \mathfrak{g} \mapsto G$, i.e. if $g \in G$ and then there is an $a \in \mathfrak{g}$, such that

$$g = \exp(a) \tag{2.5}$$

Left-Derivative: In this form the left-derivative of a function on the Lie group G in direction of the a-th basis element $t_a \in \mathfrak{g}$ can be written as

$$L_a(f(g)) := \frac{d}{dt} f(\exp(t \cdot t_a)g)|_{t=0} = \lim_{\overrightarrow{t \to 0}} \frac{f(\exp(t \cdot t_a)g) - f(g)}{t}, \tag{2.6}$$

where the word left refers to multiplication with $\exp(t \cdot t_a)$ from the left. The right-derivative can be defined analogously.

2.2 Representations

Now that we have defined Lie groups and Lie algebras solely via their group and algebra structure, we can define representations of them, which will yield matrix sets that respect the same group or algebra structure.

Representation of a Lie Group: A representation D of a Lie Group G over a Vector space V is a map from the group to $GL(V)$, the space of Linear functions on V, such that it preserves the structure of the group, i.e.

$$D(e) = 1, \;\; D(gh) = D(g)D(h), \qquad \forall g, h \in G, \tag{2.7}$$

where $e \in G$ is the neutral element.

Representation of a Lie Algebra: A representation ρ of a Lie algebra $\mathfrak{g}$ over a Vector space V is a map from the algebra to $\mathfrak{gl}(V)$, such that it preserves the structure of the algebra, i.e.

$$\rho([x, y]) = [\rho(x), \rho(y)], \qquad \forall x, y \in \mathfrak{g}, \tag{2.8}$$

where $\mathfrak{gl}(V)$ is the Lie algebra given by $GL(V)$ endowed with the commutator as its Lie bracket.

Irreducible and Reducible Representations: A representation is called reducible if there exists an invariant true subspace of V, and irreducible otherwise.

For groups such as SU(N) and SO(N) and their corresponding Lie algebras, which are originally defined in a matrix representation, we already start with a distinguished representation, called the **defining representation**. Another special representation, which is available for any Lie group / algebra and is of special mathematical interest is the adjoint representation. It gives a natural representation on the vector space given by the algebra itself and many characteristics of the Lie group can be understood in terms of the adjoint representation of its algebra. Also we will be able to define a metric on the group manifold in terms of its adjoint representation.

Adjoint representation of a Lie group: The adjoint representation $Ad : G \to GL(\mathfrak{g})$ of a Lie group G is given by

$$Ad_g(y) := gyg^{-1}, \qquad \text{for all } g \in G,\ y \in \mathfrak{g} \tag{2.9}$$

Adjoint representation of a Lie algebra: The adjoint representation $ad : \mathfrak{g} \to \mathfrak{gl}(\mathfrak{g})$ of a Lie algebra $\mathfrak{g}$ is defined by

$$ad(y)(x) := [x, y]. \tag{2.10}$$

By expanding

$$gyg^{-1} = \exp(tx) \cdot y \cdot \exp(-tx) = y + t[x, y] + O(t^2), \tag{2.11}$$

for some $x \in \mathfrak{g}$, we can see the relationship

$$\begin{aligned} &\frac{d}{dt} Ad_{\exp(tx)}(y)|_{t=0} = [x, y], \\ &Ad = \exp(ad) \end{aligned} \tag{2.12}$$

between the adjoint representation a Lie group and its Lie algebra.

Using the adjoint representation we can define a bilinear form, which will yield a metric on the group manifold.

Killing Form: The Killing form is a symmetric bilinear form $B : \mathfrak{g} \times \mathfrak{g} \mapsto \mathbb{K}$ defined by

$$B(x, y) \equiv (x, y) := Tr(ad(x) \circ ad(y)). \tag{2.13}$$

The Killing form is associative and skew symmetric and invariant under the adjoint action of the Lie group, i.e.

$$\begin{aligned} &B([x, y], z) = B(x, [y, z]), \quad x, y, z, \in \mathfrak{g} \\ &B(ad(z)x, y) = -B(x, ad(z)y), \quad x, y, z, \in \mathfrak{g} \\ &B(Ad(g)x, Ad(g)y) = B(x, y) \quad x, y \in \mathfrak{g},\ g \in G. \end{aligned} \tag{2.14}$$

It can be shown that it is non-degenerate exactly if the Lie algebra is semi-simple, in which case case the Killing form is negative definite and $-B$ defines on the Lie group a Riemannian metric, called the Killing metric. In the case of SU(N) it can be explicitly calculated and is given by

$$(a, b) = 2N \cdot Tr(a \cdot b), \qquad \text{for all } a, b \in \mathfrak{su}(N). \tag{2.15}$$

2.3 Representation Theory and Multiplets

In this section we use the previous definitions to discuss how different representations can be classified, the connection between representations and multiplets, which we are familiar with from the discussion of particles with spin, which are arranged in SU(2) multiplets, or the hadron spectrum which can be arranged into SU(3) multiplets.

Lets consider a Lie algebra $\mathfrak{g}_d$ of of dimension d and rank r, with Cartan sub-algebra $\mathfrak{h}_r \subset \mathfrak{g}_d$. We can then choose the generator such that the algebra decomposes into

$$\mathfrak{g}_d = \mathfrak{h}_r \oplus \mathfrak{e}_{d-r}, \tag{2.16}$$

where $\mathfrak{e}_{d-r}$ is the $(d-r)$-dimensional orthogonal complement to $\mathfrak{h}_r$. Now one can choose a basis $E_1, \ldots, E_{d-r}$ of $\mathfrak{e}_{d-r}$ in terms of eigenfunctions of ad_H with $H \in \mathfrak{h}_r$, i.e. satisfying

$$[H, E_j] = \alpha_j(H)E_j, \qquad \alpha_j \in H^*,\ j = 1, \ldots, d - r, \tag{2.17}$$

where α_j are elements of H^*, the dual space of H, and are called roots. Now we can consider a n-dimensional representation of the Lie algebra, where all algebra elements are given in terms of $(n \times n)$-matrices rather than as abstract algebraic elements. Since the Cartan algebra is the maximal commuting sub-algebra, all elements are simultaneously diagonalizable and we can choose an eigenbasis $e_1, \ldots, e_n$ such that for $H \in \mathfrak{h}_r$

$$He_a = M_a(H)e_a, \qquad M_a \in H^*,\ a = 1, \ldots, n, \tag{2.18}$$

where M_a are called weights. Using relation (2.17) we can show

$$HE_j e_a = (M_a(H) + \alpha_j(H))E_j e_a, \qquad j = 1, \dots, d-r,\ a = 1, \dots, n \tag{2.19}$$

$$a = 1, \dots, n, \tag{2.20}$$

i.e. that E_j-elements, the chosen basis elements of the Cartan algebra's complement $\mathfrak{e}_{d-r}$, act as ladder operators by mapping an eigenvector e_a of Cartan algebra to another eigenvector, with the eigenvalue with respect to $H \in \mathfrak{h}$ raised by $\alpha(H)$. One can show that the dimension $d-r$ and the number of ladder operators is even and that if α_j is a root, then so is $-\alpha_j$, hence we can split the basis $E_1, \dots, E_{d-r}$ into $E_1^{\pm}, \dots, E_{\frac{d-r}{2}}^{\pm}$, where if E_j^+ raises the eigenvalue of an eigenvector by α_j, then E_j^- will do so by $-\alpha_j$.

If we choose a basis $H_1, \dots, H_r$ of the Cartan algebra, then the elements $\alpha_j, M_a \in H^*$, $j = 1, \dots, d-r$, $a = 1, \dots, n$ are completely determined by the values they take for the basis elements H_i and choosing a basis $\{\beta_1, \dots, \beta_r\}$ for H^*, such that

$$\beta_i(H_j) = \delta_{ij}, \qquad i, j = 1, \dots, r \tag{2.21}$$

we can write

$$\alpha_j = \sum_i \alpha(H_i)\beta_i \equiv (\alpha_j(H_1), \dots, \alpha_j(H_r))^T = \vec{\alpha}_j \in \mathbb{R}^k \simeq H^*. \tag{2.22}$$

Hence we can depict the elements $\alpha_j \in H^*$, with $j = 1, \dots, d-r$, as vectors $\vec{\alpha}_j = (\alpha_j(H_1), \dots, \alpha_j(H_r))^T \in \mathbb{R}^r$, and likewise the elements $M_a \in H^*$ as vectors $\vec{M}_a = (M_j(H_1), \dots, M_j(H_r)^T) \in \mathbb{R}^r$, in the r-dimensional plane, where the n vectors $\vec{M}_a$ correspond to the n eigenstates of the Cartan algebra, depicted in $\mathbb{R}^r$ by their their r eigenvalues with respect to the Cartan generators $H_1, \dots, H_r$. Likewise the $(d-r)$ vectors $\vec{\alpha}_j$ represent the shifts between the eigenstates due to the ladder operators E_j in the space $\mathbb{R}$. All eigenvectors of the n-dimensional vector space, which are connected by ladder operators are part of the same, (so-called) multiplet.

Now it is possible to have several multiplets in one representation, such that the ladder operators only connect states of the same multiplet. Since then neither the ladder operators map states of different multiplets to each other and nor Cartan generators do (as the eigenvectors where chosen to be eigenvalues of the Cartan algebra) the sub-spaces spanned by each multiplet are invariant subspaces of the whole algebra, hence of the group and each multiplet spans an individual irreducible representation of the algebra, where the dimension of the spanned subspace is the dimension of the irreducible sub-representation.

We see that within an irreducible representation the states can be labeled by their eigenvalues with respect to the Cartan generators, which we depict as vectors in $\mathbb{R}$. We can get a whole irreducible representation by acting with ladder operators on an eigenvector, to get all other eigenvectors which span the representation. Furthermore

we can also label the different representation by appropriate eigenvalues. Therefore we use the eigenvalues of the Casimir operators, which are operators that are polynomes of algebra elements (hence not algebra elements themselves) and commute with all algebra elements. One can show that the number of Casimir operators that exist equals the rank of the algebra. The most easily defined Casimir operator is the quadratic Casimir operator given by

$$\Omega = \sum_i T_i T^i, \tag{2.23}$$

where $\{T^i : i = 1, \ldots, d\}$ provides a basis of the Lie algebra and $\{T_i : i = 1, \ldots, d\}$ is the dual basis with respect to the Killing metric. Now as Casimir operators commute with all algebra elements, it is easy to show that their eigenvalues are constant on each multiplet. Furthermore, one can show that the set of Casimir eigenvalues $\{c_1, \ldots, c_r\}$ are different on inequivalent representations. Hence, we can label different representations by their Casimir eigenvalues $\vec{c} = (c_1, \ldots, c_r)$ and different eigenstates within a representation by their eigenvalues with respect to the Cartan generators, $\vec{M} = (M(H_1), \ldots, M(H_N)) \in \mathbb{R}^r$.

Now let us look at the familiar case of the 3 dimensional algebra of SU(2), with rank 1. In the discussion of spin-1/2 one starts with the 2-dimensional defining representation, with the 3 algebra generators given by the 2×2 Pauli matrices. We then split the algebra into a 1 dimensional Cartan sub-algebra and its orthogonal complement, i.e.

$$\mathfrak{g}_3 = \mathfrak{h}_1 \oplus \mathfrak{e}_2 \tag{2.24}$$

and set a basis for each subspace via

$$H_1 = L_z, \;\; E_1 = L^+, \;\; E_2 = L^-. \tag{2.25}$$

The operators satisfy the relation (2.17), which, after choosing a basis of the Cartan algebra, i.e. a basis of the spin-projection operator L_z, yields that $L^\pm$ act as ladder operators on the multiplet, which is represented by the two spin-1/2 Cartan eigenvalues $+1/2$, $-1/2$ and depicted along the line $\mathbb{R}$. The Casimir operator $\vec{L}^2$ labels the spin number of particles. From the discussion of how spin particles couple to each other, we already know that the eigenvalues to the Cartan generator of the two particles are additive, hence coupling 2 multiplets of the form $-1/2, +1/2$ will yield a representation with Cartan eigenvalues $1, 0, 1$, where the 0 eigenvalue is occupied by two different states, each belonging to a different multiplet, and the space decomposes into 2 invariant subspaces $1, 0, 1$, which is identified via the Casimir eigenvalue as a spin-1 particle, and a subspace 0, which is identified as a spin-0 particle, which we write in dimensional notation as

$$[2] \otimes [2] = [3] + [1]. \tag{2.26}$$

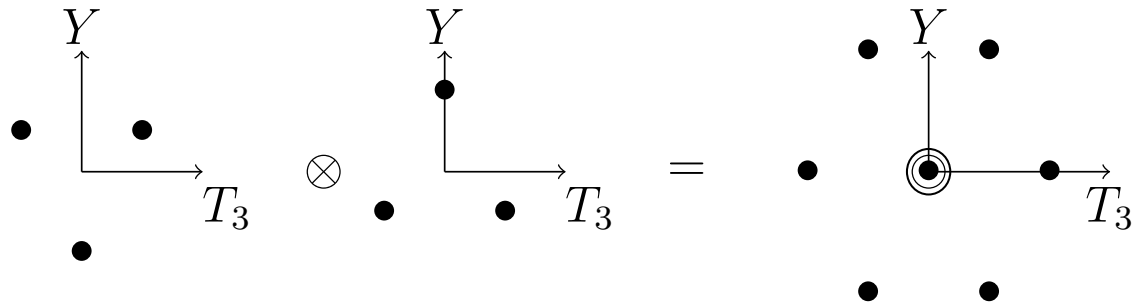

Figure 2.1: Tensor product of two triplet representation yielding an octet and singlet, i.e. $[3] \otimes [\bar{3}] = [8] + [1]$

In the case of SU(3) the dimension of the algebra is 8 and its rank is 2. Hence, we can split the algebra $\mathfrak{g}_8$ into

$$\mathfrak{g}_8 = \mathfrak{h}_2 \oplus \mathfrak{e}_6 \tag{2.27}$$

where the two Cartan generators are set to Y and T_3 (see A.31), and the ladder operators that generate the complement are set to $T^{\pm}, U^{\pm}, V^{\pm}$ (see A.32). Multiplets of SU(3) can be depicted in $\mathbb{R}^2$ by the eigenvalues with respect to the 2 Cartan generators. We have shown the form of typical multiplets in Fig. 2.1, where we have depicted the defining representation (labeled in dimensional notation as [3]) and its conjugate representation (obtained by conjugation of the defining representation's generators and labeled in dimensional notation by $[\bar{3}]$). Multiplet on the r.h.s results from a product a product of those two representations. As we can see, the pattern that emerges from the product is again obtained by vector addition of the eigenvalues of the two representation, which yields 9 states, i.e. a 9 dimensional representation. The eigenvalue $(0, 0)$ is 3-fold "occupied". One can show that one of the states at $(0, 0)$ decouples into its own invariant subspace and the 9 dimensional representation reduces to two irreducible representations denoted by $[8] + [1]$ in dimensional notation.

2.4 Dynkin Labels and Fundamental Representations

We have seen how to decompose Lie algebras into a Cartan algebra and its orthogonal complement, and use a set of Cartan generators and generators of the complement in form of ladder operators in order to depict irreducible representation in $\mathbb{R}^r$ via root and weight systems, and how to label different irreducible representations by their Casimir eigenvalues. Let us now introduce another way to label different irreducible representations in a systematic way via Dynkin labels, which will yield a classification of fundamental representations, which build in a way the basis for all other representations. In order to do so, the first step is to define an ordering of the roots (for which there will be no unique way) and weights in the space $\mathbb{R}^r$. Given an (ordered) basis $\{\beta_1, \ldots, \beta_r\}$

of H^* (which can be set for convenience again to the basis defined in (2.21)) we define a root $\vec{\alpha}_a$ to be **positive**, if the first non-vanishing entry in the expansion in terms of basis elements β_i is positive, if it is not, then it is called **negative**. In the basis 2.21 this just means that a root $\vec{\alpha}_j \in \mathbb{R}^k$ is positive if its first non-vanishing entry is positive. (Having a notion of positive and negative roots we can now equally distinguish between raising and lowering operators.) Furthermore we define positive roots which cannot be written as the sum of two other positive roots as **simple** roots, which means that the corresponding raising and lowering operators raise and lower by a minimal basic amount. The number of simple roots equals the rank of the algebra, and all other positive roots can be written as a sum of simple roots. We can then define an order for the roots, such that $\lambda \geq \mu$ if $\lambda - \mu$ is a non-negative combination of simple roots. Analogously we define and order for the weights of a representation and obtain a **highest weight**. In Fig. 2.2 we have shown the weight and root system of [3], the defining representation of SU(3), where we have depicted weights as bullets and roots as vectors. Note the transition between different weights by applying a root. The positive roots are shown in blue, and the positive roots which are also simple in red.

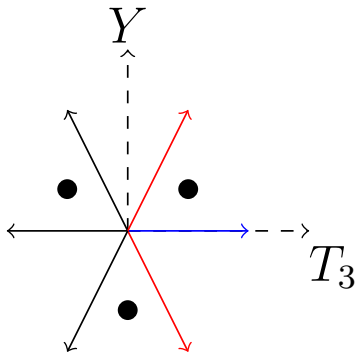

Figure 2.2: Weights (bullets) and roots (vectors) system of [3]. The positive roots are depicted in blue, the simple roots in red.

Having defined the simple weights $\vec{\alpha}_i = \sum_j \alpha_{ij}\beta_j \equiv \alpha_j \in H^*$, with $i = 1, \ldots, r$, we can define on the space of weights an inner product for a weight $\vec{\lambda} = \sum_j \lambda_j \beta_j \equiv \lambda \in H^*$ its Dynkin label via

$$\Lambda_i = 2\frac{\langle \lambda, \alpha_i \rangle}{\langle \alpha_i, \alpha_i \rangle} \in \mathbb{N}_0, \tag{2.28}$$

where Λ_i, $i = 1, \ldots, r$ are the Dynkin indices and $\vec{\Lambda} = (\Lambda_1, \ldots, \Lambda_r) \in \mathbb{N}_0^r$ is called **Dynkin Label**. The inner product $\langle ., . \rangle : H^* \mapsto \mathbb{R}$ hereby is defined via the Killing metric

$$\langle \alpha, \beta \rangle := (h_\alpha, h_\beta), \tag{2.29}$$

where the element $h_\alpha \in H$ is defined by $\alpha \in H^*$ such that $[h_\alpha, \cdot] = \alpha(\cdot) \in H^*$.

There are $r = \text{rank}(\mathfrak{g})$ so called **fundamental weights** $\vec{\omega}_i$, $i = 1, \ldots, r$ that satisfy

$$2\frac{\langle \omega_i, \alpha_j \rangle}{\langle \alpha_j, \alpha_j \rangle} = \delta_{ij}, \tag{2.30}$$

and form a basis for the weights, i.e. all weights can be expanded, such that their entries with respect to this basis are non-negative integers, hence

$$\lambda = \sum_i \Lambda_i \omega_i. \tag{2.31}$$

With this we can label a representation by the Dynkin label of its highest weight, i.e. $\vec{\Lambda}^{HW}$ and a representation is called **fundamental representation** if its highest weight λ^{HW} is a fundamental weight, i.e if

$$\begin{aligned} &\frac{\langle \lambda^{HW}, \alpha_i \rangle}{\langle \alpha_i, \alpha_i \rangle} = \delta_{pi}, \qquad \text{for some } p \in \{1, \ldots, r\} \\ &\vec{\Lambda}^{HW} = (0, \ldots, 0, \underbrace{1}_{p\text{-th position}}, 0, \ldots, 0), \end{aligned} \tag{2.32}$$

There are r fundamental representations for a Lie group of rank r and we we call a fundamental representation with the entry 1 at the p-th position of the Dynkin label the p-th fundamental representation. (Of course the order depends on the order of the basis but usually there is a standard order and in case of SU(N) the 1st fundamental representation is the defining representation, given by the defining matrices on and N-dimensional vector space).

As we saw earlier, from tensor products of representations other representations are obtained and it can show that the fundamental representations are enough to obtain all other possible irreducible representation in that way. In general we can reduce a tensor product of representations to a sum of irreducibles, i.e.

$$V_\mu \otimes V_\nu = \sum_\lambda C^\lambda_{\mu\nu} V_\lambda \tag{2.33}$$

where the indices μ, ν, λ label all possible irreducible representations (e.g. by their Dynkin labels) and the Clebsch-Gordon coefficients determine which representations occur in a given tensor product. We will later give for SU(N) a formula, with which one can calculate the sum of irreducible representation that occurs in a product of fundamental representations, from which we can read off the corresponding Clebsch-Gordon coefficients.

2.5 Integration on Lie Groups, Class functions and Characters

The integration over function on Lie groups, which will be used later in this work, relies on the construction of an appropriate measure. For $\mathbb{R}^n$ a measure is given by the Lebesque measure, which is defined in a way that ensured its translational invariance (as one needs to ensure that a given volume does not change under translation in the vector space, in order to have a meaningful integral) and with a normalization condition, such that the volume of the n-dimensional cube $[1,0]^n$ is set to one. A generalization of this measure to the manifold of Lie groups is given by the Haar measure.

The Haar measure for groups is required to have similar features. Again the volume of a given subset of the group shouldn't change if one shifts each element of the subset in a equal manner. Since we are dealing with groups and an arbitrary manifold, this shift is obviously given by the multiplication of the subset with an arbitrary group element, where due to the non-commutativity of multiplications in general one has to consider left- and right-shifts independently, which leads (similar to the translational invariance for the Lebesque measure) to the requirement of left- and right-invariance of the Haar measure. Left- and right invariance already determines the measure uniquely, up to multiplication with a constant. One has therefore a choice of normalization, and chooses the integration over the whole group to be equal to 1. When speaking of the Haar measure we will always refer to the unique Haar measure with this normalization condition.

Haar measure: The Haar measure μ on a Lie group G is therefore defined as the (as can be shown) unique measure, satisfying the conditions

$$\mu(H) = \mu(gH) = \mu(Hg), \text{ for all } g \in G, H \subset G, \tag{2.34}$$

$$\mu(G) = 1 \tag{2.35}$$

or in integral form

$$\int_{h\in H} d\mu(h) = \int_{h\in H} d\mu(gh) = \int_{h\in H} d\mu(hg), \text{ for all } g \in G, H \subset G, \tag{2.36}$$

$$\int_{h\in G} d\mu(g) = 1. \tag{2.37}$$

Construction of the Haar measure: Given an explicit parametrization of the group elements by $U = U(\alpha_1, \ldots, \alpha_{N^2-1})$ we can construct the Haar measure for SU(N) (up to a constant, which we can by normalization) via the metric tensor

$$g_{mn} = Tr\left(\frac{\partial U^\dagger}{\partial \alpha_n} \cdot \frac{\partial U^\dagger}{\partial \alpha_n}\right), \tag{2.38}$$

$$dU = \sqrt{det(g_{mn})} d\alpha_1 \cdots \alpha_n. \tag{2.39}$$

Adjoint Classes and Class functions A complex group function f on a Lie group G is a map $f : G \mapsto \mathbb{C}$. A Lie group G can be divided into different sub-manifolds (but not sub-groups), which are called adjoint classes. The adjoint class of $\langle g \rangle$ an element $g \in G$ is defined by

$$\langle g \rangle = \{hgh^{-1} | h \in G\}. \tag{2.40}$$

Adjoint classes are sub-manifolds, which are invariant under the adjoint action. A group function f is called class function, if it is constant on each class, i.e.

$$f(h) = f(hgh^{-1}) \quad \text{for all } g, h \in G. \tag{2.41}$$

Every element $g \in G$ is conjugate to an element of the maximal Torus T, i.e. of the maximal connected abelian subgroup of G. Therefore the class functions are only functions of coordinates that parametrize the maximal abelian torus T.

Characters: The character $\chi_\rho(g)$ of an element $g \in G$ in a representation ρ is given by

$$\chi_\rho(g) := Tr(\rho(g)), \tag{2.42}$$

which is the most simple class function one can think of. One can show that the characters in the fundamental representations form a basis for class functions.

The reduction of representation (2.33) carries over to characters

$$\chi_\mu(g)\chi_\nu(g) = \sum_\lambda C^\lambda_{\mu\nu}\chi_\lambda(g) \tag{2.43}$$

$$\tag{2.44}$$

Reduced Haar measure for class functions: Class functions are constant on each class, therefore integration over the redundant degrees of freedom can be executed and yields only a constant, leaving us with the so called reduced Haar-measure on the maximal abelian torus, which we could get by explicit parametrization in terms of class variables and additional variables and then integrate out the redundant degrees in equation (2.39). An easier way though is obtained by using the fact that the fundamental characters build a basis for class functions and we can therefore obtain the Haar measure via the Jacobian of the characters, hence

$$\int_G d\mu_{red} f(U) = \int_\phi d\phi_1 \dots d\phi_r \det\left(\frac{d\chi_p(U)}{d\phi_j}\right) f(U), \tag{2.45}$$

with $p, j = 1, ..., \text{rank}(G)$.

Orthogonality of characters: Integration over the characters yields the orthogonality relation

$$(\chi_\mu, \chi_\nu) := \int_G d\mu_{red} \chi_\mu \bar{\chi}_\nu = \delta_{\mu\nu}, \tag{2.46}$$

which defines a scalar product.

2.6 SU(N) Formulas

The final section of this chapter will present a short summary of formulas for SU(N) that we will need in the rest of this work. Let us first recall that SU(N) belongs to the classical Lie algebras, which are defined in terms of matrices, hence defined in a certain representation to start with. These representations are called defining representations and are denoted by a Dynkin labels $(1, 0, \dots)$ and are of of dimension N, hence labeled in dimensional notation by $[N]$. Furthermore to a certain representation we can obtain the conjugate representation by conjugation of the generators given in that representation, such a representation obtains a Dynkin label with inverted entry of the Dynkin label and has obviously the same dimension as the former one. Conjugation of the defining representation yields the conjugate representation labeled by $(0, \dots, 0, 1)$ and in dimensional notation by $[\bar{N}]$.

Reduction Formulas: Later in this work we will encounter products of fundamental representations, which we will need to reduce to a sum of irreducible representations. For products of two fundamental representation, or characters in fundamental representations, in SU(N), one can show the formulas

$$\begin{aligned} V_p \otimes V_q &= V_{(\Lambda_p+\Lambda_q)} + V_{\Lambda_{p-1}} \otimes V_{\Lambda_{q+1}}, && \text{for } p \leq q, \\ \chi_p \chi_q &= \chi_{(\Lambda_p+\Lambda_q)} + \chi_{\Lambda_{p-1}} \chi_{\Lambda_{q+1}}, && \text{for } p \leq q. \end{aligned} \tag{2.47}$$

where Λ_p is the Dynkin label of the p-th fundamental representation.

The Dimension D of a representation of SU(N), which is of rank $r = N - 1$, given by the Dynkin label $(\Lambda_1, \dots, \Lambda_r)$ can be calculated via

$$D(\Lambda_1, \dots, \Lambda_{N-1}) = \prod_{k=1}^{N-1} \left[\prod_{i=1}^{N-k} \left(1 + \frac{\sum_{j=i}^{i+k-1} \lambda_j}{k} \right) \right]. \tag{2.48}$$

Using those formulas we see that

$$(1, 0, \dots, 0) \otimes (0, \dots, 0, 1) = (1, 0, \dots, 0, 1) + (0, \dots, 0), \tag{2.49}$$

$$[N] \otimes [\bar{N}] = [N^2 - 1] + [0] \tag{2.50}$$

Hence the product of the first fundamental (defining) and the anti-fundamental representation, yields one of dimension $N^2 - 1$, which is the adjoint representation and a 0-dimensional representation, the trivial one.

The Quadratic Casimir Operator: For SU(N) we can calculate the eigenvalues of the quadratic Casimir operator (2.23) in different irreducible representations. For the p-th fundamental a fundamental representation, given by a Dynkin label with entry one at its p-th position, the Casimir eigenvalue is given by

$$c_p = \frac{N+1}{N} p(N-p). \tag{2.51}$$

Casimir eigenvalues for an irreducible representation whose Dynkin vector is obtained by adding two Dynkin vectors of fundamental representations, i.e. representations that are obtain from a product of two fundamental ones, then can be obtained by

$$c_{(\Lambda_p+\Lambda_q)} = c_p + c_q + 2\left(\min(p,q) - \frac{pq}{N}\right). \tag{2.52}$$

Reduced Haar measure: A parametrization of the maximal abelian torus in terms of

$$D = \begin{bmatrix} \exp(i\phi_1) & & & \\ & \ldots, & & \\ & & \exp(i\phi_{N-1}), & \\ & & & \exp\left(-i\left(\sum_{i=1}^{N-1}\phi_i\right)\right) \end{bmatrix}, \tag{2.53}$$

with $\phi_i \in [0, 2\pi)$, $r = \mathrm{rank}(\mathfrak{g})$ yields for the reduced Haar measure (2.45) the form

$$d\mu_{red} = \prod_{i<j} \sin^2\left(\frac{\phi_i - \phi_j}{2}\right) \prod_i d\phi_i. \tag{2.54}$$

With this we have now introduced all group theoretical concepts needed for the derivation of effective Polyakov loop models, which we will turn our discussion to in the next chapter.

Chapter 3

Effective Polyakov Loop Models

As already mentioned in the introduction, due to the sign problem, QCD at finite density is still a challenge and one way to get further insight into the QCD phase diagram is to use effective Polyakov loops models, in which the sign problem is weak enough to be dealt with [95–100]. The deconfinement phase transition of a pure Yang-Mills theory in d dimensions is determined by the dynamics of Polyakov loops [120, 121], which already motivates an effective model with Polyakov loops as the degrees of freedom. From the arguments by Svetitsky and Yaffe [122, 123] it shares in the presence of a 2nd order phase transformation universal behavior with a spin model in $d-1$ dimensions, and therefore Polyakov-loop models are for SU(2) Yang-Mills theories especially excellent candidates of effective field theories to describe this behavior. In such effective models the Polyakov loops are viewed in the sense of Landau-Ginzburg theories, as the relevant macroscopic variables of the theory and the effective theory is then obtained by averaging over all irrelevant microscopic link variables. Hence we write for the partition function

$$Z = \int DU e^{-S[U]} = \int DUDP\, \delta(P - P[U]) e^{-S[U]} = \int DP e^{-S_{\text{eff}}[P]} \tag{3.1}$$

and obtain for the so defined effective action

$$S_{\text{eff}}[P] = -\ln \int DU\, \delta(P - P[U]) e^{-S[U]}, \tag{3.2}$$

where $P_x(U) = \prod_{t=1}^{N_t} U_0(x,t)$ is the (untraced) Polyakov loop. As we will see later, integrating out all spatial links will already yield a Boltzmann factor that depends on Polyakov loops (given in terms of the microscopic link variables of the theory) only, making it possible to just substitute the remainng products of temporal link variables by Polyakov loop variables, yielding an effective theory in terms of Polyakov loop variables and for the effective action the more simple form

$$S_{\text{eff}}[P] = -\ln \left(\int DU_i \exp(-S[U]) \right) \Big|_{P=P[U]} . \tag{3.3}$$

Effective Polyakov loop models can be derived from the underlying full theory in different ways, either weak coupling methods or strong-coupling expansions are applicable, leaving out a direct derivation in the intermediate area of the deconfinement phase transition. Using the strong coupling expansion, which is inherent to lattice formulations, we can integrate out the spatial links of the lattice and calculate the effective action given by eq. (3.3). The strong coupling expansion is known to have a finite range of convergence and yielding good results until close to the phase transition. Polyakov loop models derived in this region reproduce some observables of the underlying Yang-Mills theory, like the expectation value of the Polyakov loop itself, already in leading order quite well . Other observables, such as Polyakov loop correlators and local Polyakov loop distributions, can be improved by including terms of higher order. Unfortunately, however, with increasing temperature the strong-coupling expansion eventually breaks down as non-local terms in the effective action become of increasing significance. In particular, local Polyakov-loop models typically fail to describe the full Yang-Mills theory when the temperature approaches the phase transition and one is therefore left with non-local Polyakov-loop models whose effective couplings need to be mapped to the full theory in other ways.

Given an ansatz for a non-local effective theory, inverse Monte Carlo methods will provide us with numerical ways of mapping the coupling of the full Yang-Mills theory to the effective coupling. As the aim of this work is to investigate different models, especially how to improve local models in a systematic way in order to hopefully converge to the full theory even around the phase transition, we will discuss in this chapter the various forms and ansatzes of the models we will use. It will be still worthwhile to motivate those ansatzes by a derivation via the strong coupling expansion (even though the couplings one would obtain in this way are expected to not yield the best results), as we want to improve models that hold in the strong coupling regime and possibly extend reliability to a larger region. Moreover the strong coupling expansion will reveal the general form of terms that can occur in such effective models and it will give us a guideline how to systematically add terms to our ansatz in order to obtain gradual improvements. However we will use the order, as obtained by the strong coupling expansion, only as a general guideline, as it is clear that with increasing coupling constant the relevant order of the terms should increasingly change.

In the next section we will therefore first derive effective Polyakov loops model from the strong coupling expansion for SU(N) theories in order to show the general form of non-local effective models, before we turn explicitly to the case of SU(2) in the rest of the chapter. There we will motivate different non-local ansatzes for effective models and also introduce a semi-analytical non-local model proposed by Greensite and Langfeld [124, 125], who already suggested a partially analytical mapping of the Yang-Mills coupling onto the effective couplings of non-local Polyakov loops models.

3.1 SU(N) Polyakov Loop Models from Strong Coupling Expansion

We will now show how SU(N) effective Polyakov loop models can be derived from strong coupling expansion as shown in [126, 127]. For details of the strong coupling expansion and the graphical interpretation of the arising terms we refer to [128–131]. Since we will later map the coupling constants of the full Yang-Mills theory onto the effective couplings of our models numerically via inverse Monte Carlo methods, we will drop here the explicit discussion of irrelevant factors in front of the Polyakov loop terms and be only interested in the form of the terms themselves.

In order to do the integration given in eq. (3.3), we can re-write the link depended part of Boltzmann factor of the Wilson action (1.25) as a product over all plaquettes and apply for small values of β the strong coupling expansion

$$\exp(-S(U)) = \prod_p \exp(-\beta S_p[\chi(U_p)]) = \prod_p \left(\sum_k \beta^k \frac{(\chi + \bar{\chi})^k(U_p)}{k!} \right), \tag{3.4}$$

(where $\chi(U_p)$ denotes the character of a plaquette U_p in the defining representation) to evaluate the integral order by order. However this leads to an integration over products of characters with arbitrary large powers per plaquette. In order simplify the occurring integrals over spatial links by avoiding higher powers, we can apply an character expansion,

$$\exp(-\beta S_p) = \left(\sum_R a_R(\beta) \chi_R(U_p) \right) \quad \text{with } a_R(\beta) = \int dU \exp(-\beta S_p) \bar{\chi}_R(U_p), \tag{3.5}$$

instead, where the factors $a_R(\beta)$ themselves contain the exponential function, hence contain arbitrary large powers of β, and can be expanded to

$$\exp(-\beta S_p) = \sum_{k=0}^{\infty} \beta^k \left(\sum_{R \in \text{Irrep}(k)} a_{R,k} \chi_R[U_p] \right), \tag{3.6}$$

where the second sum runs over all representation in Irrep(k), the set of all irreducible representations that occur in a reduction of the tensor product $([N] + [\bar{N}])^k$ (which can be easily seen by applying the strong couplings expansion first and then applying the character expansion to (3.4)). Since for the representations $R \in \text{Irrep}(k)$ the relation $|R| \leq k$ holds, a representation R can arise to infinite many powers k with $k \geq |R|$ but not in the powers $k < |R|$. Hence

$$a_R(\beta) = \sum_{k:(R \in \text{Irrep}(k))} \beta^k a_{R,k} = \sum_{k \geq |R|} \beta^k a_{R,k} = \mathcal{O}(\beta^{|R|}). \tag{3.7}$$

For SU(2) for example $R \in \mathrm{Irrep}(|R| + 2k)$ for every $k \in \mathbb{N}_0$, hence $a_R(\beta) = \sum_{k=0}^{\infty} \beta^{|R|+2k} a_{R,|R|+2k}$. With this we can write the overall Boltzmann factor, including the product over all plaquettes as

$$\begin{aligned} \exp(-S) &= \prod_p \left(\sum_R a_R(\beta) \chi_R(U_p) \right) = \prod_p \left(1 + \sum_{R \neq 0} a_R(\beta) \chi_R(U_p) \right), \\ a_R(\beta) &= \sum_{k(R \in \mathrm{Irrep}(k))} \beta^k a_{R,k} = \mathcal{O}(\beta^{|R|}), \end{aligned} \tag{3.8}$$

which we can interpret in a graphical way as a (possibly disconnected) surface composed by different plaquette surfaces, in possibly different representations. According to (3.3) the effective action

$$\exp(-S_{\mathrm{eff}}[P]) = \int DU_i \prod_p \left[1 + \sum_{R \neq 0} a_R(\beta) \chi_R(U_p) \right], \tag{3.9}$$

is obtained by integrating over all spatial links, for which we will have to calculate integrals of the form

$$\int DU \chi_{r_1}(UV_1) \cdots \chi_{r_n}(UV_n) \tag{3.10}$$

occuring from n plaquettes $U_n = UV_n$ intersecting in a common spatial link U. Such integrals can be in general caluclated by reducing products of character functions to a sums of irreducible representations, to see each integral will only not vanish if the trival representation is occurs in the sum (see [128]). For SU(2) 2 and 3 intersecting plaquettes can yield a non-vanishing contribution if they are for example of the form

$$\begin{aligned} &[2] \times [2] = [3] + [1], \\ &[2] \times [2] \times [3] = [5] + [3] + [3] + [1]. \end{aligned} \tag{3.11}$$

For the integration of a spatial link, where (at most) two plaquettes intersect, and other thereby emerging integrals we will make use of the integration rules

$$\int DU \chi_r(XU) \chi_s(U^{-1}Y) = \delta_{rs} d_r^{-1} \chi_r(XY), \tag{3.12}$$

$$\int DU \chi_r(UXU^{\dagger}Y) = d_r^{-1} \chi_r(X) \chi_r(Y), \tag{3.13}$$

where d_r is the dimension of the representation r.

From (3.12) it is (with $s = 0$) clear that terms that do not vanish in the integral cannot have spatial links that are occupied only once, hence cannot have a spatial boundary. Examples for contributing surfaces are given by the closed surface of an elementary (smallest possible) cube or an elementary ladder, a surfaces of N_t plaquettes, which are placed next to each other in timelike direction, such that the surfaces wraps around the lattice. Other possibilities of contributing surfaces can be build by putting elementary surfaces together in different ways. They might be disconnected, share only a common lattice point, a common link or be attached to each other in a common plaquette. In the last case the shared plaquette of course only arises once and one needs to check that it comes in an appropriate representation, such that the the resulting surface will still contribute. For SU(2) and elementary surfaces in the fundamental representation for example, the common plaquette of the resulting surfaces shown in Fig. 3.1 can according to (3.11) be either in the adjoint or in the trivial representation (i.e. be removed completely).

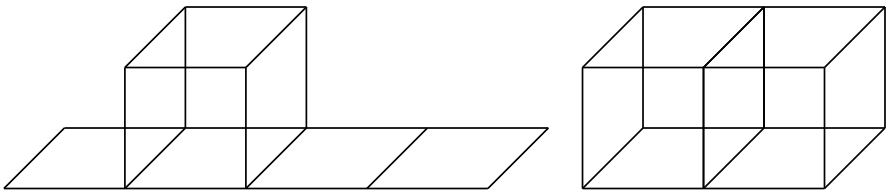

Figure 3.1: Ladder with cube attached (left), double cube (right)

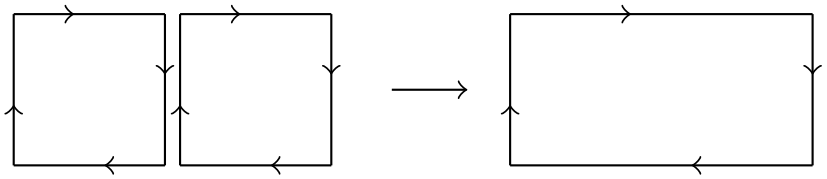

Figure 3.2: Graphical interpretation of the integration rule 3.12

In order to perform the integration over to spatial links of such contributing surfaces we can interpret eq. (3.12) in a graphical way as shown in Fig. 3.2. Integrating over a common link of two character functions of two equally oriented neighboring plaquettes will make the two associated surfaces join into one, which represents the joining of two character function into one. The argument of the character function is then the boundary of the new surfaces with its orientation inherited directly from the arguments of the former character functions (i.e. surfaces) that were joined.

Applying this graphical integration rule successively, one can join more and more plaquettes that are seperated by a spatial links, until we have joined all connected[1] plaquettes into a single surface (i.e. a single character function) and have thereby exhausted the integration rule (3.12), which then cannot be used for the integration of remaining link variables anymore.

Figure 3.3: Elementary ladder (left) and elementary cube (right) after integration of spatial links

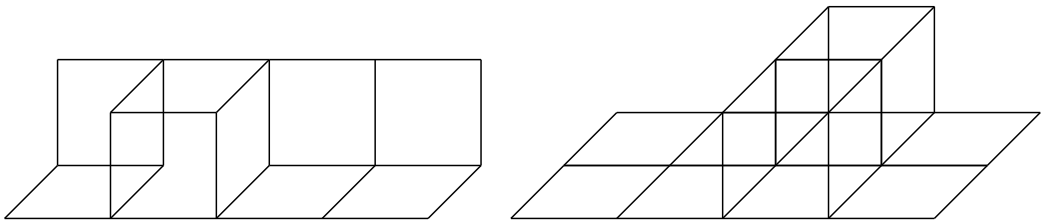

Figure 3.4: Surfaces yielding an interaction term between Polyakov loops at diagonal distance $\sqrt{2}a$ and straight distance $2a$

For the elementary cube and elementary ladders the intermediate results (which is trivial for the elementary ladder and in the case of the cube graphically dervied in the appendix B.1) are shown in Fig. 3.3, which correspond to terms of the form

$$S_{\text{cube}} = \chi_r \left(\left(\prod_i U_i \right) \left(\prod_i U_i \right)^{-1} \right) = \chi_r(\mathbb{1}) = const., \tag{3.14}$$

$$S_{\text{ladder}} = \chi_r(U P_i U^\dagger P_{i+1}^\dagger). \tag{3.15}$$

We see that elementary cubes, and similarly other closed surfaces, can contribute, even after performing the remaining spatial integrations, only constant terms to the

[1]Note that from now on, whenever we speak of connected surfaces we will implicitly mean connected via spatial links. Since we integrate only over spatial links, the integration over surfaces that are connected only via timelike link variables will decompose just like for disconnected surfaces. Hence for our purposes we will refer to both cases as disconnected.

effective action. For the elementary ladder the remaining integrals will narrow down to an integral over the spatial link on the left and on the right end of the ladder (seemingly two links identified with each other by periodicity of the lattice). By applying rule (3.13) this will yield an interaction term between two Polyakov loops of the form

$$\int DU\ \chi_r(UP_iU^\dagger P_{i+1}^\dagger) \sim \chi_r(P_i)\bar{\chi}_r(P_{i+1}). \tag{3.16}$$

It can be easily checked that doing the same for other surfaces that wrap around the lattice in temporal direction, such as shown in Fig. 3.1 (left), will in the same way also yield interaction terms between Polyakov loops. Wider connected surfaces, such as shown in Fig. 3.4, will yield interaction terms between Polyakov loops at larger distances. (Note the extra decorations with additional spatial plaquettes in Fig. 3.4 connecting the otherwise disconnect elementary ladders, yielding one interaction pair at larger distances instead of a product of two neighboring interaction terms. We have shown in appendix B.2 and B.3 that for two elementary ladders without additional spatial decorations each of the ladders independently leads to an Polyakov interaction pair just like two completely unconnected surfaces, whereas spatial connection between the two elementary ladders yields one connected interaction term at larger distances). Taking into account that contributing terms in the integral (3.9) can consist of multiple disconnected components, each yielding interaction terms between Polyakov loops, the effective Boltzmann factor takes the form

$$\begin{aligned}\exp(-S_{\text{eff}}) = c(\beta) + \sum_r \sum_{R_1,\ldots,R_r} \sum_{<x_i,y_i>} c^{R_1,\ldots,R_r}_{x_1,y_1,\ldots,x_r,y_r}(\beta) \prod_i^r S^{R_i}_{x_i,y_i} \\ \text{with } S^R_{x,y} = \chi_R(P_x)\bar{\chi}_R(P_y) + c.c.,\ <xy>^2 \in \mathbb{N},\end{aligned} \tag{3.17}$$

where $< x, y >$ is the lattice distance between the lattice sites x,y and the products consist strictly of disconnected components.

Now we can naively determine the content of the effective action by simply applying the logarithm to the Boltzmann factor in the form above and then expanding it. This would lead to higher powers of the terms above, yielding a fairly complicated form for the effective action, involving arbitrary combinations of disconnected interaction pairs between Polyakov loops, which are themselves of arbitrary power, i.e. winding number. However one can suspect that the effective action should only be a sum of connected terms, and that disconnected products in the Boltzmann factor arise only due to taking the exponential of the sum. If this is true then disconnected terms of the same form, arising at different powers in the logarithmic expansion, should cancel each other due to the alternating sign in the logarithmic expansion. This suspicion is supported by the argument that the free energy

$$F = -\frac{1}{V}\log(Z), \tag{3.18}$$

and therefore also

$$F^* = -\frac{1}{V_{d-1}} \log\left(\int DU_i \exp(S)\right) = \frac{S_{\text{eff}}}{V_{d-1}} \tag{3.19}$$

should exist in the thermodynamical limit $V \to \infty$. Therefore the effective action itself should grow linearly with the spatial volume V_{d-1}. One can show that precisely terms with disconnected components occur with a multiplicity proportional to higher powers of V_{d-1}. This can be seen by noticing that rotating or translating a term's disconnected components separately on the lattice will not change its contribution to the effective action. Hence terms obtained from each other by rotating and translating their disconnected components independently can be grouped together. Now the number of possible ways to arrange each disconnected term on the lattice is proportional to the number of lattice points, hence V_{d-1}. Therefore the multiplicity, with which the different kind of terms on the lattice occur, is proportional to V_{d-1}^q, where q is the number of disconnected components. Hence only connected components should arise in the effective action[2]. Using this result, we can just expand the logarithm and drop contributions coming from terms with multiple disconnected parts to see that the effective action will be of the form

$$\begin{aligned} S_{\text{eff}} &= c(\beta) + \sum_r \sum_{R_1,\ldots,R_r} \sum_{<x,y>} C_{x,y}^{R_1,\ldots,R_r}(\beta) \prod_i^r S_{x,y}^{R_i} \\ \text{with } S_{x,y}^R &= \chi_R(P_x)\bar{\chi}_R(P_y) + c.c., \ <xy>^2 \in \mathbb{N}. \end{aligned} \tag{3.20}$$

where the occurring product is now connected and therefore there the factors in the product all come with the same lattice indices x, y. Every interaction term in the representation R contributes a factor $a_R(\beta)^n$ to the overall constant $C_{x,y}^{R_1,\ldots,R_n}(\beta)$, where n is the number of plaquettes the interaction term is obtained from. Note that this number is not unique, as different surfaces yield the same interaction term and one can decorate a surface with additional spatial plaquettes without changing its contribution to the effective action. However for nearest neighbor interaction it is clear that the minimum number of plaquettes for a interaction pair is N_t. Hence every term that is of a new form will first arise to an order pN_t. Therefore we can take into account the contribution of all different type of terms by increasing the order in β by multiple powers pN_t and take into account all terms of the form

$$S_{x,y}^{R_1} \cdots S_{x,y}^{R_r}, \qquad \text{with } \sum_{i=1}^r |R_i| = p \tag{3.21}$$

with the overall coupling $a_{R_1}(\beta)^{N_t} \ldots a_{R_r}(\beta)^{N_t}$. Surfaces that consist of plaquettes that are not multiples of N_t then contribute to a sub-order which can be taken into account

[2]In fact using the "moments and cumulants method" one can show (see [128]) that when taking the logarithm disconnected surfaces will not contribute anymore ensuring the existence of F^* and the free energy in the thermodynamical limit.

afterwards by calculating their contributing corrections to the former couplings. For non-local interactions the situation is more complicated, since some terms' leading order is not a multiple of pNt. Examples of such surfaces are shown in Fig. 3.4, whose leading order contributions are of the orders $\beta^{2\,N_t+2}$ and $\beta^{2\,N_t+6}$. We therefore cannot keep track of all terms in correct order, if we just look at orders of the form β^{pN_t}. We will talk about this more in the explicit discussion of SU(2).

Now the occurrence of interaction terms of higher winding number in addition to those of higher representation is somewhat redundant, since higher winding numbers can be reduced. In a strictly analytical treatment within the strong coupling expansion it makes sense to keep both, the higher representations and the higher winding numbers, since the latter will emerge at higher order of β. Within the IMC method we can not really make a difference between terms according to their order, since the couplings will still have to be determined, but only by the form of the terms themselves. It therefore makes sense to further reduce terms of higher winding number and we can write the effective action (see [102, 103]) in the form

$$-S_{\text{eff}} = \sum_{P,Q} \sum_{x,y} \lambda_{P,Q}(\beta)(\chi_{P,x}\chi_{Q,y} + c.c.), \tag{3.22}$$

where sum then runs over pairs of Dynkin labels P, Q such that $\chi_P\chi_Q$ contains the trivial representation. For SU(2) with labels $P = (p)$, $Q = (q)$ this is given by $p = q \bmod 2$, whereas for SU(3) with $P = (p_1, p_2)$, $Q = (q_1, q_2)$ we have $p_1 + q_1 = p_2 + q_2 \bmod 3$. This ansatz, with all couplings treated as independent parameters, can be derived entirely by arguments using center symmetry [132], and does not necessarily rely on an a derivation via the strong coupling expansion. However a derivation from the strong coupling expansion can provide an ordering scheme to progressively add terms.

Note that in this form, due to the reduction of higher winding numbers, which leads to interaction pairs of mixed representation and due to the regrouping of higher and lower order terms of the same form, it is in general difficult to keep track of all terms contributing to a main order of the form pN_t. However for SU(2) we will be able to write down the general form for all terms that first occur to any given main order quite easily. We will show this in the next section.

3.2 Explicit Nearest Neighbor Form for SU(2)

As we have seen, the representations of interaction terms contribute to the order in β just like their distance (or rather the number of plaquettes involved to span the distance). Also have we mentioned that sub-orders can arise, due to additional spatial plaquettes that an elementary ladder (or other surfaces) can be decorated with. This makes it fairly complicated to write down non-local models, where all terms to an certain order in β are added simultaneously. If one for example takes into account large distances, one has to consider smaller representations for those distances, than for the short distances, so that

the overall order in β is the same. However such complicated expressions are beyond feasible and might not be necessary, since in the strong coupling limit we do not have to add many terms to the effective model in order to obtain good results, and in the area of interest, where the phase transition occurs, the order provided by the strong coupling expansion is not reliable in the first place. Gradually adding terms to the leading order contribution while sticking strictly to the order given by the strong coupling expansion might be unnecessarily complicated. In order to obtain a more simple systematic way of improving models, instead of adding all terms that belong to the same order in β simultaneously, which are hard to keep track of (especially when taking non-local terms into account), we will take look at the terms occurring at a certain order of β, when taking nearest neighbor interactions into account only. Interaction terms of higher winding number will thereby be reduced, as discussed in the last section, and grouped together with lower order terms of the same form. Having obtained a certain order for nearest neighbor interaction terms, we then increase the interaction distances for all interaction terms, without being concerned about the additional contribution of terms to the order in β coming from the increased interaction distance. I.e. we make our models non-local by ordering all terms only by the order in β of their nearest neighbor analogs.

Considering only nearest-neighbor interaction terms for now, we can derive the $SU(2)$ effective action easily. As we discussed in the previous sections, in order too obtain interaction terms at larger distances, one has to put elementary ladders together and connect them with additional spatial plaquettes. Therefore neglecting spatial plaquettes in eq. (3.9), we immediately arrive at an effective action only containing nearest neighbor interactions, which can be written (see [128, 133]) as

$$-S_{\text{eff}} = \sum_{<x,y>} \ln\left[1 + \sum_{p_1}^{\infty} \kappa_p \chi_p(P_x)\chi_p(P_y)\right], \quad \kappa_p(\beta) = a_p(\beta)^{N_t} = -\left[\frac{I_{p+1}(\beta)}{I_1(\beta)}\right]^{N_t}. \tag{3.23}$$

Expanding and ordering the terms occurring in the effective action (as shown in [103]) by the power of β to which they arise (which is now strictly an integer multiple of N_t, since no sub-orders occur due to the lack of spatial plaquettes), we can write the action $-S_{\text{eff}}$ as a sum of the terms

$$\begin{aligned} S_1 &= \sum_{<x,y>} \kappa_1 \chi_{1,x}\chi_{1,y}, \\ S_2 &= \sum_{<x,y>} (\kappa_2 \chi_{2,x}\chi_{2,y} - \frac{1}{2}\kappa_1^2 \chi_{1,x}^2 \chi_{1,y}^2), \\ S_3 &= \sum_{<x,y>} (\kappa_3 \chi_{3,x}\chi_{3,y} - \kappa_1\kappa_2 \chi_{1,x}\chi_{1,y}\chi_{2,x}\chi_{2,y} + \frac{1}{3}\kappa_1^3 \chi_{1,x}^3 \chi_{1,y}^3), \\ &..., \end{aligned} \tag{3.24}$$

where $S_p \sim \beta^{pN_t}$. We can see that, in agreement with our previous statement, the terms in S_p proportional to $\beta^{p \cdot N_t}$ are given by all products of interaction pairs $\chi_{r_i,x_i}\chi_{r_i,y_i}$ such

that $\sum_i r_i = p$. Reduction of all terms of higher winding number leads to the form

$$\begin{aligned} S_1 &= \sum_{<x,y>} \lambda_{11}^{(1)} \chi_{1,x}\chi_{1,y}, \\ S_2 &= \sum_{<x,y>} \lambda_{22}^{(2)} \chi_{2,x}\chi_{2,y} + 2d \sum_x \lambda_{20}^{(2)} \chi_{2,x}, \\ S_3 &= \sum_{<x,y>} \left[\lambda_{11}^{(3)} \chi_{1,x}\chi_{1,y} + \lambda_{33}^{(3)} \chi_{3,x}\chi_{3,y} + \lambda_{13}^{(3)} (\chi_{1,x}\chi_{3,y} + \chi_{3,x}\chi_{1,y}) \right], \\ &\ldots \end{aligned} \tag{3.25}$$

with

$$\begin{aligned} \lambda_{11}^{(1)} &= \kappa_1 & \lambda_{11}^{(3)} &= -\kappa_1\kappa_2 + \frac{4}{3}\kappa_1^3, \\ \lambda_{22}^{(2)} &= \kappa_2 - \frac{1}{2}\kappa_1^2, & \lambda_{20}^{(2)} &= -\frac{1}{2}\kappa_1^2, \\ \lambda_{33}^{(3)} &= \kappa_3 - \kappa_1\kappa_2 + \frac{1}{3}\kappa_1^3, & & \\ \lambda_{13}^{(3)} &= -\kappa_1\kappa_2 + \frac{2}{3}\kappa_1^3. & & \end{aligned} \tag{3.26}$$

We see that terms of the same form will occur to different order and grouping them together we can write the action as a sum of the terms

$$\begin{aligned} \tilde{S}_1 &= \sum_{<x,y>} \lambda_{11} \chi_{1,x}\chi_{1,y}, \\ \tilde{S}_2 &= \sum_{<x,y>} \lambda_{22} \chi_{2,x}\chi_{2,y} + \sum_x \lambda_{20} \chi_{2,x}, \\ \tilde{S}_3 &= \sum_{<x,y>} \left[\lambda_{33} \chi_{3,x}\chi_{3,y} + \lambda_{13} (\chi_{1,x}\chi_{3,y} + \chi_{3,x}\chi_{1,y}) \right], \\ &\ldots \end{aligned} \tag{3.27}$$

with $\lambda_{pq} = \lambda_{pq}^{(max(p,q))} + \lambda_{pq}^{(max(p,q)+2)} + \lambda_{pq}^{(max(p,q)+4)} + \ldots$.

This provides us with an ordering scheme in β for the ansatz (3.22), which is meaningful for the IMC method, since terms of the same form are grouped together.

3.3 Extended Linear Polyakov Models for SU(2)

Now we are ready to take the former results in order to write an ansatz for our first non-local linear Polyakov loop model (where linear refers to the linear dependence on the coupling constants). Taking the local action given by (3.27) we can write it in general form as

$$S = \sum_{p=1}^{p_{\max}} \tilde{S}_p, \qquad \tilde{S}_p \quad = \sum_{q \in \{p, p-2, \dots p\%2\}} \sum_{<x,y>=1} \lambda_{pq} (\chi_{p,x}\chi_{q,y} + \chi_{q,x}\chi_{p,y}) \tag{3.28}$$

and then extending it to a non-local version, where we take the same form for all terms, no matter at which distance and sum over all possible distances in lattice unit, hence we obtain the form

$$\boxed{S_{\text{xlin}} = \sum_{r^2=1}^{r_{\max}} \sum_{p=1}^{p_{\max}} \tilde{S}_{p,r}, \qquad \tilde{S}_{p,r} = \sum_{q \in \{p, p-2, \dots p\%2\}} \sum_{<x,y>=r} \lambda_{pq,r^2} (\chi_{p,x}\chi_{q,y} + \chi_{q,x}\chi_{p,y}).} \tag{3.29}$$

This will be our first class of non-local Polyakov loop models, which we will refer to as *full linear* or *extended linear* Polyakov loop model, since in principle it contains all terms one can possible get by sending $p_{\max}, r_{\max} \to \infty$. Later on we will investigate the cases where $p_{\max} = 1, 2, 3$.

3.4 Simple Linear Polyakov Models for SU(2)

As we already mentioned, the order given by the strong coupling expansion is only meant as a rough guideline for improving the leading order contribution, but not meant too strictly as it is not reliable in the region of the phase transition. Therefore it is not clear if all terms to a given index p in the previous form of the action (3.29) are still of the same relevance and we might simplify this model, which will be complicated enough provided that we will go to large distances $r_{\max}$, by only taking parts of the terms to the same order p into account. Furthermore in the previous form of the action (3.29) or in general (3.27), we expanded all function and reduced terms of higher winding numbers completely. The IMC method will treat each of those couplings as an independent parameter, thereby neglecting all relations between those couplings, which occur when expanding the logarithm and hold in the strong coupling limit. This is on the one hand an advantage, since the relationships given by the strong coupling expansion are expected to not hold near the phase transition, where we mainly want to improve our models. Neglecting the constraints will give the model more freedom to reproduce the results of the full Yang-Mill theory as well as possible. However it is known that too much freedom can affect the performance of the IMC method negatively (see [102]). Strictly speaking this was shown for SU(3), where the IMC method is very sensitive to the number of coupling constants and one can see such an effect already when taking into account just a few coupling constants. However our models for SU(2) will include

a large number of coupling constants, far beyond common calculations and we cannot exclude the occurrence of a similar effect at a number of degrees of freedom that large. Therefore it might be useful to simplify the model (3.29) and reduce the number of coupling constants. A straight forward simplification is to not take into account terms that arise only from terms with higher winding number, i.e. the interaction terms with mixed representations. For such a simplification the model is then given by

$$\boxed{S_{\text{lin}} = \sum_{r^2=1}^{r_{\max}} \sum_{p=1}^{p_{\max}} \tilde{S}_{p,r}, \quad \tilde{S}_{p,r} = \sum_{<i,j>=r} \lambda_{pp,r^2} \chi_{p,i} \chi_{p,j},} \tag{3.30}$$

which leads to another class of linear non-local models, which we refer to as the *simple linear* Polyakov-loop models. A simplification by neglecting Polyakov loops with multiple winding number can also be interesting, since the next model we will discuss somewhat prioritizes the effect of higher winding numbers by summing them up into a logarithmic form, before taking into account contributions from higher representations or larger distances. This simplification is therefore in a way complementary to the prioritizing of larger winding numbers in the next model.

Note that if p is even in the model above, then the sum over q will include 0, hence the trivial representation with $\chi_0(U) = 1$ for all $g \in G$. Hence the interaction pairs proportional to λ_{p0,r^2} do not really dependent on the second Polyakov loop in the trivial representation and therefore not on the distance and we will summarize all terms of the same form in the coupling constant $\lambda_{p0,0}$, leaving us for this kind of interaction terms with the introduction of only 1 coupling constant, which does not depend on the distance. This situations occurs for $p = 2$, where

$$\sum_{r^2} \sum_{<i,j>=r} \lambda_{20,r^2} \chi_{p,i} \chi_{0,i} = \lambda_{20,0} \sum_i \chi_{2,i} \tag{3.31}$$

introduces a potential term $\chi_{2,i} = \chi_{1,i}^2 - 1$ into the action.

3.5 Logarithmic Resummation for SU(2)

In the previous section we have improved the local Polyakov loop leading order term

$$\lambda_1 S_1 = u^{N_t} \sum_{<ij>} \chi_{1,i} \chi_{1,j}, \tag{3.32}$$

of the effective action $S = \lambda_1 S_1 + \lambda_2 S_2 + \ldots$, where $u = a_1(\beta)$ as defined in (3.23), by first adding higher representations that arise directly due to the character expansion involved, but also from reduction of terms with higher winding numbers that occur due to the expansion of the logarithm, and then by increasing the interaction distance of such terms, making the model non-local. Another way to improve the local model (as shown in [130, 131]) is, instead of reducing terms of higher winding number and grouping all

similar terms together, to do a resummation of terms of higher winding number. Hereby one also takes into account the contribution that come from decorations of elementary ladders with additional spatial plaquettes, which have been initially neglected, in order to get an improved local action, which we can then again extend to a non-local version.

Let us first discuss the resummation of the elementary ladder and higher order graphs which arise from its decoration with spatial plaquettes. In Fig. 3.5, 3.6 we can see two of such surfaces resulting in the same nearest neighbor interaction pair $\chi_{1,i}\chi_{1,i+1}$, but of higher sub-orders β^{N_t+4} and β^{N_t+8}. Hence the form of the resulting terms will be the same, only their contribution to the effective coupling will be different.

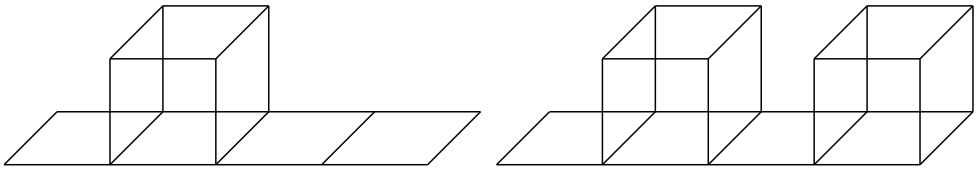

Figure 3.5: Elementary ladder with decorations leading to an order in β proportional to $\sim (N_t + k)$, $k = 4$ (left), $k = 8$ (right)

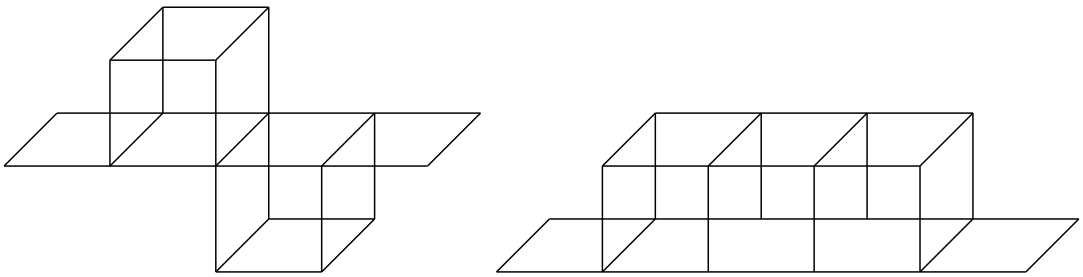

Figure 3.6: Elementary ladder with decorations leading to an order in β proportional to $\sim (N_t + 8)$

Following the calculations in [130, 131] we can calculate explicitly the contributions to the effective action of the sub-order surfaces given shown in Fig. 3.5 and Fig. 3.6 (left) which are given by

$$\phi_1 = u^{N_t}[4N_t u^4]S_1, \tag{3.33}$$

$$\phi_2 = u^{N_t}\left[\frac{1}{2!}(4N_t u^4)4(N_t - 3)u^4\right]S_1, \tag{3.34}$$

$$\phi_1 = u^{N_t}[4N_t u^4 3N_t u^4]S_1, \tag{3.35}$$

where the powers of u in the square brackets arise due to the additional plaquettes of which each contributes a factor u and the additional factors take into account the combinatoric multiplicity of such decorations. The factors N_t takes into account the number of different positions where a cubic decoration can be placed onto the elementary ladder (hence the factor $N_t - 3$ instead of N_t in ϕ_2, taking into account the 3 unavailable positions for the second cubic decoration). The factor 4 in front of N_t takes into account the number of spatial directions one can direct a cubic decoration. Note that the factor 3 instead of 4 in front of the 2nd cubic decoration in ϕ_3 again arises due to the fact that one has to subtract one direction, which would lead to a double cube decoration, belonging to another class of surfaces.

Neglecting higher order terms, we can then write the sum of the decorated elementary ladders as

$$\phi_1 + \phi_2 + \phi_3 = u^{N_t} exp[N_t(4u^4 - 12u^8)]S_1, \tag{3.36}$$

where of course the polynomial in the exponent reflects only a partial resummation of higher order terms. For example there are, as already mentioned, double cube decorations of order u^6 or triple cube decorations of order u^8 (Fig. 3.6 (right)), which are not included. However similar calculations have also been presented in [130, 131] up to the order u^{10}, which yield for $\lambda_1(u, N_t)$

$$\lambda_1(u,2) = u^2 \exp\left[2(4u^4 - 8u^6 + \frac{134}{3}u^8 - \frac{49044}{405}u^{10}\right], \tag{3.37}$$

$$\lambda_1(u,3) = u^3 \exp\left[3(4u^4 - 4u^6 + \frac{128}{3}u^8 - \frac{36044}{405}u^{10}\right], \tag{3.38}$$

$$\lambda_1(u,4) = u^4 \exp\left[4(4u^4 - 4u^6 + \frac{140}{3}u^8 - \frac{37664}{405}u^{10}\right], \tag{3.39}$$

$$\lambda_1(u,N_t \geq 5) = u^{N_t} \exp\left[N_t(4u^4 - 4u^6 + \frac{140}{3}u^8 - \frac{36044}{405}u^{10}\right]. \tag{3.40}$$

In general the effective coupling will then be of the form

$$\lambda_1(u, N_t) = u^{N_t} exp[N_t P(u, N_t)], \tag{3.41}$$

where the polynomial $P(u, N_t)$ takes into account higher order corrections from all possible decorations. Now doing a resummation of the terms of higher winding number in (3.24) will again yield an logarithmic form

$$\sum_{<ij>} \left(\chi_{1,i}\chi_{1,j} - \frac{\lambda_1^2}{2}\chi_{1,j}^2\chi_{1,i}^2 + \frac{\lambda_1^3}{3}\chi_{1,i}^3\chi_{1,j}^3 - \dots \right) = \sum_{<ij>} \ln(1 + \lambda_1\chi_{1,i}\chi_{1,j}) \tag{3.42}$$

for the action, where the coupling $\lambda_1(u, N_t)$ is now the full effective action, with sub-order contributions by decorations taken into account (in contrast to the logarithmic action (3.23)).

3.6 Logarithmic Polyakov Models for SU(2)

Doing the same resummation for Polyakov terms in higher representations and with larger interaction distances, we can motivate another class of generalized non-local ansatzes for Polyakov models, which we will investigate later on, given by

$$\boxed{S_{\log} = \sum_{r^2=11}^{r_{\max}} \sum_{p=1}^{p_{\max}} \tilde{S}_{p,r}, \quad \tilde{S}_{p,r} = -\sum_{<i,j>=r} \ln\left(1 + g_{pp,r^2} \chi_{p,i} \chi_{p,j}\right),} \tag{3.43}$$

with coupling constants g_{pp,r^2}, which we refer to as the *logarithmic* Polyakov-loop models.

Again we will later investigate the cases $p_{\max} = 1, 2, 3$. For the action above, we can see that we run into a sign problem unless we satisfy the condition

$$0 < 1 + g_{pp,r} \chi_{p,i} \chi_{p,j} \tag{3.44}$$

and for the 3 cases mentioned we can see from

$$\left.\begin{array}{ll} \chi_1 = \chi_1 & \in [-2, 2] \\ \chi_2 = (\chi_1^2 - 1) & \in [-1, 3] \\ \chi_3 = \chi_1(\chi_1^2 - 2) & \in [-4, 4] \end{array}\right\} \Rightarrow \chi_{p,i}\chi_{p,j} \geq \begin{cases} -4, & p = 1 \\ -3, & p = 2 \\ -16, & p = 3 \end{cases} \tag{3.45}$$

that the condition is satisfied if the effective couplings satisfy the conditions

$$g_{pp,r} < \begin{cases} 1/4 = 0.25, & p = 1, \\ 1/3 \simeq 0.33, & p = 2, \\ 1/16 \simeq 0.06, & p = 3. \end{cases} \tag{3.46}$$

In the results sections of this work we will later see that this conditions are indeed satisfied for SU(2) on the full range of interest.

3.7 Semi-Analytical Polyakov loop Model from Relative Weights Method

Later on in this work we will try to make sense of the fall-off of the non-local couplings with the interaction distance, try to relate it to the correlation length of the theory and investigate the fall-off in order to determine a possibly analytical behavior. This is in hindsight of possible extensions of investigations to SU(3) gauge theories especially important, since a known analytical behavior would reduce the number of needed free parameters drastically, which the SU(3) IMC method is, as mentioned, very sensitive to. In this context we will introduce another non-local model proposed by J. Greensite and K. Langfeld [124], which is quite interesting, since it already comes with the fall-off for the non-local couplings, with respect to the interaction distance, given in analytical form. The action of this model is given by

$$\boxed{S_{\mathrm{GL}} = -\frac{1}{8}c_1 \sum_x \chi_x^2 + \frac{1}{2}c_2 \sum_{x,y} \chi_x Q(x-y)\chi_y,} \tag{3.47}$$

where the couplings c_0 and c_1 are determined numerically but the operator Q, determining the fall-off of the couplings, is given by

$$\boxed{Q(x-y) = \begin{cases} (\sqrt{-\nabla^2})_{xy}, & |x-y| \leq r_{\max}, \\ 0, & |x-y| > r_{\max}. \end{cases}} \tag{3.48}$$

Its eigenvalues can can be determined by Fourier transformation of the lattice momenta

$$(\sqrt{-\nabla^2})_{xy} = \frac{1}{L^3}\sum_k k_L \exp(i\vec{k}\cdot(\vec{x}-\vec{y})),$$
$$\text{with} \qquad k_l = \sqrt{4\sum_{i=1}^{3}\sin^2\left(\frac{1}{2}k_i\right)}, \qquad k_i = \frac{2\pi}{L}m_i, \;\; \vec{m}\in V. \tag{3.49}$$

and are depicted in Fig. 3.7.

Note the different values at certain values of r, i.e. at $r = 3$ coming from two different vectors $(3,0,0)$, $(2,2,1)$ with the same length, and the missing values for some values of r, due to the non-existence of a 3-dimensional integer vector with such a length, e.g. on a 3 dimensional lattice there is no integer vector $\vec{v}$ with $|\vec{v}|^2 = 7$.

On a $16^3 \times 4$ lattice at $\beta = 2.22$ the constants c_1 and c_2 are determined numerically in [124] and given by

$$c_1 \approx 4.417(4), \qquad c_2 \approx 0.498(1). \tag{3.50}$$

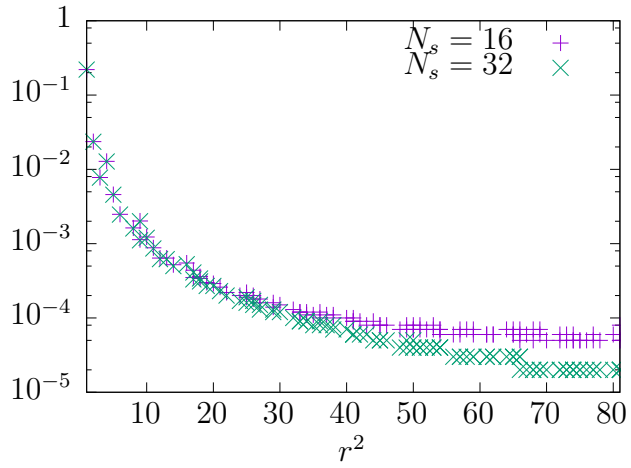

Figure 3.7: Eigenvalues of $(-\sqrt{-\nabla^2})_{r=|x-y|}$ for differnt lattices with $N_s = 16, 32$

As can be seen, ansatz (3.47) proposed by Greensite and Langefeld is quite similar to our ansatzes (3.29) and (3.30). If we set $p_{\max} = 1$ in our linear ansatzes, add an additional term $\lambda_{11,0} \sum_i \chi_{1,i}^2$ we can roughly identify the models by applying the mapping

$$\begin{aligned} &\lambda_{1,0} = -\frac{1}{8} c_1 + \frac{1}{2} c_2 \, Q(0) \\ &\text{and} \quad \lambda_{1,r^2} = c_2 \, Q(r) \\ &\text{with} \quad Q(r) \approx \frac{1}{|\{x : |x| = r\}|} \sum_{|x|=r} Q(x). \end{aligned} \tag{3.51}$$

This concludes our discussion of effective Polyakov loop models. Having derived different ansatzes for non-local effective Polyakov loop models, we will show in the next chapter how to map the full Yang-Mills theory via inverse Monte-Carlo methods onto those non-local ansatzes.

Chapter 4

Inverse Monte-Carlo Method

As already mentioned our aim is to map the coupling of the full Yang-Mills theory to different non-local Polyakov loop models in order to investigate them. In general we cannot map the couplings of the full theory to those of the effective Polyakov-loop models (3.30) and (3.43) analytically. Using the strong coupling expansion to find approximations for such mappings does not work due to the sheer number of couplings and terms involved, and even more importantly due to the breakdown of the strong coupling expansion itself in the main area of interest. Therefore we need other methods to obtain a mapping between the couplings. There are different methods available to do so, such as treating the couplings of the effective theories as independent parameters to investigate the theory and then map those couplings, via matching of different observables, back to the coupling of the full theory. Other methods, such as the inverse Monte-Carlo method (IMC) [101–103], which we will use in this work, use a more direct approach to find a mapping between the couplings. In the IMC method we first generate configurations of the full theory via Monte-Carlo methods, calculate the corresponding configurations in terms of the degrees of freedom of the effective theory, and then use the latter to determine the couplings of the effective theory in the IMC step (see Fig. 4.1).

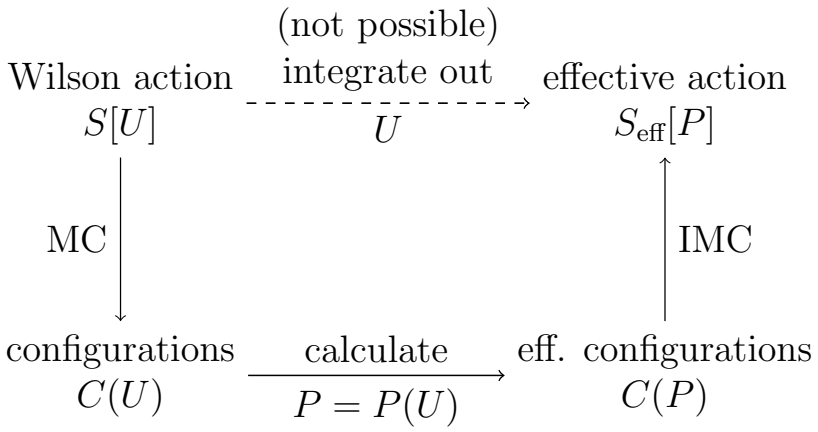

Figure 4.1: Inverse Monte-Carlo-Method

In principle the IMC step is done by taking an ansatz for an effective action $S_{\text{eff}}(\lambda)$ with yet to determine coupling constants λ. As in the derivation of Dyson-Schwinger equations (DSEs) we use that expectation values of total derivatives with respect to the fields in the effective action must vanish and require that this remains true when replacing the effective theory with the full theory for the calculation of these expectation values via, i.e.

$$0 = \left\langle \frac{\delta S_{\text{eff}}}{\delta \varphi}(\lambda) \right\rangle_{\text{eff}} \stackrel{!}{=} \left\langle \frac{\delta S_{\text{eff}}}{\delta \varphi}(\lambda) \right\rangle_{\text{full}} . \tag{4.1}$$

This requirement means that if we view the total derivative itself as an observable, its expectation value must vanish if calculated on a set of configuration of the variables of the effective theory, which are distributed with respect to the measure of the full theory, and obtained by reducing the full theory‘s variables to effective ones. The requirement implicitly determines the coupling constants of the effective theory.

4.1 Geometric Ward-Identities and DSE's

In order to apply the IMC method we first will need to derive a Dyson-Schwinger equation, which we can impose the requirement (4.1) onto. For a pure gauge theory we will have to consider derivatives and integrals with respect to the gauge field variables. Since in lattice gauge theory the gauge degrees of freedom are given in terms of link variables, which are elements of a gauge group G, in order to derive a DSE we need to consider derivatives and integrations with respect to group elements. The left invariance of the Haar measure yields for the left derivative L_a of a function f on G

$$\begin{aligned} &\int d\mu(g)(L_a f)(g) = \int d\mu(g) \frac{d}{dt} f(\exp(t \cdot T_a) g) = \frac{d}{dt} \int d\mu(g) f(\exp(t \cdot T_a) g) = \\ &\frac{d}{dt} \int d\mu(\exp(t \cdot T_a) g) f(\exp(t \cdot T_a) g) = \frac{d}{dt} \int d\mu(g)(L_a f)(g) = 0, \quad f \in L_2(G)\,, \end{aligned} \tag{4.2}$$

where $g \in G$ is a group element and T_a is the a-th generator of the algebra, which can be used to derive a DSE from geometric Ward-identities [134]. The aim hereby is to calculate the derivative in the equation above, on an appropriate choice for the function f, such that it inserts the Boltzmann factor into the integral equation and we can write it as an expectation value, leaving us with the desired DSE, which we can use for the IMC method. Since the full and effective theories can only depend on class functions of the gauge group, we want to use the equation above also in a way that only involves class functions, i.e. write a class function as a derivative of other class functions.

This is achieved by

$$\vec{L} \cdot (F\vec{L}\tilde{F}) = F\vec{L}^2\tilde{F} + \vec{L}F \cdot \vec{L}\tilde{F}. \tag{4.3}$$

For class functions F and $\tilde{F}$, the choice (4.3) is then a class function itself, which can be proven (see C.1) by first showing that $\vec{L}^2$ acts as the quadratic Casimir operator and therefore commutes with all group elements and then using the fact that invariance of the Killing metric $\mathrm{Tr}(T_aT_b)$ under the adjoint action $T_a \to h^{-1}T_ah$ implies that $h^{-1}T_ah$ can be expanded as $R_a^cT_c$ with an orthogonal matrix R, to show invariance under the adjoint action of the second term in 4.3. Inserting the function (4.3) into the identity 4.2 leaves us with an integration over the adjoint classes,

$$0 = \int d\mu_{red}\vec{L} \cdot (F\vec{L}\tilde{F}) = \int d\mu_{red}(F\vec{L}^2\tilde{F} + \vec{L}F \cdot \vec{L}\tilde{F}), \tag{4.4}$$

with the appropriate measure given by the reduced Haar measure. Making an appropriate choice of the function $\tilde{F}$, calculating the derivatives and reducing higher powers of character function will then leave us with a master equation, which we will be able to write, by insertion of the Boltzmann factor via choice of the function F, in form of an Dyson-Schwinger equation.

In the first step we set $\tilde{F} = \chi_p$, for some $p \in \{1, ..., r\}$ and then calculate the first part on the r.h.s of equation 4.4. By applying the eigenvalue equation

$$\sum_a L_a^2\chi_p(g) = -c_p\chi_p(g) \tag{4.5}$$

for the Laplacian $\vec{L}^2$, we can write the first term in the sum of 4.4 as

$$F\vec{L}^2\tilde{F} = -c_p\chi_p(g)F. \tag{4.6}$$

In the next step we then calculate the second term on the r.h.s of eq. 4.4. Using the fact that the fundamental characters χ_q, with $q \in \{1, \ldots, r = \mathrm{rank}(G)\}$, provide a basis for class functions, we can apply a character expansion

$$L_aF(\chi) = \sum_{q=1}^{r} \frac{\partial F(\chi)}{\partial \chi_q(g)} L_a\chi_q(g). \tag{4.7}$$

Reducing then all terms $\chi_\mu\chi_\nu$ to

$$\chi_\mu\chi_\nu = \sum_\lambda C_{\mu\nu}^\lambda\chi_\lambda, \tag{4.8}$$

where $C_{\mu\nu}^\lambda$ are Clebsch-Gordon coefficients and the sum runs over all irreducible representations λ, we can write

$$\sum_a L_a^2\chi_p\chi_q = \sum_a((L_a^2\chi_p)\chi_q + 2(L_a\chi_p)(L_a\chi_q) + \chi_p(L_a^2\chi_q)) = \tag{4.9}$$

$$-\sum_a(c_p + c_q)\chi_p\chi_q + \sum_a 2(L_a\chi_p)(L_a\chi_q) = -\sum_\rho C_{pq}^\rho c_\rho\chi_\rho \tag{4.10}$$

and therefore get

$$(\vec{L}\chi_p)\cdot(\vec{L}\chi_q) = \frac{1}{2}\sum_a \left[(c_p + c_q)\chi_p\chi_q - \sum_\rho C^\rho_{pq} c_\rho \chi_\rho\right], \tag{4.11}$$

and for the second term in the sum of 4.4

$$\vec{L}F \cdot \vec{L}\tilde{F} = \vec{L}F \cdot \vec{L}\tilde{\chi}_p = \sum_{q=1}^{r} \frac{\partial F(\chi)}{\partial \chi_q(g)} \vec{L}\chi_q(g) \cdot \vec{L}\chi_p(g). \tag{4.12}$$

Inserting equations 4.6 and 4.11 into equation 4.4, one derives the master equation

$$\boxed{\begin{aligned} 0 &= \int_G d\mu_{red} \left\{ \frac{1}{2}\sum_q K_{pq} \frac{\partial F(\chi)}{\partial \chi_q(g)} - c_p \chi_p(g) F \right\}, \\ K_{pq} &:= \left[(c_p + c_q)\chi_p\chi_q - \sum_\rho C^\rho_{pq} c_\rho \chi_\rho\right], \end{aligned}} \tag{4.13}$$

where C^ρ_{pq} are Clebsch-Gordon coefficients, c_ρ eigenvalues of corresponding Casimir operators, the first sum runs over all fundamental representations q and the second sum runs over all irreducible representations ρ.

One equation of the form (4.13) holds independently for every point on the $d-1$ dimensional lattice of our effective theory. Therefore, inserting a unity in terms of $\Pi = \exp(-S_{\text{eff}})$ times its inverse, one can write the lattice average of these equations in the form of expectation values. In the last step we replace the measure for these expectation values with that of the full theory,

$$V^{-1} \sum_{i\in L} \left\langle \frac{1}{2}\sum_q K_{pq,i} \frac{\partial \vec{F}_i}{\partial \chi_{q,i}} \Pi(\vec{\lambda})^{-1} - c_p\, \chi_{p,i}\, \vec{F}_i\, \Pi(\vec{\lambda})^{-1} \right\rangle_{\text{full}} = \vec{0}. \tag{4.14}$$

Moreover, we have collected sets of as yet unspecified class functions per lattice site i in large vectors $\vec{F}_i$ because their number needs to match that of the couplings in the ansatz for the effective action, i.e. $\dim(\vec{F}_i) = \dim(\vec{\lambda})$, so that the resulting system of DSEs (4.14) can be solved to determine the couplings $\vec{\lambda}$ via the IMC method.

Since the function Π usually factorizes into a product, by setting the functions $\vec{F}_i \equiv \vec{f}_i\Pi$ most of the factors Π^{-1} cancel and we obtain

$$\boxed{V^{-1} \sum_{i\in L} \left\langle \frac{1}{2}\sum_q K_{pq,i} \left(\frac{\partial \vec{f}_i}{\partial \chi_{q,i}} + \vec{f}_i \frac{\partial \ln \Pi_{q,i}(\vec{\lambda})}{\partial \chi_{q,i}} \right) - c_p\, \chi_{p,i}\, \vec{f}_i \right\rangle_{\text{full}} = \vec{0},} \tag{4.15}$$

where $\Pi_{q,i}$ denotes the factor of Π which depends on the lattice index i and the representation q.

In general this equation is of non-linear depenence of the coupling constants $\vec{\lambda}$ and solving it will require non-linear methods but in the case of a linear depenence, as for our linear Polyakov loops models, the effective action and its derivatives with respect to the characters can be written as

$$\ln \Pi(\vec{\lambda}) = \vec{S}^T \cdot \vec{\lambda}, \tag{4.16}$$

$$\frac{\partial \ln \Pi_{q,i}(\vec{\lambda})}{\partial \chi_{q,i}} = \frac{\partial \vec{S}^T_{q,i}}{\partial \chi_{q,i}} \cdot \vec{\lambda}, \tag{4.17}$$

an we get the matrix equation $\vec{\lambda} = A_p^{-1} \vec{v}_p$, with

$$\boxed{\begin{aligned} A_p &= \sum_{i \in L} \left\langle \frac{1}{2} \sum_q K_{pq,i} \left(\vec{f}_i \cdot \frac{\partial \vec{S}^T_{q,i}}{\partial \chi_{q,i}} \right) \right\rangle_{\text{full}}, \\ \vec{v}_p &= -\sum_{i \in L} \left\langle \frac{1}{2} \sum_q K_{pq,i} \left(\frac{\partial \vec{f}_i}{\partial \chi_{q,i}} \right) - c_p \, \chi_{p,i} \vec{f}_i \right\rangle_{\text{full}}, \end{aligned}} \tag{4.18}$$

which can be solved by matrix inversion.

4.2 IMC for SU(2) Polyakov-Loop Models

For the case of a SU(2) gauge theory, where we have proposed three classes of models (extended linear, simple linear and logarithmic models), we can now insert into the geometric DSE the factors Π, where $\Pi = \Pi_{\text{xlin}}$ for the extended linear model (3.29), $\Pi = \Pi_{\text{lin}}$ for the simple linear model (3.30) and $\Pi = \Pi_{\text{log}}$ for the logarithmic model (3.43) respectively. Since there is only one fundamental representation we set $p = q = 1$ and use eq. 2.51, 2.52, 2.47 to determine all Casimir eigenvalues and Clebsch-Gordon coefficients involved, which yields

$$\begin{aligned} &c_0 = 0, \;\; c_1 = 3/2, \;\; c_2 = 4, \\ &C^0_{11} = 1, \;\; C^2_{11} = 1, \end{aligned} \tag{4.19}$$

and hence

$$K_{11,i} = 3\chi^2_{1,i} - 4\chi_{3,i}. \tag{4.20}$$

By then setting the functions $\vec{F}_i \equiv \vec{f}_i \Pi$ most of the factors Π^{-1} in (4.15) cancel and it remains to make a choice for the functions $\vec{f}_i$, such that we avoid any coupling constant from only occuring in terms that contain odd powers of some Polyakov loop $\chi_{l,i}$, which would then lead to an independence of eq. (4.15) of that coupling after group integration.

A convenient choice to achieve this is given for the simple linear and logarithmic models (where only interaction terms with Polyakov loops in the same representation contribute) by

$$f_{l,d,i} = \frac{1}{\lambda_{ll,d}} \frac{\partial \ln(\Pi_{ll,d,i})}{\partial \chi_{1,i}}, \qquad \text{and} \qquad f_{l,d,i} = \frac{1}{g_{ll,d}} \frac{\partial \Pi_{ll,d,i}}{\partial \chi_{1,i}}, \tag{4.21}$$

with $(\vec{f_i})_{d+(l-1)\cdot r_{max}^2} = f_{l,d,i}$ for the quadratic distance $d \in \{1, \ldots, r_{max}^2\}$ and the representation $l \in \{1, \ldots, p_{max}\}$. $\Pi_{ll,d,i}$ now denotes the factor of the product Π with interactions between Polyakov loops only at squared distance d with one of the loops sitting at lattice point i and both in representation l.

For the extended linear model we need additional functions due to the interaction terms with mix representations, which introduce the coupling constants $\lambda_{20,0}$ (which does not depend on the distance due to the trivial representation of one of the two Polyakov loops in the interaction terms) and λ_{13,r^2}. For the additional coupling constants we introduce equally many new functions

$$f_{0,0,i} = \frac{1}{\lambda_{02,0}} \frac{\partial \ln(\Pi_{20,0,i})}{\partial \chi_{1,i}}, \qquad \text{and} \qquad f_{p_{max}+1,d,i} = \frac{1}{\lambda_{13,d}} \frac{\partial \ln(\Pi_{13,d,i})}{\partial \chi_{1,i}}, \tag{4.22}$$

With this we can now apply the IMC method to our different SU(2) Polyakov loop models.

Part II

Results and Conclusion

Chapter 5

Logarithmic vs. Linear Models

In this and the following chapters we will present our results for the effective Polyakov loop models as obtained by IMC methods. Generating the configurations of the full Yang-Mills theory has been done with a local Hybrid-Monte-Carlo (HMC) algorithm, where a number of 1000 configurations has been used in this work (unless explicitly mentioned otherwise). Via IMC we have minimized the geometric DSE (4.14) with respect to the effective coupling constants, in order to map different values of the Yang-Mills coupling constant β onto the coupling constants of different effective models. For the linear models all dependences on the coupling constants are linear and eq. (4.14) reduces to a matrix equation of expectation values which have been solved by simple matrix inversion. In the logarithmic case we solve the then non-linear eq. by applying a secant method. Doing so we have used the obtained coupling constants $\vec{\lambda}(\beta)$, to simulate different observables $\left\langle O(\vec{\lambda}(\beta)) \right\rangle_{\text{eff}} = \langle O(\beta) \rangle_{\text{eff}}$ in the effective theories, which are presented as functions of β and compared to their results $\langle O(\beta) \rangle_{\text{YM}}$ as obtained by simulations of the full theory. We want to stress that the IMC algorithm provides us with coupling constants that contain numerical errors, where we drop the error interval for simulations of the effective theories due to the computational costs. Therefore error bars in plots for the effective theories only contain statistical errors due the simulation itself but not the errors resulting from determining the effective coupling constants in the IMC method. For the simulation of the effective theories we have used the basic Metropolis algorithm. We consider effective models with different values of r^2_{max} up to 81, and p_{max} up to 3. This leads to a maximum number of independent coupling constants up to $81 \cdot 3 = 243$ for the logarithmic and simple linear model. For the extended linear model we obtain a maximum number of 325 independent coupling constants. In this chapter we will start by comparing the logarithmic model to the two different (simple and extended) linear models on a lattice with $N_t = 4$. First in the local case, with Polyakov loops only in the fundamental representation included, then we will add higher representations, before we look at the non-local case. The lattices used for this chapter are all of the size $16^3 \times 4$ unless mentioned otherwise.

5.1 Local models in fundamental representation

First we compare the linear and the logarithmic models with only nearest neighbor interactions and taking into account only fundamental Polyakov loops ($r^2_{\max} = 1$ and $p_{\max} = 1$). Note that at this level the simple and the extended linear models coincide and differences only occur for $p_{\max} \geq 2$.

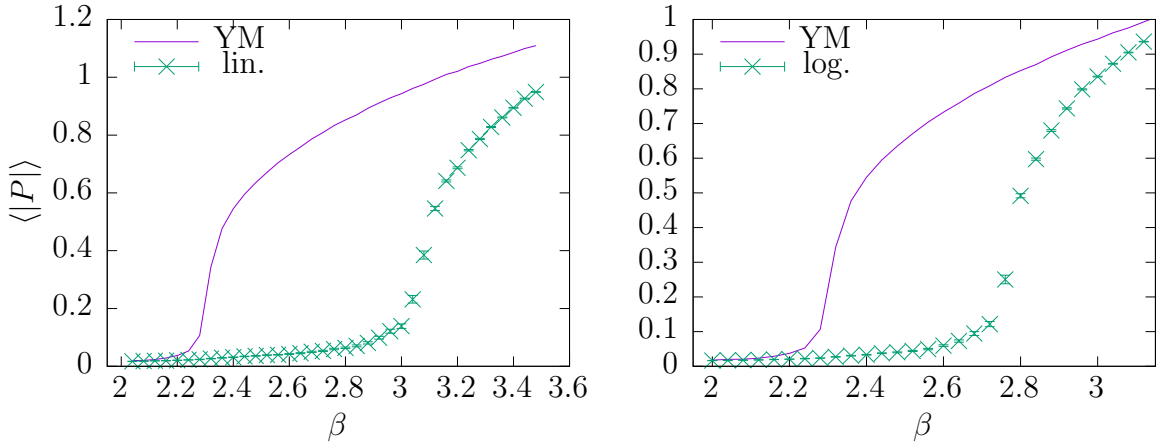

Figure 5.1: Polyakov loop expectation value $\langle |P| \rangle$ for local models in fundamental representation: Linear model (left) and logarithmic model (right)

In Fig. 5.1 we compare $\langle |P| \rangle$, the expectation value of the absolute value of the (non-normalized) fundamental Polyakov loop ($P = \chi_1$), as a function of β, for the full Yang-Mills theory to the effective local models in the fundamental representation (linear model on the left, logarithmic on the right). In both cases we see that the value of the Polyakov loops are matched very poorly in the center symmetry broken phase. However, both effective models show a phase transition from a center symmetric to a broken phase and the form of the Polyakov loop as a function of β is qualitatively correct. Compared to the critical value $\beta_c \approx 2.30$ of the full Yang-Mills theory, the values of β, where the effective models undergo a phase transition, are shifted to significantly larger values. The logarithmic resummation improves this and shifts the effective critical value towards its Yang-Mills value compared to the linear model. This is obviously due to the interaction terms of higher winding number implicitly included into the logarithmic form, whereas the linear form only contains the leading order term of the strong coupling expansion.

In Fig 5.2 (left) we have depicted the local Polyakov loop distributions of the effective models and the full model at different values of β, right before the phase transition and slightly in the broken phase. In. Fig. 5.2 (right), we have shown the same again, but divided the local Polyakov loop distribution by the scaling factor of the reduced $SU(2)$ Haar measure, i.e. the Vandermonde potential, which describes the local Polyakov loop distributions of the Yang-Mills theory (see [135]). The (reduced) $SU(2)$ Haar measure

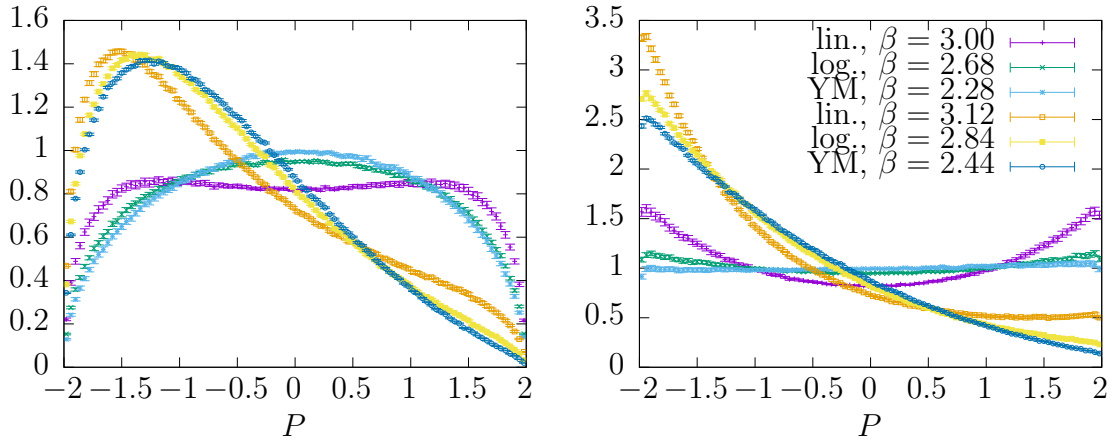

Figure 5.2: Local Polyakov loop distributions of the local linear and logarithmic models compared to the full theory immediately before the phase transition and in the broken phase (left); divided by the $SU(2)$ Haar measure (right). The legend on the right applies to both figures.

in terms of the (non-normalized) Polyakov loop $P = \mathrm{Tr}\,\mathrm{Diag}\,(\exp(i\phi)), (\exp(-i\phi)) = 2\cos(\phi)$ is given by (see 2.54)

$$\frac{2}{\pi}\sin^2(\phi)d\phi = \frac{2}{\pi}\sin^2(\phi)\left|\frac{\partial P}{\partial \phi}\right|^{-1} dP = \frac{1}{\pi}\sqrt{1-\frac{P^2}{4}}dP. \tag{5.1}$$

We see that the distribution of the Yang-Mills theory in the symmetric phase is given by the symmetric Haar measure, whereas for the effective linear model we can see a deformation compared to the full theory, which leads to a flattening with a local minimum around $|P| = 0$ and two global maxima emerging on the sides. In the logarithmic model the deformation is very small, compared to the linear case. In the broken phase, the distributions become asymmetric and the maximum of the full theory shifts from $P = 0$ to larger values of $|P|$. The deformation of the local Polyakov distribution of the linear model clearly carries on into the broken phase, which agrees with the results in [136].

5.2 Local models with higher representations

As a next step we take into account higher representations for the local effective models, first for the linear model, then for the logarithmic one. Note that from now on we will include terms for our models that were labeled by $p_{\max} = 2, 3$. Hence there will be a difference between the simple linear model (which we will label in plots and equations by "lin.") and the extended linear model (labeled by "xlin.").

5.2.1 Simple Linear Model

In Fig. 5.3 (left) we compare the Polyakov loop expectation value $\langle|P|\rangle$ for the local simple linear model, where we gradually increase via the value of $p_{\max}$ the number of representations taken into account, to the full theory. We do the same for the local Polyakov loop distributions in Fig. 5.3 (right) with the local linear model at $p_{\max} = 1, 3$ only. As we can see, in the linear model the results for the expectation value of the Polyakov loop are improved significantly, if we add up to three representations, reaching roughly the same quality as the logarithmic model with the fundamental representation only. However the critical coupling is still far from that of the full theory and the small improvement between $p_{\max} = 2$ and $p_{\max} = 3$ indicates that this would not improve further even if we take into account higher representations. The shape of the local Polyakov loop distributions do not seem to improve on increase of $p_{\max}$, still showing a significant flattening around zero and too high values away from zero.

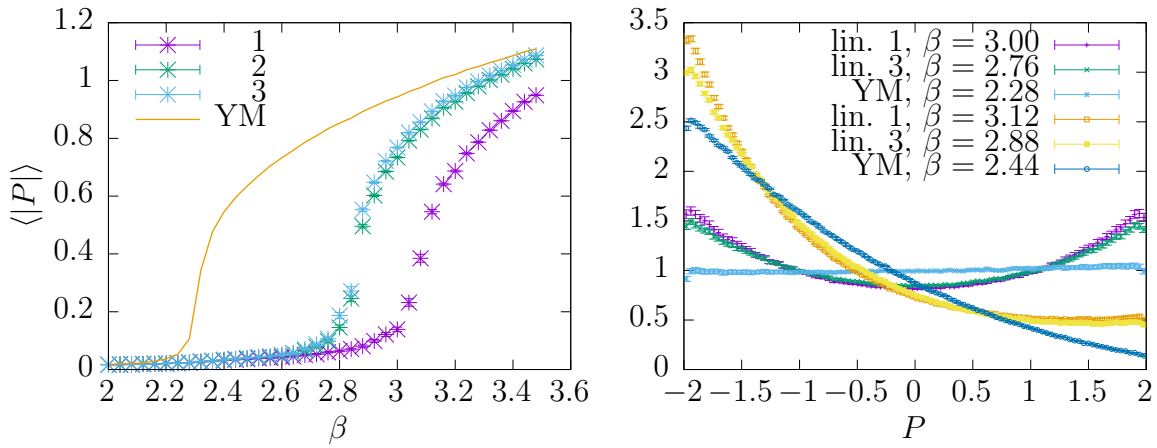

Figure 5.3: Polyakov loop expectation value $\langle|P|\rangle$ for the local simple linear model with $p_{\max} = 1, 2, 3$ compared to the full Yang-Mills theory (left) and local Polyakov loop distributions of the local simple linear model with $p_{\max} = 1, 3$ compared to the full theory at fixed value of $\langle|P|\rangle$, corresponding to values of β shortly before and after phase transition (right).

Furthermore, in Fig. 5.4 we compare the coupling constants of the effective linear models for fundamental and adjoint interaction terms as obtained by the inverse Monte-Carlo method to the prediction of the strong coupling expansion. We see that our results differ significantly from the predictions in the region of interest with $\beta \gtrsim 2.2$, indicating the breakdown of the strong coupling expansion around the phase transition and beyond. However as we see by the Polyakov loop expectation values and local distributions, also with the numerically matched coupling constants, results of the full theory are still matched only poorly by the local simple linear model, due to the very restricted ansatz.

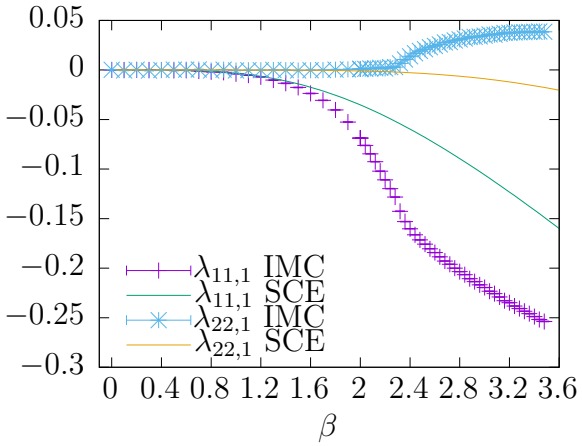

Figure 5.4: Couplings of the local interaction terms in fundamental ($\lambda_{11,1}$) and adjoint ($\lambda_{22,1}$) representation calculated in the simple linear model from IMC (dots) vs. analytical prediction from strong coupling expansion (lines)

5.2.2 Logarithmic Model

When adding higher representations in the local logarithmic model, the results for the expectation value of the Polyakov loop model and shape of local Polyakov loop distributions do not improve much (Fig. 5.5). This is due to the fact, that the logarithm arises from the resummation of terms of higher winding number and implicitly contains higher order representations. The proper resummation of higher representations can also been seen in Fig. 5.6 (left), where we have plotted the resulting couplings of the fundamental representation of the logarithmic model after expansion of the logarithm vs. the fundamental and the adjoint coupling constants of the linear model. We have also plotted in Fig. 5.6 (right) the coupling constants of the local logarithmic model with three representations and we see that they are small enough, satisfying the three conditions (3.46), preventing us from running into a sign problem on the range of interest. This will be also true for the non-local action, as the coupling constants of the non-local parts decrease with the distance and are smaller than the local coupling constants.

5.2.3 Extended Linear Model

So far we have seen that increasing $p_{\max}$ until a value of two or three, i.e. taking into account local higher order terms in β, improves the result for the simple linear model, such that the expectation value of the Polyakov loop is roughly of the same quality as the logarithmic model in the fundamental representation only. However the shape of local Polyakov loop distributions is still deformed significantly with no noticeable improvement at all. The logarithmic model seems to neither improve when looking at the Polyakov loop expectation value, nore the local distributions.

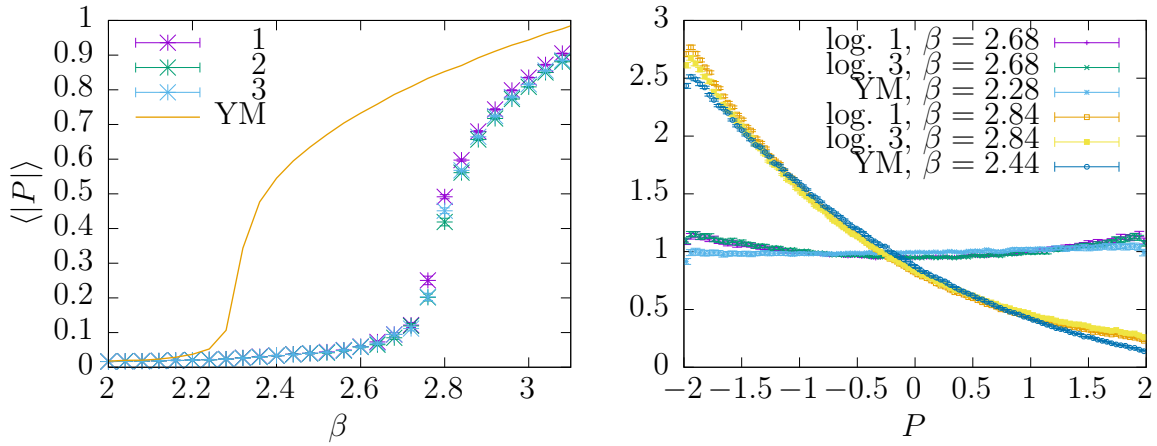

Figure 5.5: Polyakov loop expectation value $\langle |P| \rangle$ for the local logarithmic model with $p_{\max} = 1, 2, 3$ compared to the full Yang-Mills theory (left) and local Polyakov loop distributions of the local simple linear model with $p_{\max} = 1, 3$ compared to the full theory at fixed value of $\langle |P| \rangle$, corresponding to values of β shortly before and after phase transition (right).

In. Fig. 5.7 we see that for increasing $p_{\max}$ the extended linear model also improves the expectation value of the Polyakov loop, yielding approximately the same quality as the other local models (simple linear and logarithmic). However in contrast to the simple linear model, the shape of the local Polyakov loop distributions is improved significantly already at $p_{max} = 2$, such that the shape is very similar to that given by the logarithmic model. Hence the shape of the distributions, which is given for the full theory by the Haar measure at small β, is improved by the mixed interaction term between adjoint and trivial representation proportional to $\lambda_{20,0}$, which is equivalent a quadratic potential term

$$\lambda_{20,0}\, \chi_{2,i}\, \chi_{0,j} = \lambda_{20,0}\, (\chi_{1,i}^2 - 1)\, \chi_{0,j} = \lambda_{20,0}\, (\chi_{1,i}^2 - 1). \tag{5.2}$$

By expansion of the logarithmic model with $p_{\max} = 1$, it is apparent that such a potential term is implicitly also contained in the logarithmic model. Hence similar improvements in the local Polyakov loop distributions are achieved by logarithmic resummation and by adding a potential term in the extended linear ansatz.

5.3 Non-local Models

The seemingly convergence (when increasing $p_{\max}$) in all local models towards a similar Polyakov loop expectation value and critical coupling constants, which are still far from the values of the full theory, suggests that further improvements in the region of the phase transition won't be obtained by adding more nearest-neighbor terms to our ansatzes. Instead, we must take into account non-local interaction terms, which we will

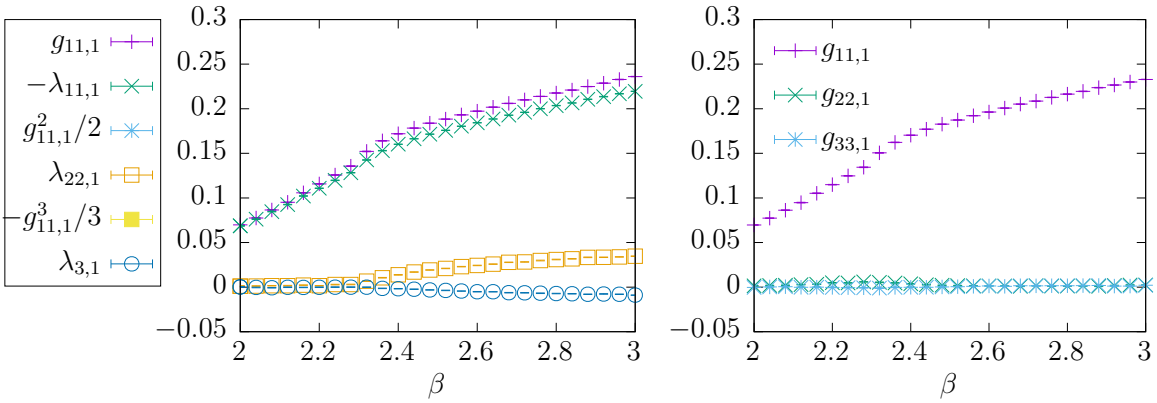

Figure 5.6: IMC couplings for the linear model as obtained by expansion of the logarithmic model vs. IMC coupling constants of the simple linear model (left). Coupling constants of the logarithmic model (right).

do in this section. We will gradually increase the interaction distance $r_{\max} = 1, 2, \ldots, 9$ to improve the models. However, we want to stress again, that the order in which we add terms, by increasing the interaction distance, is motivated by the strong coupling expansion, where higher distances are of higher order in β. As the strong coupling expansion breaks down at large values of β, near the phase transition, the order in which independent terms contribute should change as well. Hence it is not clear if the models improve in a monotone way, when increasing the maximal distance and if values of operators will converge in a clear way to a certain value at all. In fact, we will see that this is not the case for the logarithmic model.

For the local logarithmic model we saw in the last sections that is was sufficient to consider interaction terms in the fundamental representation. In Fig. 5.8 (left) we see that increasing the maximum interaction distance taken into account on a lattice of the size $16^3 \times 4$ results in the expectation value of Polyakov loops being improved first, but when increasing the interaction distance further, the values for the Polyakov loop do not converge to the full theory but we have some kind of "overshooting" instead. The suspicion, that this overshooting is a finite volume effect, which vanishes on larger lattices, cannot be confirmed. This overshooting vanishes first on the larger lattice of size $32^3 \times 4$ (Fig. 5.8 (middle)), but then we see that adding higher representation terms does (in contrast to the local case) change results significantly for the non-local model. The overshooting re-occurs on the larger lattice when taking into account higher representations (Fig. 5.8 (right)). All together there seems to be a competing effect of adding higher order terms, which leads to an overshooting Polyakov loop expectation value, and increasing the lattice size, which together lead to a non-monotone behavior. This makes a correct convergence on fixed lattices sizes and also in the thermodynamical limit unlikely.

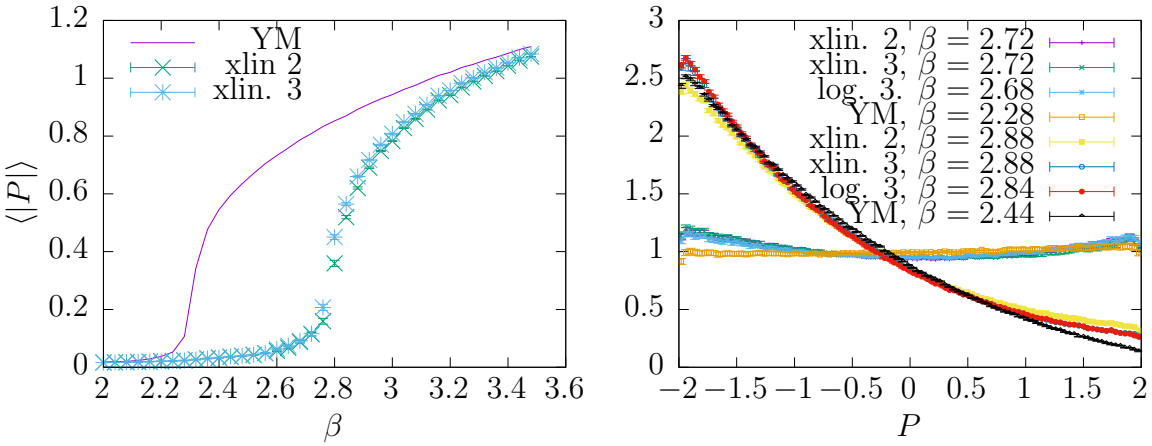

Figure 5.7: Polyakov loop expectation value $\langle |P| \rangle$ for the local extended linear model with $p_{\max} = 2, 3$ compared to the full Yang-Mills theory (left) and local Polyakov loop distributions of the local extended linear model with $p_{\max} = 2, 3$ compared to the full theory at fixed value of $\langle |P| \rangle$, corresponding to values of β shortly before and after phase transition (right).

Similar investigations for the linear models show a very different behavior. In Fig. 5.9 we have plotted the expectation value of the Polyakov loop of the non-local simple Polyakov loop model compared to the full theory, when increasing the interaction distance taken into account gradually. We have done this for the non-local model with $p_{\max} = 1$ (left), $p_{\max} = 2$ (middle) and $p_{\max} = 3$ (right). We see that increasing the interaction distance in all three cases leads to a monotone improvement of Polyakov loop expectation values, where no overshooting occurs. Furthermore taking into account higher representations yields the same result as in the local case, the improvement slows down around $p_{\max} = 3$, indicating that even higher representation should not change results too much. The Polyakov loop expectation values seem to converge for $p_{\max} = 2, 3$ in the non-local case to values very close to those around the full theory. Nevertheless the model approaches the full theory very slowly around the critical $\beta_c \approx 2.30$, indicating that we need to increase $r_{\max}$ much further in this region, if we want to obtain a better approximation. This is expected considering that the correlation length peaks at β_c.

We have checked on a larger lattice of $N_s = 32$ that this results do not change for the simple linear model. Also the extended linear model shows a similar behavior, with the Polyakov loop expectation values being hardly distinguishable from those of the simple model.

The qualitatively different behavior of the logarithmic and linear models, where the logarithmic model fails to describe the full theory correctly when generalizing it to the non-local case can be understood by realizing that the logarithm is a resummation of formally similar terms that are of different winding number. When grouping those terms together for the resummation into a logarithmic form, one uses relations between the

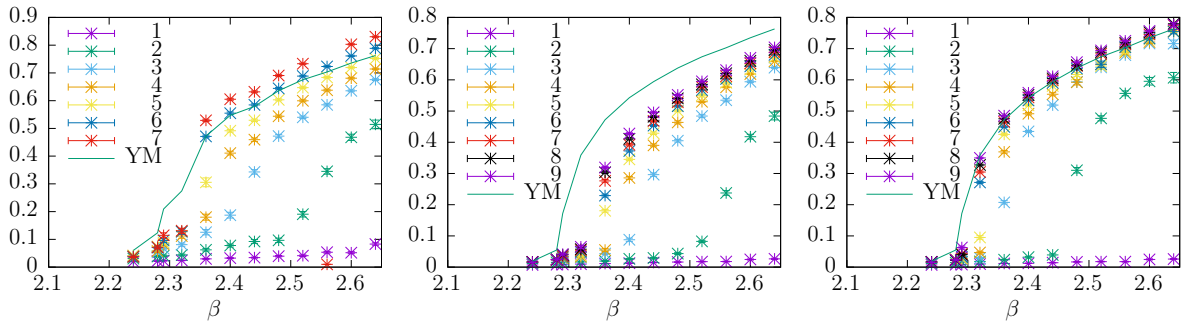

Figure 5.8: Polyakov loop expectation value for the log. model with $p_{\max} = 1$ on a $16^3 \times 4$ lattice (left), $p_{\max} = 1$ on a $32^3 \times 4$ lattice (middle) and $p_{\max} = 3$ on a $32^3 \times 4$ lattice (right)

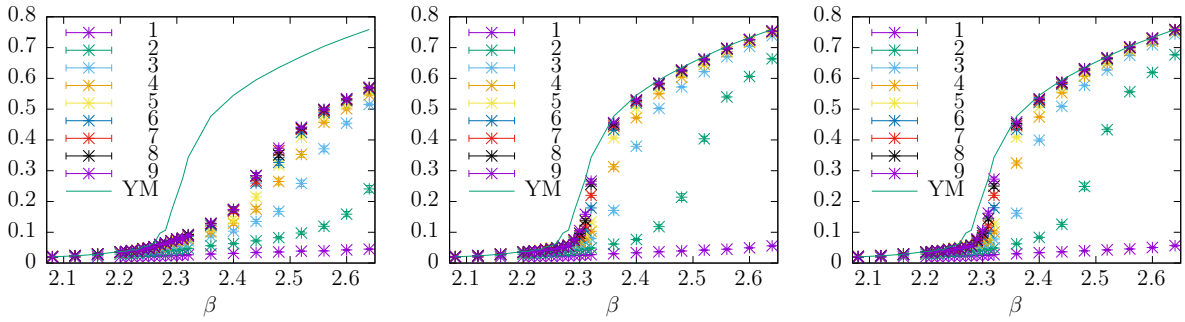

Figure 5.9: Polyakov loop expectation value for the non-local simple linear model with $p_{\max} = 1$ (left), $p_{\max} = 2$ (middle) and $p_{\max} = 3$ on a $16^3 \times 4$ lattice

coupling constants of those terms, which is only justified in the strong coupling limit but fairly unclear for larger values of β. The linear ansatz provides a much more general ansatz that can be justified even without the strong coupling expansion. Restrictions are not imposed and the coupling constants of all terms are left independent, giving the IMC method more freedom. We must conclude that the logarithmic model seems not to be suitable as an ansatz for highly non-local models, in contrast to the linear models, which both show a similar behavior. Therefore we will drop further investigations of the logarithmic model and will investigate the linear ansatzes in more detail in the next chapter.

Chapter 6

The Linear Models in Detail: Simple vs. Extended Model

After having seen that the logarithmic model seems not to be an useful ansatz for highly non-local models, we will discuss in this chapter the two classes of linear models in more detail. We will investigate and compare the behaviors of different observables when increasing the non-locality $r_{\max}$ at different values of β, with special interest in the region of the deconfinement phase transition on lattices of the size $16^3 \times 4$. We will also discuss the convergence of the different models in the large $r_{\max}$ limit and investigate their behavior on larger lattices with $N_t = 4, 6, 8$.

6.1 Comparing Observables for Large $\mathbf{r_{max}}$ at $\mathbf{N_t}$=4

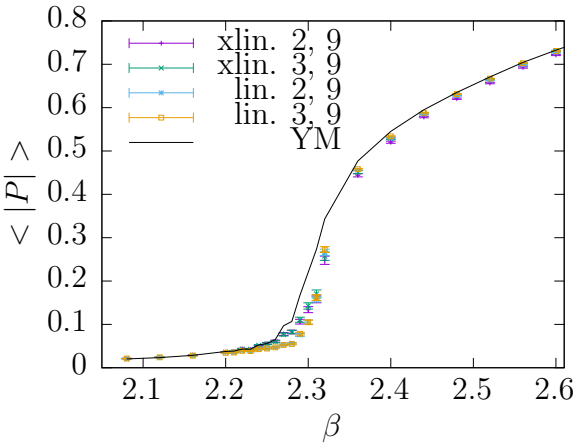

Figure 6.1: Polyakov loop expectation value for the simple linear model and extended linear model with $p_{\max} = 2, 3$ and $r_{\max} = 9$

As mentioned, in the non-local case the expectation value for the Polyakov loop looks very similar for the simple linear and extended linear models. Instead of plotting the Polyakov loop expectation value of the extended model in detail as well, we have plotted in Fig. 6.1 a direct comparison of the Polyakov loop expectation values of the simple linear and the extended linear model.

We compare the simple and extended linear model with $p_{\max} = 2, 3$ and $r_{\max} = 9$. We can see that the extended linear model yields slightly better results right before the phase transition and around the phase transition, but shortly after the phase transition the simple model seems to yield better results. The differences are hardly noticeable for the Polyakov loop expectation values. Also it is not clearly visible if we get an improvement in every step in which we are increasing the interaction distance, as there is hardly a difference for the models with large maximal interaction distances, say for $r_{\max} = 8$ and $r_{\max} = 9$. However taking a look at other observables such as Polyakov loop correlation functions and local Polyakov loop distributions, we get a better insight. In Fig. 6.2 we show the correlation functions of the simple linear and extended linear model with $p_{\max} = 3$ at different values of β, while gradually increasing the interaction distance and we see in fact more clearly now an improvement in every step when increasing the interaction distance, especially in the broken phase.

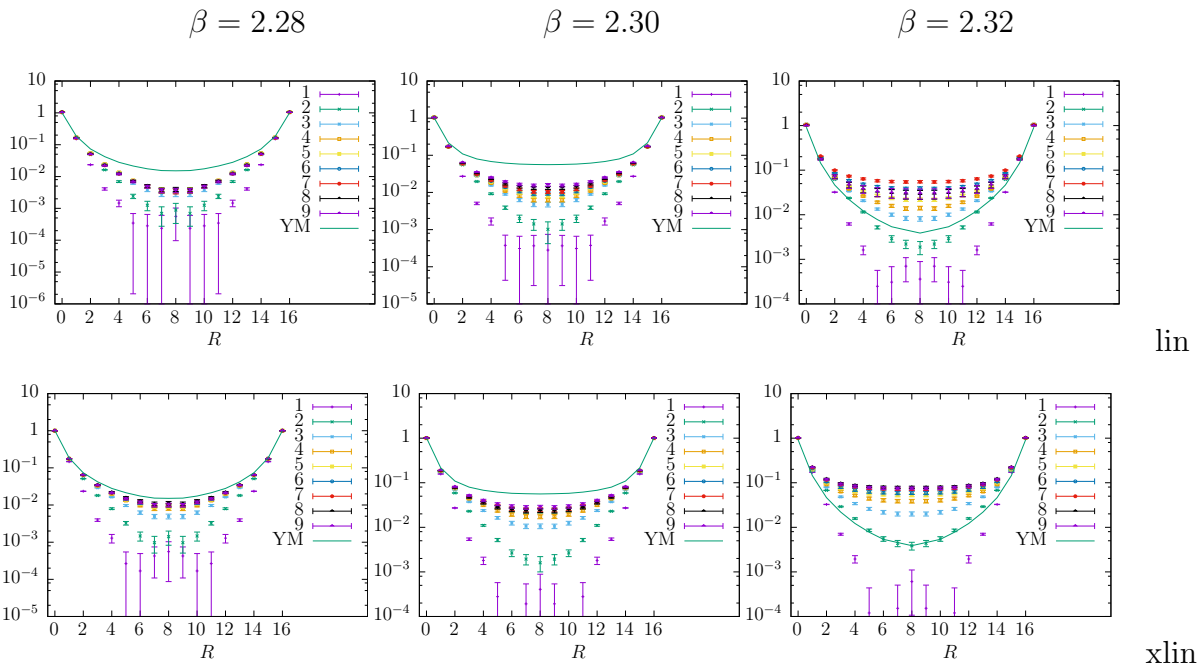

Figure 6.2: Polyakov loop correlation functions of the non-local simple linear model (top) and the extended linear model (bottom) with $p_{\max} = 3$ at $\beta = 2.28$ (left), $\beta = 2.30$ (middle), $\beta = 2.32$ (right)

Before the phase transition and right at the Yang-Mills phase transition (Fig. 6.2 left and middle), where the effective models are still in the unbroken phase, we can clearly see that the Yang-Mills correlation function is matched the best by the effective model with the largest interaction distance. We can also see that the extended linear model yields better results. Slightly in the broken phase (Fig. 6.2 right) it looks like the Yang-Mills correlator is best matched by linear models with short interaction distances of about $r_{\text{max}} = 2, 3$. However the seemingly better match is misleading, as we have to remember that correlation functions before and after a phase transition look qualitatively very similar and only flatten right around the phase transition. As the full Yang-Mills theory is already in the broken phase at $\beta = 2.32$, while the effective models with short maximal interaction distances are still deep in the unbroken phase, their correlation functions look similar by coincidence. In order to compare our models to the full theory, we must keep in mind that the full model is already in the broken phase and compare its correlation functions to the effective models that are also in their broken phases, i.e. whose correlation functions are past their flattest form. When increasing at fixed value of β the interaction distance for the effective models we clearly see that for larger interaction distances the correlation functions start to flatten, and for even larger distances they start to sink again towards the Yang-Mills results, indicating that the critical value β_c for models with larger interaction distances gets closer and closer to the full theory's value. Looking at the correlation function that started to sink again only, we can clearly see that the larger the interaction distance, the better we match the Yang-Mills correlation functions. Furthermore we see that the simple linear model takes over in the broken phase and approximates the full theory better than the extended model, which can be seen even more clearly in Fig. 6.3, where we have plotted the correlation functions of the simple and extended linear models at $r_{\text{max}} = 9$ and $r_{\text{max}} = 2, 3$ in the broken phase at $\beta = 2.32$.

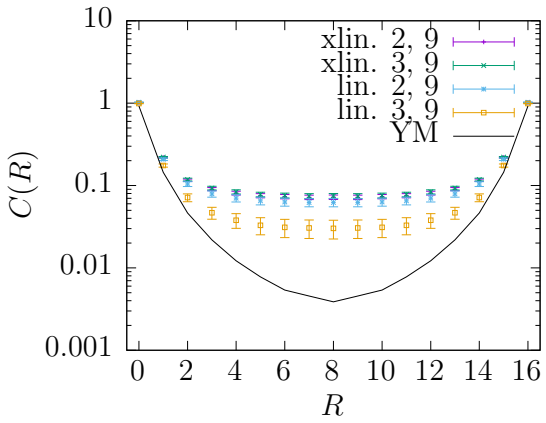

Figure 6.3: Correlation functions of the simple and extended linear models at $p_{\text{max}} = 2, 3$ and $r_{\text{max}} = 9$ in the broken phase at $\beta = 2.32$

The reason for the switch in qualities between the competing models (linear and extended linear) before and after the phase transition is unclear and can only be speculated about. A possible reason is the IMC method itself, which might be more precise (especially after the phase transition) when not taking into account too many terms, hence yielding better result for the simple model. Another reason might be the breakdown of the order of terms given by the strong coupling expansion around and after the phase transition. We already saw that the interaction terms of mixed representation and especially the interaction term between fundamental and trivial representations (the quadratic potential term), improves results significantly before the phase transition, enforcing a more Haar measure like, symmetrical local distribution of Polyakov loops. This might need to be suppressed again in the broken phase. The breakdown of the order given by the strong coupling expansion leaves the possibility for so far neglected higher order terms gaining importance in the broken phase, which could possibly cancel the effect of the potential term. After all, it was already expected that the order, which holds in the strong coupling limit, changes in the broken phase, and it was also unclear if the IMC method will be stable considering the huge number of coupling constants taken into account. Therefore a steady improvement of the models when adding higher order terms could not be expected easily in the first place and it is an even more astonishing result that increasing interaction distances gradually also improves results steadily even when we go as far as $r_{\max} = 9$, which requires the introduction of up to 325 coupling constants.

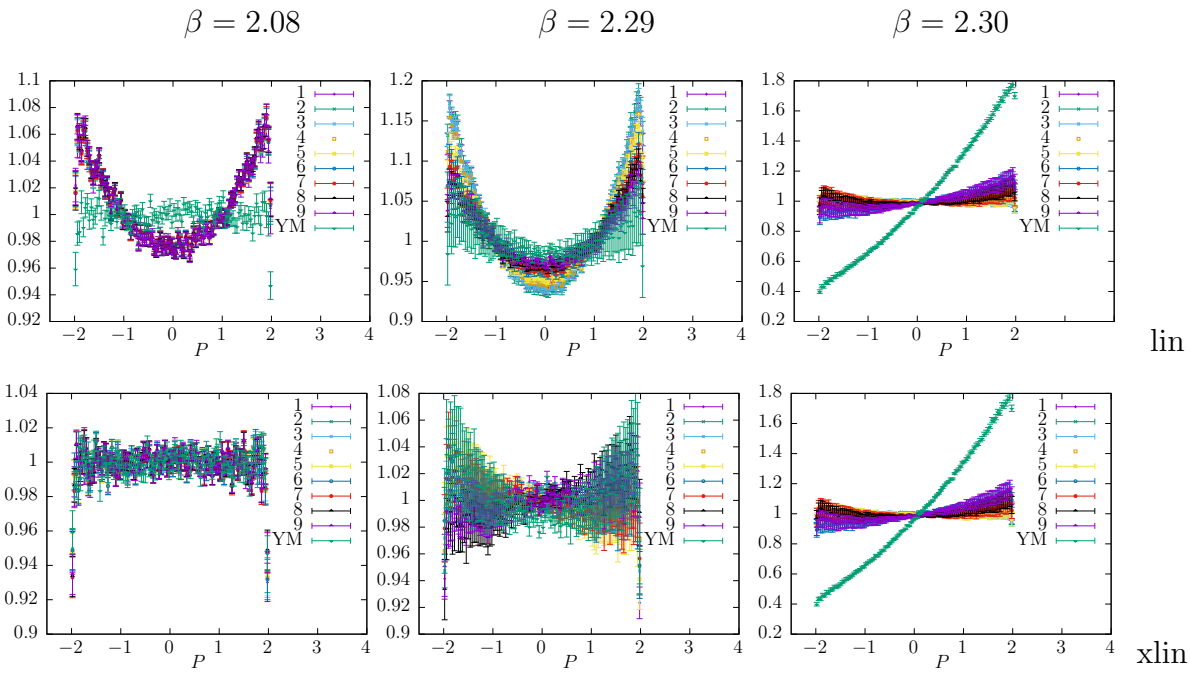

Figure 6.4: Local Polyakov loop distributions of the non-local simple linear model (top) and the extended linear model (bottom) with $p_{\max} = 3$ and $r_{\max} = 1, \ldots, 9$ at $\beta = 2.08$ (left), $\beta = 2.29$ (middle), $\beta = 2.30$ (right)

Another observable of interest is the local Polyakov distribution. We saw earlier in the local case, that only the extended linear model gives the right shape for the distributions in the unbroken phase. In Fig. 6.4 (right) we see that as the critical coupling of the effective models moves closer to the Yang-Mill critical value, results for the distributions get also improved in the broken phase and around the phase transitioning. Around the phase transition the local Polyakov loop distributions of the simple model gets more Haar-measure like, as we increase non-locality, however the extended model still yields a better shape for the distributions, and deep into the unbroken phase results for the effective models do not improve at all. Hence for small values of β only the extended model yields a distribution given by the Haar-measure, whereas the simple model preserves its deformed shape. Again we see that the extended model yields better results in the unbroken phase, where it is the potential term that leads to Haar-measure like distribution. In fact making the models non-local does not improve the shape of the distributions at all for small β, as can be concluded from Fig. 6.5 (left), where we have plotted the simple and extended linear models at $r_{\max} = 9$ and $p_{\max} = 3$, compared to the local extended model with $p_{\max} = 2$ and the local logarithmic model with $p_{\max} = 1$. Furthermore we see from the local Polyakov distribution in Fig. 6.5 (right) more clearly that the simple model again yields better results in the broken phase.

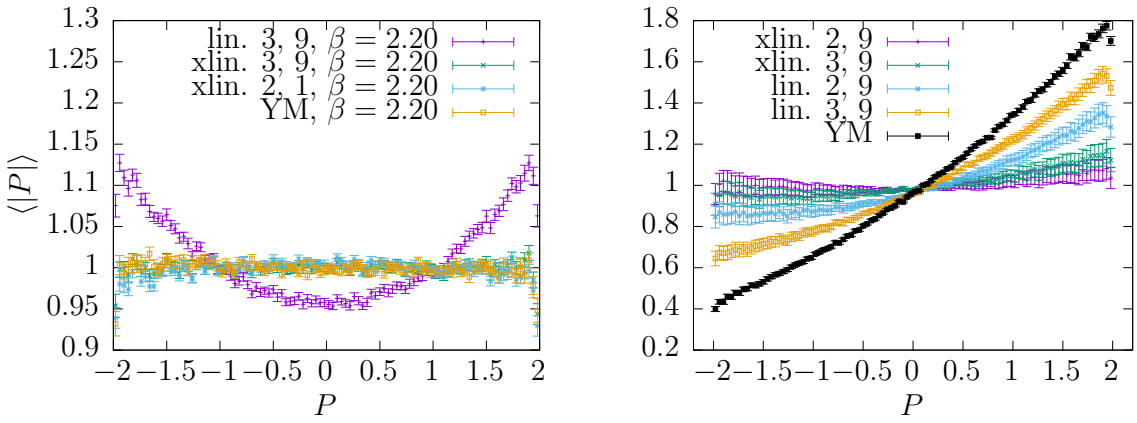

Figure 6.5: Local Polyakov loop distributions of the linear models with $p_{\max} = 2, 3$ and $r_{max} = 9$ on a $16^3 \times 4$ lattice with $\beta = 2.20$ (left) and $\beta = 2.32$ (right)

Let us summarize our results before we move on to the next section. So far we have seen that making the linear models non-local and gradually increasing the maximum interaction distance improves the models steadily. We have seen in multiple observables that before the phase transition the extended model yields better results, due to the potential term, which dominates the shape of the Polyalov loop expectation value and local Polyakov loop distributions. However, after phase transitioning the simple effective model quickly takes over and yields slightly better results in the region where center symmetry is broken.

6.2 Convergence via r_{max} at N_t=4

As we can describe the Yang-Mills theory at least deep in the broken and deep in the unbroken phase fairly well by either the non-local extended or simple linear model, we see that at least in certain regions we do not need to include all terms occurring in the strong coupling expansion to obtain correct results with the effective models. Furthermore we saw almost no improvement when increasing $p_{\max}$ from 2 to 3 for our linear models on the one hand but on the other hand a steady improvement when increasing the interaction distance, even in the area around and after the phase transition, which is the area described by the effective models with the least accuracy. This raises naturally the question if it is necessary to include all possible interaction terms into our models in order to converge towards the full theory, or if its enough to increase the interaction distance while keeping $p_{\max} = 3$ fixed. Therefore in this section we will try to determine the behavior of the linear models under increase of $r_{\max}$ for a fixed value $p_{\max} = 3$ and fixed timelike lattice extend $N_t = 4$. The area of interest here is mainly the region right after the phase transition, where we have the least accurate match between the effective models and the full theory.

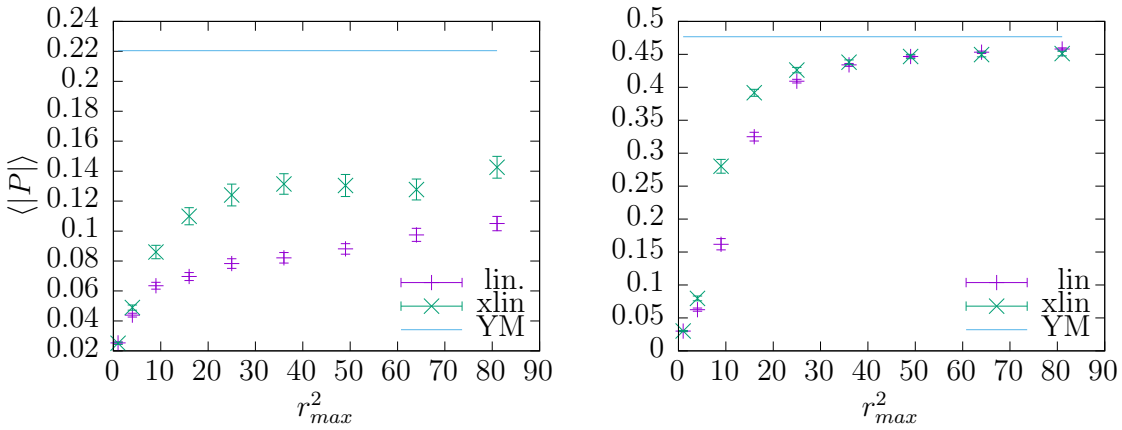

Figure 6.6: Polyakov loop expectation value for the simple and extended linear model with $p_{\max} = 3$ as a function of r^2_{max} for $\beta = 2.30$ (left) and $\beta = 2.36$ (right)

Since on the lattice the quadratic lattice distance r^2 takes integer values with only a few possibilities not applicable (for example a squared distance r^2 equal to 7 or 15 cannot be realized on a 3-dimensional lattice), for our effective models the number of coupling constants up to a maximum distance $r_{\max}$ grows quadratically with the maximum distance. Hence we cannot increase the maximum distance taken into account much further in order to investigate convergent behavior in the limit of large $r_{\max}$, as the number of coupling constants would grow and increase computational costs quickly. Instead we try to extrapolate the obtained results for $r_{\max} = 1, \ldots, 9$ to larger values. However this turns out difficult, as 9 reference points are not a lot to obtain a reasonable extrapolation and observables are not necessary expected to behave under increasing

value of $r_{\max}$ in a way that can be extrapolated easily. In Fig. 6.6 we have plotted for the simple and extended linear model with $p_{\max} = 3$ the expectation value of the Polyakov loop as a function of the (squared) maximum interaction distance $r^2_{\max}$ compared to the Yang-Mills value. We have plotted the results around the Yang-Mills phase transition (left) and in the broken phase (right). As we can see again in the broken phase the model approaches a value very close to the Yang-Mills value but due to the lack of date a reasonable extrapolation and determining a limit is not possible. Around the phase transition at $\beta = 2.30$ we see that the improvement of the values of the effective model is significantly slowed down and it is not clear if the theory converges to the Yang-Mills result, rather it seems very unlikely. However drawing the conclusion that the model does not converge to the right result around $\beta = 2.30$ might be a bit rash. Keeping in mind the form of the Polyakov loop expectation value as a function of β, which is growing quickly around the phase transition but is relatively constant before and after, and taking into account that increasing the maximum interaction distance shifts the critical coupling of the effective models closer to the Yang-Mills value, hence shifts the quickly growing region of the Polyakov loop expectation value to lower values, the growth of $\langle |P| \rangle$ slightly above the Yang-Mills phase transition is expected to speed up under increase of $r_{\max}$ once the critical value of the effective model is shifted into the region, making an extrapolation of data difficult.

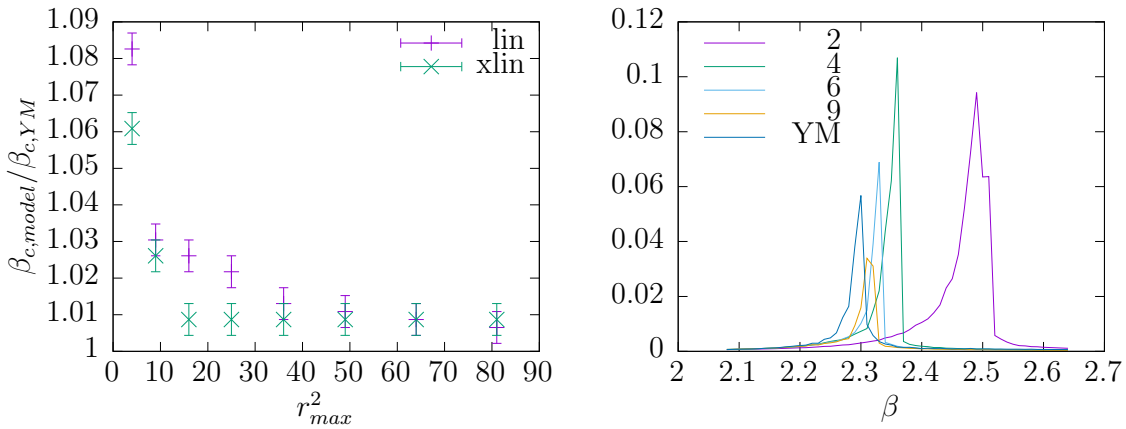

Figure 6.7: Critical value $\beta_{\text{c,model}}/\beta_{\text{c,YM}}$ of the effective theories with $p_{\max} = 3$ normalized to the Yang-Mills critical coupling as a function of r^2_{max} (left); Polyakov loop susceptibilities of simple linear model at $N_t = 4$, $N_s = 16$ (right)

A better way for investigating convergent behavior might be to directly extract the critical value $\beta_{\text{c,model}}$ of the effective models as a function of the (squared) maximum interaction distance, which we have plotted (normalized to the critical value $\beta_{\text{c,YM}}$) for the simple and extended linear model in Fig. 6.7 (left). The critical values β_c have been extracted from the Polyakov loop susceptibilities as shown for the simple linear model in Fig. 6.7 (right). Again we see in Fig. 6.7 a quick improvement of the critical value towards a value close to the one of the full Yang-Mills theory, which slows down at larger

values of $r_{\max}$, where the limit value is difficult to determine due to the limited number of data points.

Overall determining limits of the models for large maximum interaction distances is difficult due to the expected change of behavior with growing $r_{\max}$ and lack of functional form of certain observables such as $\langle |P| \rangle$ on the one hand, and a lack of sufficient data points, which is difficult to improve due to the quadratic growth of number of degrees of freedom with the maximum interaction distance on the other hand.

6.3 Increasing the Lattice Size: N_t=4,6,8

Up until now we have only investigate lattices with temporal extend of $N_t = 4$. As we could not determine convergent behavior of the effective models under increase of the maximum interaction distance, we will turn our investigation to larger lattices in this section, where we consider lattices with $N_t = 4, 6, 8$, from which we will try to make predictions for the effective models in the thermodynamical limit.

Before we do so, we want to discuss appropriate spatial extends for the different values of N_t, in order to avoid too large finite volume effects. So far we have used the proven aspect ratio of $N_s/N_t = 4$, where finite volume effects are expected to be small. Having kept this aspect ratio, we have plotted the Polyakov loop expectation values for the simple (top) and extended (bottom) linear models with $p_{\max} = 3$ and with gradual increase of $r_{\max}$ on lattices with $N_t = 4, 6, 8$ (left,middle,right) in Fig. 6.8. It shows that on lattices with larger temporal extend (especially on the $N_t = 8$ lattice) the quality of the effective model after the phase transition seems to decrease with increasing N_t. On the $N_t = 8$ lattice there opens up a huge gap between the effective models with $r_{\max} = 9$ and the full Yang-Mill theory. In addition to the gap, the effective models seems to show small signs of an additional phase transition, which is located around the Yang-Mill transition, before the proper phase transition of the effective models. To make sure that these effects are not finite size effect and that the aspect ratio of 4 is justified, we will discuss in this section finite volume effects in more detail. We will look into finite volume effects on lattices with $N_t = 4$ and $N_t = 8$, as calculations are the cheapest on the former one, and the gap between the effective model and the full theory, as well as the sign of the additional phase transition, are the most obvious on the latter one.

6.3.1 Finite volume effects at N_t=4

In order to investigate finite size effects on a lattice with $N_t = 4$, we have plotted in Fig. 6.9 the Polyakov expectation value for the simple linear model with $p_{\max} = 3$ at increasing maximum interaction distance with an aspect ratio of 4, i.e. $N_s = 16$ (middle). We have also decreased and increased the aspect ratio by a factor of 2 by setting

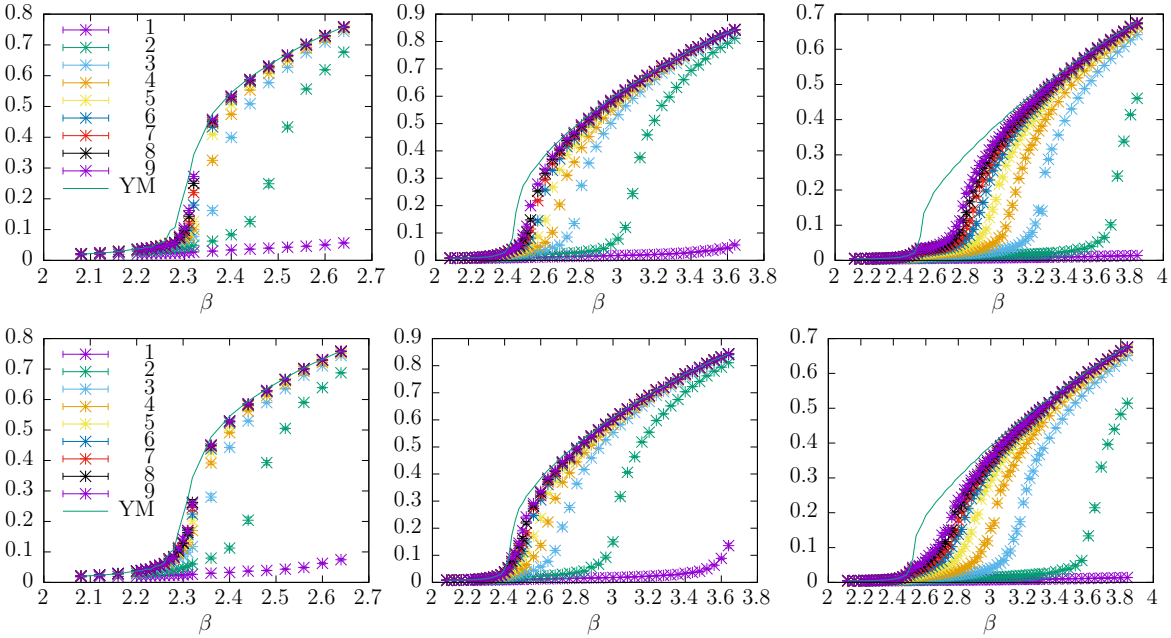

Figure 6.8: Polyakov loop expectation value of simple linear model (top) and extended linear model (bottom) with $p_{\max} = 3$, on a lattice with $N_t = 4, 6, 8$ (left,middle,righ) at fixed aspect ratio of $N_s/N_t = 4$

$N_s = 8$ (left), where we expect severe finite volume effects and $N_s = 32$ (right), to show no significant change in results when increasing the aspect ratio beyond 4. Indeed we see an increase of the aspect ratio beyond the value 4 does not change results much, but decreasing it by 2 leads to a more smeared out phase transition in both, the full and effective theories, resulting in a small gap opening up between the full theory and the effective models. It is worth noticing that the gap seems to open up due to the less sharp phase transition of the full theory and the shifted critical value for the coupling constant of the effective theory (see Fig. 6.10).

On the one hand this shows that at least for lattices with $N_t = 4$ an aspect ratio of 4 is justified, on the other hand the gap opening up between full and effective theory and the slow rising of the Polyakov loop expectation value suggest that for $N_t = 8$ the gap between effective model and full theory and the small sign of an additional phase transition might also be finite volume effects, as similarities between the Polyakov loop expectation values on the $8^3 \times 4$ and the $32^3 \times 4$ lattices are apparent. This makes a further discussion of the aspect ratio on the lattice with $N_t = 8$ necessary.

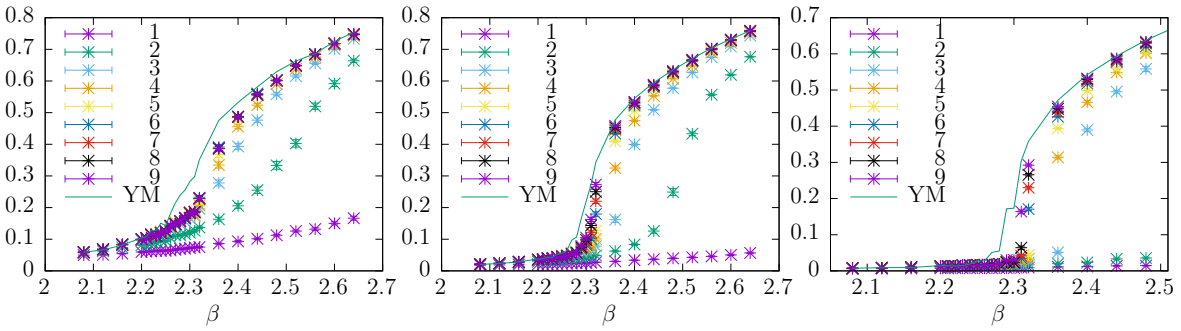

Figure 6.9: Polyakov loop expectation value of the simple linear model with $p_{\max} = 3$, $N_t = 4$ and $N_s = 8, 16, 32$ (left, middle, right)

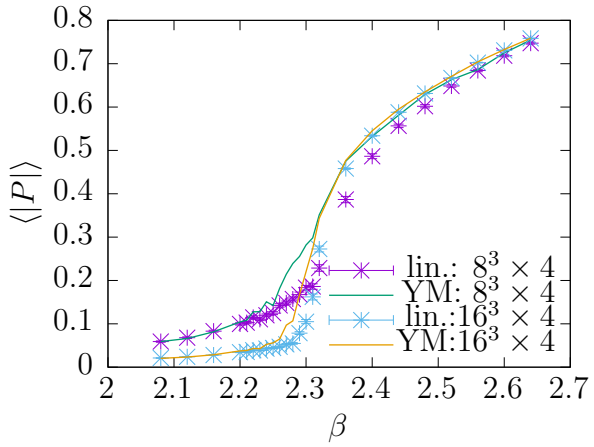

Figure 6.10: Polyakov loop expectation value of the simple linear model with $p_{\max} = 3$ and $r_{\max} = 9$ on lattices with $N_t = 4$, $N_s = 8, 16$

6.3.2 Finite volume effects at N_t=8

In Fig. 6.11 we have plotted the Polyakov loop expectation value for the simple linear model with $p_{\max} = 3$ on a lattices with $N_t = 8$. On the lattice with $N_s = 16$ (left), we see in comparison to the lattice with $N_s = 32$ (right) a slight finite size effect in the full theory. On the larger lattice the rise of the Polyakov loop expectation value is a bit sharper right around β_c. However this effect is not strong as in the case of $N_t = 4$ as the phase transition is less sharp for $N_t = 8$ anyways.

When comparing the effective models we see that increasing the aspect ratio from 2 to 4 indeed leads to a decrease of the small sign of the additional phase transition around the critical Yang-Mills value. Hence the small sign of the phase transitioning in the effective model seems not to be purely a finite size effect. Rather it seems like the

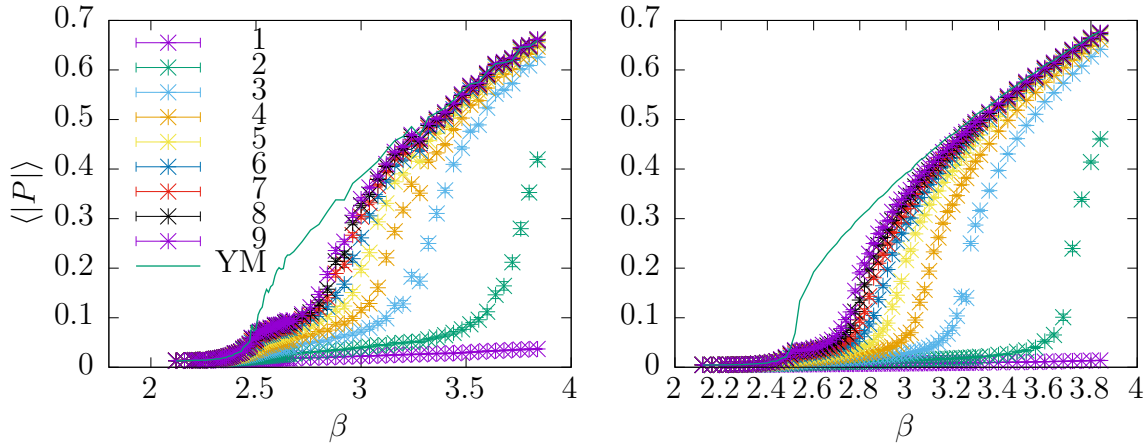

Figure 6.11: Polyakov loop expectation value of the simple linear model with $p_{\max} = 3$, $N_t = 8$ and $N_s = 16, 32$ (left,right)

Polyakov loop expectation value of the highly non-local effective models are following the values of the full theory until near the Yang-Mills phase transition, but eventually start to deviate right at the phase transition, when the strong coupling expansion breaks down and the order of terms given by the expansion does not apply any longer. The qualitative change in behavior at the phase transition can also be seen in the dominant coupling constant $\lambda_{11,1}$ for interaction terms between nearest-neighbor Polyakov loops in the fundamental representation, which we have plotted for the simple and extended linear model with $p_{\max} = 3$ and $r_{\max} = 9$ on lattices with an aspect ratio of 4 and $N_t = 4, 6, 8$ in Fig. 6.13 (right). The horizontal lines indicate the critical Yang-Mills coupling constant (line at lower value of β) and the critical coupling of the effective model (line at higher value of β), as obtained by the peak position of Polyakov loop susceptibilities, at $N_t = 4$ (green), $N_t = 6$ (yellow), $N_t = 8$ (blue). We see that on all lattices a kink in the fundamental coupling constants occurs around at the critical value of β in the Yang-Mills theory, rather than the at the critical value in the effective models. This can be seen more clearly for the lattices of $N_t = 6, 8$, as for growing temporal lattice extend the critical values of the Yang-Mills theory and the effective model tend to drift further and further apart from each other. Due to the more smeared out phase transition, for small lattices the Polyakov loop expectation value in the effective models (although having their own proper phase transition at larger values of β) start to "feel" the phase transition of the full theory and rise before such a deviation occurs. Increasing the lattice size on the other hand will result in a more sharp phase transition and hence in a smaller rise in the Polyakov loop expectation values of the effective models before their results start to deviate from the Yang-Mill results. But still the rise indicates that the effective models "feel" the phase transition of the full theory before properly phase transitioning at larger values of β themselves. (We will later in section 7.3, where we will investigate the analytical structure of the coupling constants and their fall-off with

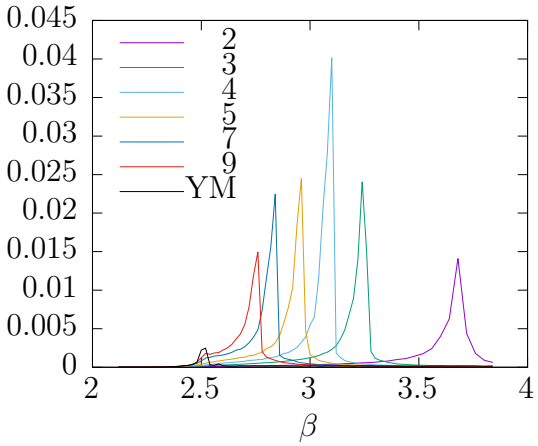

Figure 6.12: Polyakov loop susceptibilities for the simple linear model with $p_{\max} = 3$ on a $32^3 \times 8$ lattice

the interaction distance, see additional signs for the effective models "feeling" the phase transition of the full theory.) However the gap that opens up between the full theory and the effective models, which indicates a growing difference in the values of critical constants, seems not to decrease for larger aspect ratios. In fact, when increasing the aspect ratio the sharpening of the phase transition results in the decrease of the additional bump in the Polyakov loop expectation value, while the position and shape of the actual phase transition does not change. Therefore the gap between the full theory and the effective models becomes even clearer. We conclude that the gap between model and full theory is not a finite size effect but results from missing terms in our ansatz. This is supported by the fact that the extended model yields a smaller gap than the linear model (compare Fig. 6.8 top, right vs. bottom, right), indicating that the gap results from the lack of interaction terms with Polyakov loops in higher representations and mixed representations. For $N_t = 4$ we actually saw a similar behavior where the extended model yields better results in a small region after the phase transition, before the simple model takes over. This region where higher and mixed representation terms become more important seems to be of increased size for $N_t = 8$ and most likely suggests that narrowing down the gap requires taking into account even more representation terms. We also see, in contrast to the $N_t = 4$ lattice, no region in the broken phase where the simple model takes over again and yields better results than the extended model (see Fig. 6.13). This holds also true when comparing local Polyakov loop distributions and correlation functions.

It is interesting to note that for the lattice of $N_t = 8$ our ordering and improvement scheme, although resulting in a gradual improvement of results, deforms the shape of the Polyakov loop expectation value as a function of β due to the small bump around the Yang-Mills phase transition. Furthermore the deformation looks quite different for the simple linear and for the extended linear model. This raises the question if the

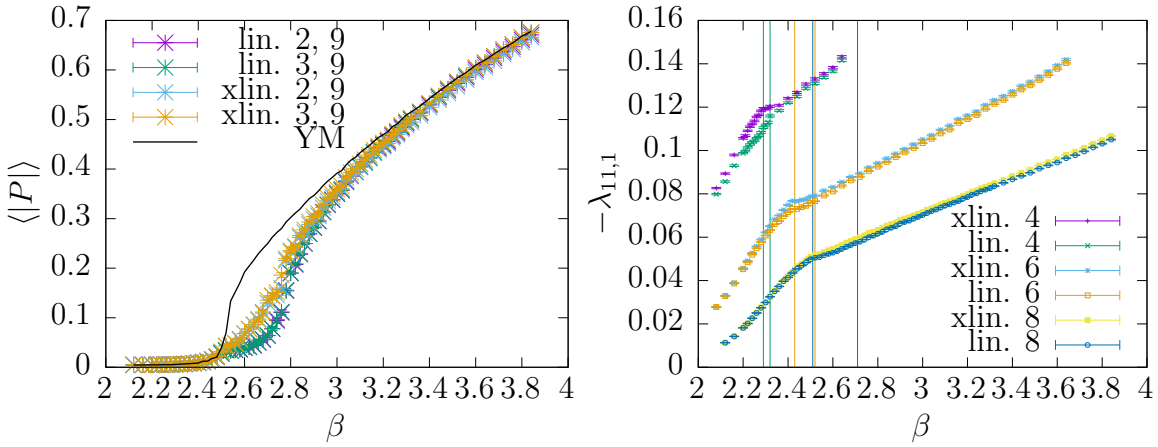

Figure 6.13: Polyakov loop expectation value for simple and extended linear model with $p_{\max} = 2, 3$ and $r_{\max} = 9$ on a $32^3 \times 8$ lattice (left); dominant coupling constant $\lambda_{11,1}$ for the simple and extended linear model with $p_{\max} = 3$, $r_{\max} = 9$ on lattices $N_s/N_t = 4$, $N_t = 4, 6, 8$ (right). The horizontal lines indicate the critical Yang-Mills coupling constant (line at lower value of β) and the critical coupling of the effective model (line at higher value of β), as obtained by the peak position of Polyakov loop susceptibilities, at $N_t = 4$ (green), $N_t = 6$ (yellow), $N_t = 8$ (blue)

improved models still yield the same universal behavior as the full model. From the Svetitsky-Yaffe conjecture, we know that short-range Polyakov loop models yield the same universal behavior as the full Yang-Mills theory. Furthermore we expect Polyakov loop models where all significant terms are taken into account to exhibit, as an expansion of the Yang-Mills theory, also the same universal behavior. However, for our models, where different truncation schemes have been applied, preservation of universal behavior is not clear for all values of $r_{\max}$, since Polyakov loop models with long-range interaction terms are neither subject to the Svetitsky-Yaffe conjecture, nor are they near the phase transition (especially for large values of N_t) a good approximation of the full Yang-Mills theory. In principle it is at least possible that we change universal behavior or that only carefully chosen truncation schemes leave the universal behavior of the theories unaffected.

However, concerning the aspect ratio, the fact that a growing aspect ratio seems to only decrease the additional bump in the effective theories indirectly by sharpening the phase transition of the full theory and that changes are already fairly small for an increase of the aspect ratio from 2 to 4, seems to justify further use of the ratio 4. Furthermore the position and form of the actual phase transition in the effective models seems not to be influenced much by finite size effects either. This can be seen by comparing the critical coupling constants, read off from the Polyakov loop susceptibilities of the simple linear model with $p_{\max} = 3$ in Fig. 6.12, to the position of the phase transition in Fig. 6.11 (right). We see that the position of the peak in Polyakov loop susceptibilities is not

disturbed by the small additional rising in the Polyakov loop expectation value for an aspect ratio of 4 and agrees with the actual phase transition, which also speaks for an aspect ratio of 4 being sufficient.

6.3.3 Comparing $\mathbf{r_{max}}$ at $\mathbf{N_t}$=4,6,8

Although we could not determine convergence of the effective models on a lattice of fixed size in the large $r_{\max}$ limit we can still try to compare the effective models at fixed $r_{\max}$ at different lattice sizes. Comparing how well the effective models approximate the full theory on different lattices sizes will then hopefully give us some insight about the thermodynamical limit. However, the gap that opens up between the effective model and the full theory on lattices with larger temporal extend is actually difficult to compare to the smaller gap on lattices with smaller values of N_t, since with increasing temporal extend the phase transition gets shifted and blurred out over larger areas in the β-axis, resulting in a very different form of the Polyakov loop expectation value as a function of β. Scaling the critical values to 1, by plotting the Polyakov loop expectation value as a function of $\beta/\beta_{\mathrm{c,YM}}(N_t)$, yields a better way for comparing the the effective models. In Fig. 6.14 we have shown the resulting functions for the simple linear and extended linear model at $p_{\max} = 3$. The critical coupling constants of the Yang-Mills theory, which are depending on N_t, have been calculated according to [135] via

$$\beta_c(N_t) = a_0 + b_0 \log(N_t) - \log(\log(N_t))^{c_0}, \tag{6.1}$$

with $a_0 = 1.1579(6)$, $b_0 = 0.9398(1)$, $c_0 = 1.627(2)$.

As we see, scaling down the Polyakov loop expectation values results on all lattices in a critical Yang-Mills value of 1, but besides that the shape of the Polyakov loop expectation values still differ a lot as a function of β. A direct comparison is still difficult, but it seems unlikely that the gap, which is opening up between effective models and full theories on lattices with larger values of N_t, can be explained by scaling alone. Rather it seems to be indicating a loss of quality of the approximation given by the effective models at fixed $r_{\max}$ with increasing timelike extend of the lattices. This loss of quality at constant interaction distance actually makes sense, as the interaction distance $r_{\max}$ is given in lattice units. If at all, then we should expect a comparable quality of results with fixed maximal interaction distance in physical units ($r_{\max} \cdot a$), instead of a fixed value of $r_{\max}$. As the critical temperature on lattices with different temporal extends should be constant, we can conclude from

$$\frac{1}{T_c} = a(\beta_c) N_t \tag{6.2}$$

that the lattice spacing at the critical coupling should decrease with increasing temporal extend of the lattice. Therefore with increase of N_t we should also increase the lattice

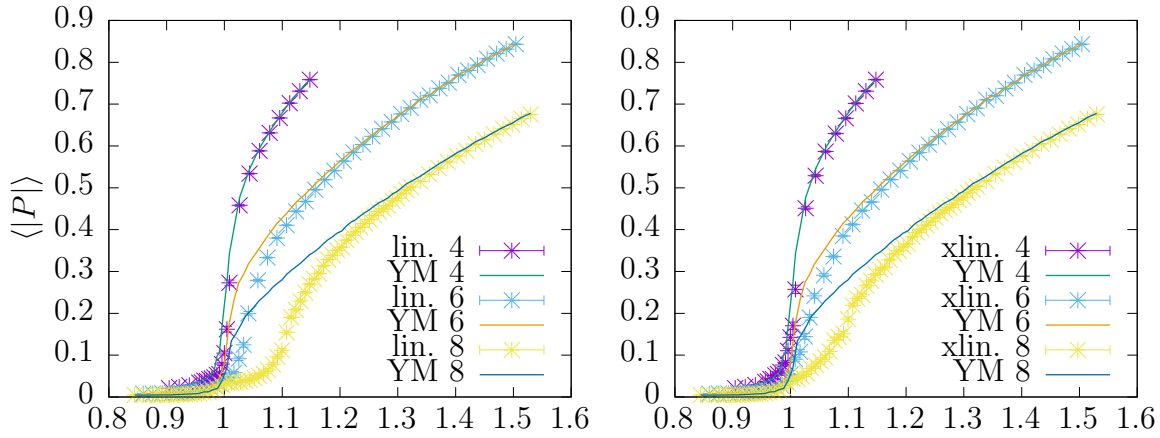

Figure 6.14: Polyakov loop expectation value as a function of $\beta/\beta_{\mathrm{c,YM}}$ for the simple (left) and extended (right) linear model with $p_{\max} = 3$ and $r_{\max} = 9$ on lattices with $N_t = 4, 6, 8$

distance $r_{\max}$ in order to obtain a constant maximum physical interaction distance. In the following we will compare effective models on lattices with $N_t = 4, 6, 8$ where we choose the maximal lattice interaction distance $r_{\max}$ such that the corresponding physical distance is approximately constant on the different lattices, in order to make predictions about the models in the thermodynamical limit.

Considering equation (6.2) and demanding the critical temperature of the Yang-Mill theories to be constant on lattices of different size, we get a rough estimation of how to increase the maximal lattice interaction distance $r_{\max}(N_t)$ in order to obtain a constant distance $r_{\max} \cdot a$ in physical units. As the critical temperature is constant, the lattice spacing $a(\beta_c(N_t))$ should be proportional to N_t^{-1}. Therefore we must chose $r_{\max}(N_t) \sim N_t$. As the simulations taken into account are restricted to $r_{\max} = 1, \ldots, 9$, we do not have much choice but to set

$$r_{\max}(N_t) = N_t \qquad \text{or} \qquad r^2_{\max}(N_t) = N_t^2 \tag{6.3}$$

to compare results on the different lattices with size $N_t = 4, 6, 8$.

In Fig. 6.15 we have compared the critical coupling constants (normalized by the Yang-Mills critical coupling) of the effective simple linear (left) and extended linear model (right) for $p_{\max} = 3$ as a function of $r^2_{\max}$ on lattices with $N_t = 4, 6, 8$. The critical coupling constants have been determined again by the position of the peak in Polyakov loop susceptibilities. The yellow line fitted to the data points

$$\left(r^2_{\max}(N_t), \beta_{\mathrm{c,model}}/\beta_{\mathrm{c,YM}}(N_t)\right) = \left(N_t^2, \beta_{\mathrm{c,model}}/\beta_{\mathrm{c,YM}}(N_t)\right), \qquad N_t = 4, 6, 8, \tag{6.4}$$

should be approximately constant for a constant quality of the effective models with fixed value $p_{\max} = 3$ and fixed maximum interaction distances in physical units. However this is not the case, indicating that with growing lattice size the critical coupling is

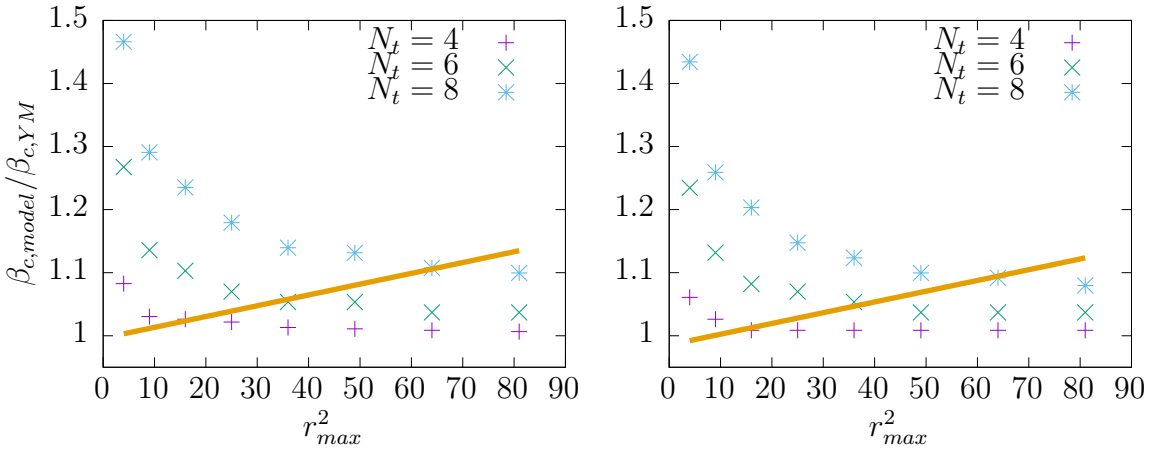

Figure 6.15: $\beta_{\mathrm{c,model}}/\beta_{\mathrm{c,YM}}$ as a function of r^2_{max} for different $N_t = 4, 6, 8$ at $N_s = 16$

not approximated equally well by models with similar physical interaction range. This agrees with our previous observation that with growing N_t higher order representations seem to gain importance around the Yang-Mills phase transition and that on lattices with large temporal extend we cannot get away with a simple truncation of interaction terms by setting $p_{\max} = 3$.

Before moving on to the next part of our investigations, let us summarize this chapter. We have tried to determine the behavior of the non-local models in the limit of large interaction distances and also in the thermodynamical limit for fixed physical interaction distances. Determining the limit of our models for large maximum interaction distances at fixed lattice size turned out to be difficult. On the $N_t = 4$ lattice we saw that we approximate the full theory very well, however a convergence to the full theory could neither be confirmed nor disproven as a reliable way of determining limits of observables was not possible. Furthermore we made arguments that suggest that in the thermodynamical limit we will not be able to approximate the full theory by simply increasing the maximum interaction distance of the models. Instead, we must take into account terms of higher order, which include higher representations and mixed representations of Polyakov loops.

Chapter 7

Non-Local Couplings of the Linear Models

In this chapter we will now investigate the fall-off of the non-local coupling constants with respect to the interaction distance and try to find an analytical form which describes the fall-off. The coupling constants λ_{pq,r^2} typically decrease quickly for larger values of p, q, r^2.

The coupling constants of interaction terms including a representation with $p = 3$ are already so small compared to their errors, that, regarded as a function of r^2, a certain structure is not really recognizable. However for λ_{11,r^2}, λ_{22,r^2} (the coupling constants of the interaction terms in fundamental and adjoint representation), plotting the coupling constants as a function of the interaction distance typically yields a fall-off with the distance of the form shown in Fig. 7.1, where a structure is clearly visible. The coupling constants tend to show an exponential fall-off with respect to the interaction distance for smaller interaction distances, followed by an almost constant plateau at larger distances. As the structure is the clearest for λ_{11,r^2}, we will focus on those coupling constants in the following detailed discussion of possible analytical forms, with their values obtained by the IMC method for the simple linear model with $p_{\max} = 3$.

7.1 The constant plateau

Although for fixed value of β the form of the coupling constants $\lambda_{11,r^2}(\beta)$ as a function of the interaction distance r^2 (Fig. 7.1) shows an exponential fall-off for small distances, taking into account the plateau at larger distances, the overall shape seems to coincide the most with a fall-off described, as proposed by Greensite and Langfeld, by the Laplacian kernel Q (3.48). However in such non-local models one typically applies a hard cut-off to the interaction distances taken into account, as the arguments made by Svetitsky and Yaffe suggest that an effective spin model for the full Yang-Mills theory should contain only short-range interactions. Hence such an cut-off is applied at relatively short distances (see [124]). Therefore before investigating the analytical form of

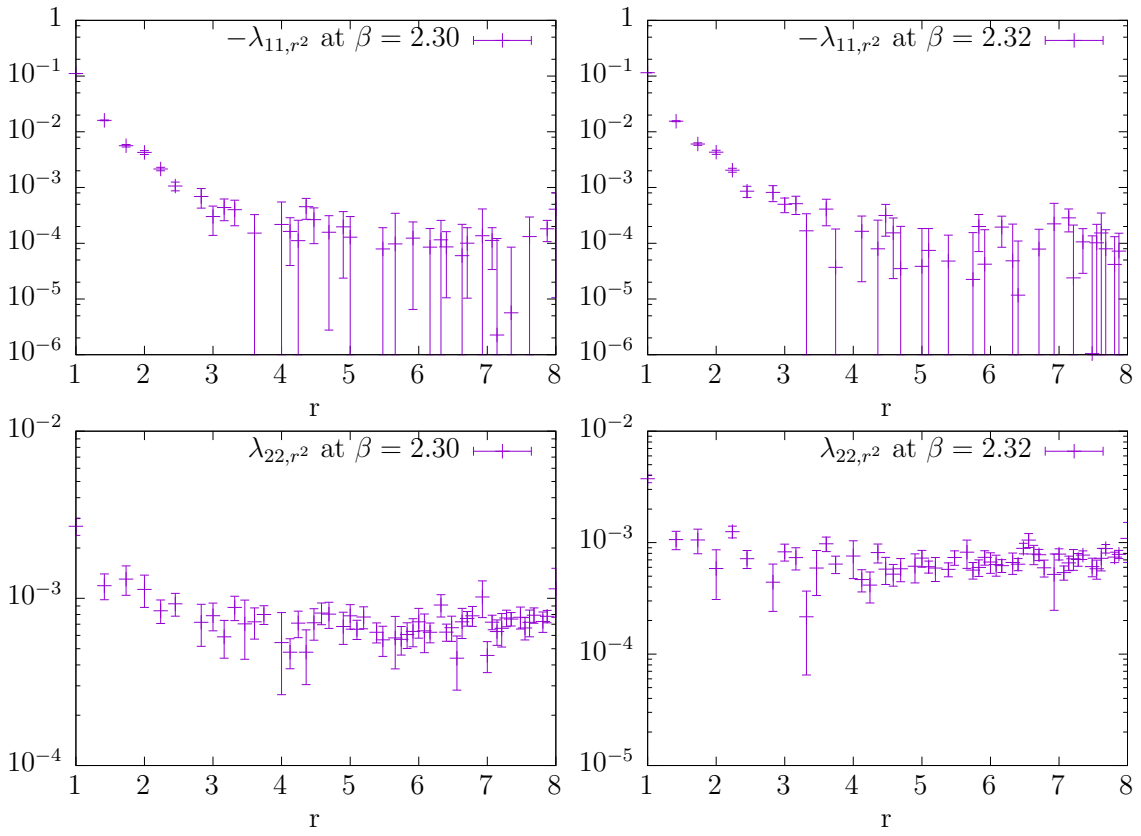

Figure 7.1: Coupling constants for of the interaction terms in fundamental (top) and adjoint (bottom) representation as a function of the interaction distance r at $\beta = 2.30$ (left) and $\beta = 2.32$ (right) taken from the simple linear model with $p_{\max} = 3$

the non-local coupling constants, we will first discuss if such a hard cut-off at larger distances is justified, when trying to obtain an effective model that goes beyond universal behavior and yields an accurate approximation for the full theory and we will discuss if the plateau reached in the coupling constants is physical or only due to statistical errors. Although we have seen that increasing the maximum interaction distance up to 9 gradually improves our effective models, without further investigation one cannot exclude the possibility that such an improvement only occurs because the interaction terms at larger distances compensate for statistical errors in the original configurations of the Yang-Mills theory, thereby allowing the coupling constants for the short distance interaction terms to attain values closer to their "true" values. In this sense adding larger distance interaction terms might only yield a stabilization of the IMC method for the short term coupling constants. In this section we will argue that this scenario seems not to be the case and that the specific values of the large distance coupling constants are of relevance for improvements of the models, hence cannot be explained by statistical errors alone.

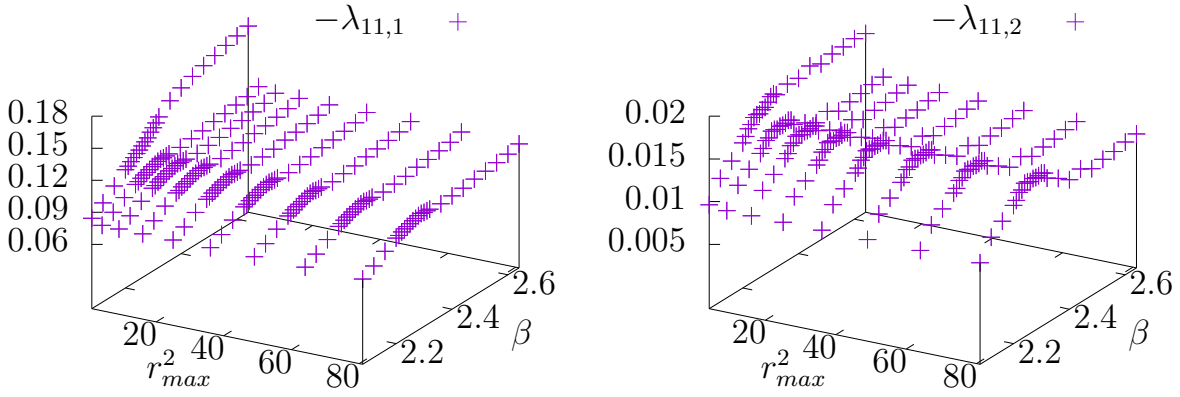

Figure 7.2: Coupling constants $\lambda_{11,1}$, $\lambda_{22,1}$ as a function of $r^2_{\max}$ taken from linear model with $p_{\max} = 3$

A first argument for the large distance terms being of relevance beyond stabilization of the short term coupling constants is obtained by realizing that an increase $r_{\max} \to r'_{\max}$ of the maximal interaction distance usually effects primarily coupling constants λ_{pp,r^2} with r close to $r_{\max}$. Especially for the dominant coupling constants, such as λ_{11,r^2} with small values of r^2, increasing the maximum interaction distance further than a few steps leaves the results for those coupling constants almost unchanged, which seems the contradict the stabilization argument. In Fig. 7.2 we have plotted the coupling constant of the fundamental interaction terms at interaction distance $r^2 = 1$ (left) and at interaction distance $r^2 = 2$ (right) as a function of β and of the maximum interaction distance $r^2_{\max}$. We see that when increasing the maximum interaction distance, the coupling constants quickly converge to a value and then do not change too much anymore with any further increase of the maximum interaction distance. This suggests that increasing the maximum interaction distance mainly effects the coupling constants of interaction terms with distance close to the maximum interaction distance.

Furthermore in Fig. 7.3 we have plotted again the Polyakov loop expectation value for the simple linear model, where we have taken into account interaction distances until $r_{max} = 9$ in the calculation of the coupling constants via the IMC method, but then applied a position space cut-off, where we have dropped for the simulation of the effective theory all interaction terms at distances larger than that cut-off. We applied a cut-off at $r_{max} = 3$ (left) and $r_{max} = 6$ (right). The plots show that for a fixed cut-off value the best result is obtained by taking in the IMC method only interaction terms into account until that cut-off. If we take more terms into account, and then drop them in the simulation afterwards results become less accurate is the effective model. Hence the larger distance interaction do not act as a stabilization for the IMC results at short

distances only but really improve the effective models by the specific value they take. At least for the maximum interaction distances considered here, a hard cutoff seems not to be justified and we have to take into account the shape of the fall-off over the whole interaction range when trying to determine the analytical form.

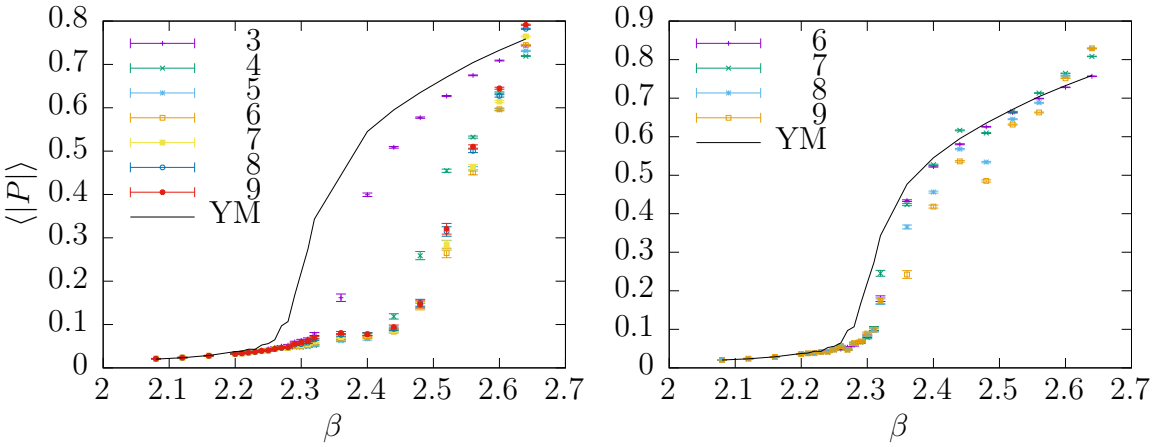

Figure 7.3: Polyakov loop expectation value for simple linear model with $p_{max} = 3$ and $r_{\max} = 3$ (left), $r_{\max} = 6$ (right) in simulation of the effective theories, where the coupling constants up to distance 3 and 6 have been calculated via IMC method with interaction terms up to a maximum distance $r_{\max} = 3, \ldots, 9$ (left) and $r_{\max} = 6, \ldots, 9$ (right)

7.2 Laplacian Fit

Having established that the actual value of the large range coupling constants are relevant for the improvement of our models, we cannot simply ignore them when trying to explain the analytical form of the fall-off in Fig. 7.1. In this context comparing the fall-off of the coupling constants with the fall-off of the Laplacian kernel Q (3.48), one sees that the shape of the fall-offs are very similar. Therefore we have fitted at $\beta = 2.32$ the coupling constants λ_{11,r^2} to $-c_2 Q(r)$ via the free variable c_2. In Fig. 7.4 we see that the shape of the coupling constants then agree very well.

We have done the same for the linear model at $p_{max} = 1$ with an additional potential term $\lambda_{11,0} \sum_i \chi_{1,i}^2$. The obtained model is then very similar to the model (3.47) proposed by J. Greensite and K. Langfeld. On a lattice of with $16^3 \times 4$ and at $\beta = 2.22$ we have applied to our couplings λ_{pp,r^2} (calculated in the IMC method) the mapping 3.51. A fit to our coupling constants obtained with the IMC-Method leads to $c_1 = 3.6(7)$ and $c_2 = 0.42(7)$, which are not too far from the values $c_1 \approx 4.417(4)$ and $c_2 \approx 0.498(1)$, calculated by Greensite and Langfeld.

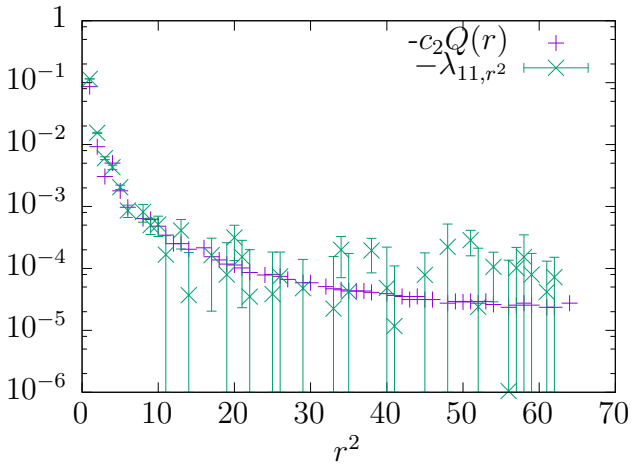

Figure 7.4: Fit of $-c_2Q(r)$ to coupling constants λ_{11,r^2}, obtained by IMC for the simple linear model with $p_{max} = 3$ at $\beta = 2.32$, yielding the fitted value $c_2 = 0.39 \pm 0.07$

These results suggests that a Laplacian form $Q(r)$ might indeed be the correct ansatz in order to describe the coupling constants as a function of the interaction distance. However, as mentioned, in the work of Greensite and Langfeld such a Laplacian form has only been used for short-range interaction terms, where a hard cut-off is applied at $r_{max} = 3$. In Fig. 7.5 we have therefore plotted the Polyakov loop expectation value for the simple linear model (left) and the simple linear model with an additional potential term (right), where we have applied the mapping 3.51 upfront and calculated the remaining coupling constants c_1, c_2 directly via the IMC method, to then simulate the resulting effective models. However, instead of applying a cut-off at $r_{\max} = 3$, we go beyond that value and again gradually increase the maximum interaction distance up to the value 9. The results reveal that the Laplacian fall-off seems to describe the Yang-Mills theory well in the center symmetric phase until right before the phase transition with a cut-off applied at $r_{max} = 3$. However it fails to describe the theory in the broken phase. Trying to improve results in the broken phase by increasing the cut-off value $r_{\max}$ fails, as an unphysical peak around the Yang-Mills phase transition occurs when going to large values for r_{max}. This suggests that the Laplacian kernel Q yields only in the unbroken phase, where it is sufficient to include short range interaction terms, a good approximation for the coupling constants, but cannot be used beyond that for highly non-local models. Although the match of the independent coupling constants and the coupling constants related via the Laplacian kernel Q presented in 7.4 seemed to be qualitatively well, the resulting models yield quite different results.

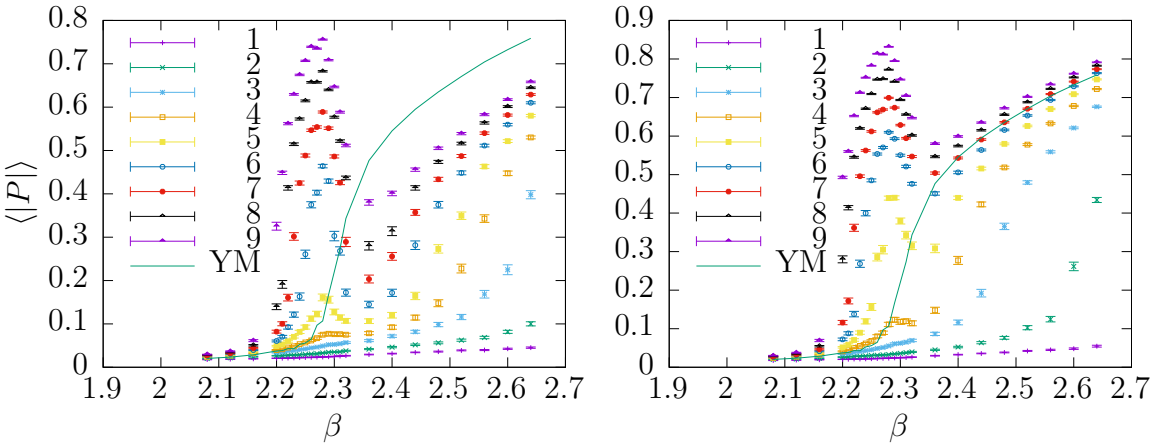

Figure 7.5: Polyakov loop expectation value for the linear model (left) and simple linear model with an additional potential term (right) both with $p_{max} = 1$, with number of coupling constants for non-local terms reduced to 1 by assuming a Laplacian slope

7.3 Exponential Fit

Since a complete description of the non-local coupling constants as a function of the interaction distance, as depicted in Fig. 7.1, seems to be difficult and not matching the Laplacian Kernel $Q(r)$, let us now focus on the short distance part, which seems to obey an exponential fall-off. We already noticed earlier that an approximation of the full theory with non-local effective models is less accurate in the region around the phase transition and requires taking into account interaction terms of larger distance and higher representations in the effective action. The exponential fall-off of the coupling constants at short interaction distances might reflect the need for large range interaction terms. In order to quantify this behavior we will apply an exponential fit, which will be dominated by the first few coupling constants, and define a correlation length $\xi(\beta)$ in order to check for critical scaling via

$$\lambda(r) \propto a(\beta) \cdot \exp\left(-\frac{r}{\xi(\beta)}\right). \tag{7.1}$$

The resulting characteristic length as a function of β for fixed temporal extend and two different values $N_s = 16, 32$ is shown in Fig. 7.6. As can be seen, there is a rather small peak in the characteristic length around $\beta_c \approx 2.30$, which seems not to scale with the spatial volume at all. In Fig. 7.7 we have done the same for different values $N_t = 4, 6, 8$ at constant aspect ratio equal to 4. As we see with increasing value of N_t the size of the peak grows (Fig. 7.7 (left)), corresponding to a growth of the correlation the long range coupling constants in the large N_t limit. However this describes the growth of characteristic length in lattice units. Dividing the characteristic length by N_t (Fig. 7.7 (right)) gives us a rough estimation of the characteristic length in physical units and we see

that the characteristic length measured in physical units actually decreases in the large N_t limit. The non-scaling for large N_s and the decrease in physical units for large N_t might suggest that the effective models become local again in the thermodynamical limit.

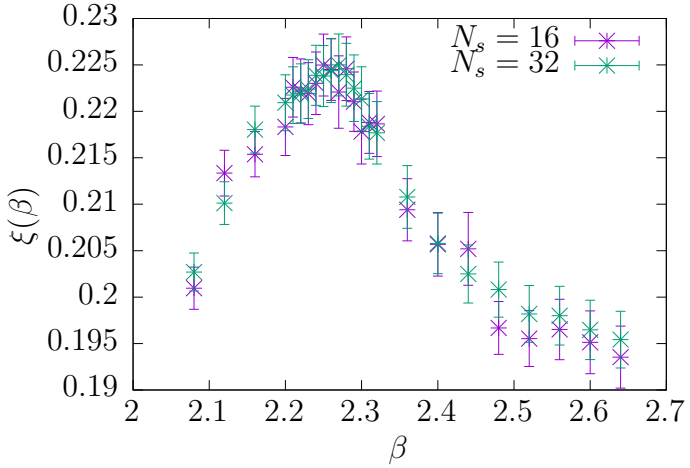

Figure 7.6: Characteristic length $\xi(\beta)$ of the coupling constants λ_{11,r^2} as a function of β for different values $N_s = 16, 32$ at $N_t = 4$

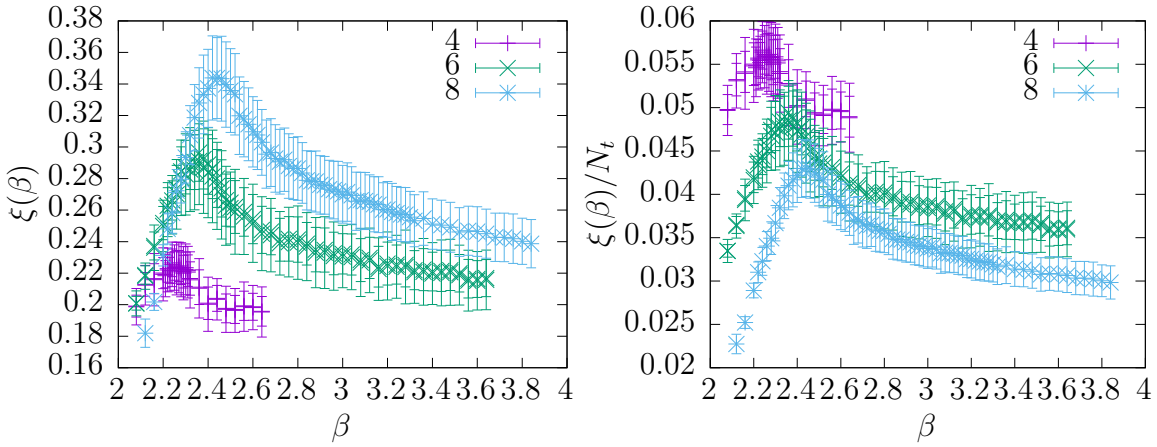

Figure 7.7: Characteristic length $\xi(\beta)$ (left) and $\xi(\beta)/N_t$ (right) of the coupling constants λ_{11,r^2} as a function of β for different values $N_t = 4, 6, 8$ at fixed aspect ratio 4

An interesting feature of the peak in the characteristic length is that it arises around the phase transition of the full theory instead of the effective model, which can be seen very clearly for $N_t = 8$, where the difference between critical Yang-Mills value and critical values of the effective model is the largest. In Table 7.1 we have summarized the

N_t	β_c		
		simple lin. model	
	YM	Pos. of peak in char. length $\xi(\beta)$	Pos. of peak in susceptibilities
4	2.30	2.25 ± 0.05	2.32 ± 0.05
6	2.43	2.35 ± 0.07	2.52 ± 0.05
8	2.51	2.44 ± 0.06	2.71 ± 0.05

Table 7.1: Critical value β_c from Yang-Mills theory obtained by eq. (6.1) vs. critical value from of the simple linear model ($p_{\max} = 3$, $r_{\max} = 9$) by determining the peak in the characteristic length $\xi(\beta)$ (7.1) and determining the peak in the Polyakov loop susceptibility.

critical values β_c of the full Yang-Mills theory as obtained by eq. 6.1 vs. the critical value for the simple linear model ($p_{\max} = 3$, $r_{\max} = 9$) determined by the location of the peak in the characteristic length $\xi(\beta)$ vs. the critical value obtained by the location of the peak in the Polyakov loop susceptibility. As we see the peak in Fig. 7.7 is approximately at the phase transition of the full theory, instead of the phase transition of the effective model. This means that even though the effective models critical coupling constants are shifted to larger values, the information about the critical coupling of the full theory is still contained in the effective model. We have seen earlier a related behavior in the effective models, where the dominant coupling constant $\lambda_{11,1}(\beta)$ showed a kink at the Yang-Mills phase transition.

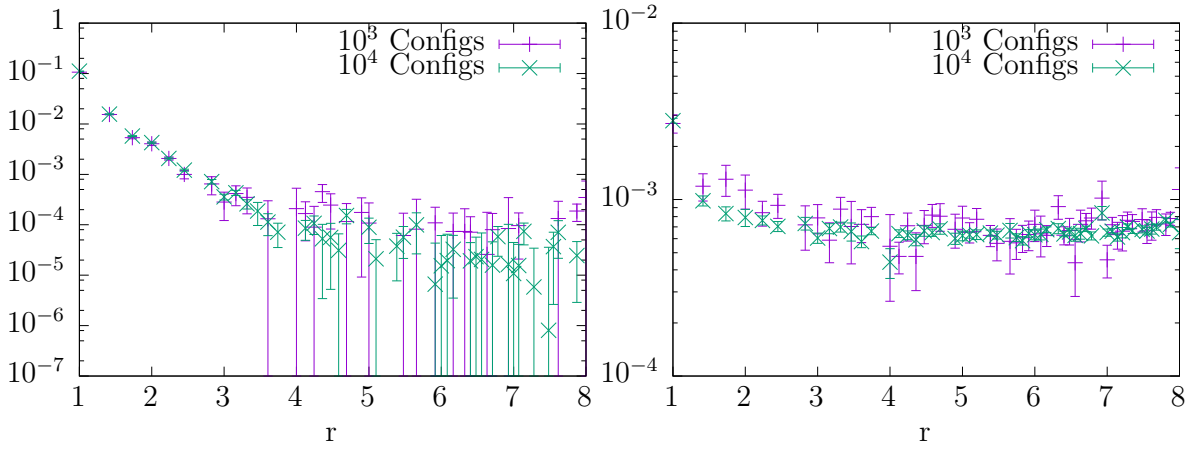

Figure 7.8: Coupling constants λ_{11,r^2} for the fundamental (left) and λ_{22,r^2} for the adjoint (right) representation as a function of the distance r taken from model with $p_{max} = 3$ at $\beta = 2.30$ for 10^3 and 10^4 configurations compared

The fact that the characteristic length, which is defined by an exponential fit of the coupling constants, has a peak exactly at the critical coupling constant of the full theory, suggests that, even though at larger distances the coupling constants reach a plateau, there might be more to an exponential fit than we first assumed. We have argued earlier that we cannot cut off the plateau, as the value of the long range coupling constants are important for the improvement of results in the effective models. We had argued that their taken values can therefore not be completely disregarded as statistical errors. However, keeping in mind the significance of the exponential fall-off, we can suspect that the values at large distances are shifted away from their "true" values due to errors. It seems plausible that with more accuracy the exponential fall-off should extend to large interaction distances. If this is true, then the plateau should sink towards the extrapolation of the exponential fit at short distances, when we increase the accuracy of the calculations by increasing the number of configurations. In Fig. 7.8 we have plotted the coupling λ_{11,r^2} as a function of the interaction distance for different numbers of configurations (10^3 and 10^4). It seems that increasing the number of configurations by a factor of 10 indeed yields a slight sinking of the plateau. Although this effect is very small and therefore does not prove our assumption, it at least leaves the possibility that our suspicion is right and we would get an over all more exponential form with sufficient accuracy.

Concluding this chapter we have seen that the non-local coupling constants as a function of the interaction distance yield an exponential fall-off at short interaction distances and a constant plateau at larger ones. We have found arguments that applying a hard-cutoff for large distance interactions seems not to be justified if one wants to go beyond universal behavior and obtain an approximation of the full Yang-Mills theory in term of non-local Polyakov loop models. Furthermore we have seen that a Laplacian kernel $Q(r)$ seems to describe the non-local fall-off only for small values of β before the phase transition, where one can neglect long range interaction terms. However, such a description breaks down after the phase transition where one has to take into account interaction terms at larger distances. We have furthermore found that approximating the fall-off by an exponential function reveals critical behavior of the effective models in the corresponding characteristic correlation length, suggesting that in spite of the long range plateau, and exponential fall-off seems the most plausible ansatz to describe the non-local behavior of the coupling constants. We then found signs that for large enough accuracy the plateau might indeed sink and yield an exponential fall-off over a larger range.

Chapter 8

Conclusion and Outlook

In this work we have investigated for the $SU(2)$ Yang-Mills theory different non-local Polyakov loop models. After having introduced the basic physical theory, including concepts of quantum field theory, Lie groups and Lie algebras, we discussed how to derive different effective Polyakov loop models and ordering schemes in the strong coupling limit. We then introduced the inverse Monte-Carlo method and explained how to use it in order to map the Yang-Mills theory at given values of the coupling constant β to the coupling constants of our effective models, which have been used as free parameters for the IMC method. In the results chapter we have then used the obtained effective coupling constants $\lambda(\beta)$ to simulate different observables $\langle O(\beta)\rangle_{\text{eff}}$ for the non-local effective models and compared them to the results $\langle O(\beta)\rangle_{\text{YM}}$ of the full Yang-Mills theory, in order to investigate the non-local models.

We saw that in case of a $SU(2)$ theory the IMC method works fairly well, producing consistent improvements for the models by a gradual increase of the number of degrees of freedom taken into account, even up to a number of 325. In the first results chapter we saw that for local theories a logarithmic resummation of higher order terms occurring in the strong coupling expansion improves results, especially local Polyakov loop distributions, significantly compared to the linear model, where shapes of local Polyakov loop distributions near and in the broken phase are deformed and the value of the critical coupling is shifted to larger values compared to the full theory. Taking into account local terms with higher representations, we saw that the logarithmic model does not improve much. Although the linear model does improve, it is not until we include a potential term that shapes of Polyakov loop distributions in the broken phase can be reproduced correctly.

In all cases, the critical value β_c of the effective local models seems to converge to a similar value still shifted significantly away to larger values compared to the Yang-Mill result. We saw that we have to take into account non-local terms in order to fix this. Trying to extend the logarithmic models to the non-local case, we run into problems regarding the convergence of observables in the logarithmic model. The expectation value of the Polyakov loop does not improve gradually when increasing the non-locality

of the logarithmic model and a convergence to the Yang-Mills theory seems rather unlikely, forcing us to drop the logarithmic model as an useful ansatz for non-local models in order to derive effective models that provide us with good results in the region of the phase transition. On the other hand both classes (simple and extended) non-local linear models provide suitable ansatzes for non-local effective models, yielding gradual improvements in every step, when increasingly taking into account terms of higher orders. On a lattice with $N_t = 4$ the effective linear models already provide very good approximations of the full theory at $p_{\max} = 3$ and $r_{\max} = 9$. We argued that this good behavior, compared to the difficult behavior of the logarithmic models, arises from the fact that linear ansatzes provide much more general ansatzes and in contrast to the logarithmic models, which assume certain relations between different terms, which only hold true in the strong coupling limit.

In spite of the gradual improvements of the linear models by increase of the maximum interaction distance, improvements near the phase transition seemed to rather slow, which, as we argued, reflects the large range correlation of the Yang-Mills theory at the phase transition, forcing us to take into account terms of even higher order and distances in order to obtain further improvements in that region. Further investigations of convergence of the linear models in the limit of large interaction distances on a lattice of fixed size have proven to be rather difficult and we therefore turned to arguments that let us speculate about the behavior of the models in the thermodynamical limit. Therefore we first showed that an aspect ratio $N_s/N_t = 4$ yields, even for the highly non-local models, finite size effects that are rather small. We then investigated the effective models on larger lattices with $N_t = 4, 6, 8$ and $N_s/N_t = 4$. The results on the larger lattices suggested that at fixed physical maximum interaction distance, the effective linear models yield approximations with decreasing accuracy as we increase the temporal extend of the lattice. We argued that this is due to the fact that including terms with Polyakov loops in higher and mixed representations gain significance when increasing the value of N_t.

In the last results-chapter of this work we then focused on investigating the non-local behavior of the effective models. We tried to determine the analytical form of the fall-off of the non-local coupling constants with the interaction distance. We showed that the coupling constants as a function of the interaction distance typically show an exponential fall-off at short distances, followed by a plateau at larger ones. We argued that the plateau at larger distances cannot be neglected and that the values of the coupling constants at larger distances indeed are important in providing improvements for the effective models. We found that, although the fall-off qualitatively looked like it could be described by the Laplacian kernel Q, proposed by Greensite and Langfeld, it is only in the center symmetric phase, where including short range interactions is sufficient, an appropriate description of the coupling constants, but leads to wrong results in the broken phase. An exponential fit of the coupling constants at short distances defines an characteristic length associated with the coupling constants, which describes their correlation at large distances. We saw that this characteristic length exhibits critical behavior

around the phase transition of the full Yang-Mills theory, instead of the effective phase transition, which seems to suggest that indeed an exponential fall-off of the coupling constants is be the most reasonable ansatz between the suggestes ones. Therefore we argued that, even though the values of the coupling constants at large distances cannot be neglected completely, their values as obtained by the IMC method could be shifted to larger values due to statistical errors and that increasing the accuracy of the calculations should provide an exponential fall-off for the non-local coupling constants over a larger range of interaction distances. Increasing the number of configurations we found a small decrease of the plateau, which left the possibility for our argument to hold true. But as the decrease was rather small, it provided no reliable proof for our claim.

As for future ways in order to progress this work, it would be interesting to further check the possibility of an exponential form for the fall-off of the non-local couplings. Therefore we could apply the IMC method and simulations to effective models that assume an exponential fall-off already in the ansatz for the action. A calculation of critical exponents of our effective models might also yield interesting insights, since (as already mentioned) spin models with long-range interaction terms are not subject to the Svetitsky-Yaffe conjecture and it is therefore not clear if the various ways of gradually extending truncation schemes and taking into account more interaction terms leaves the universal behavior of the models unaffected. Furthermore we can extend the non-local ansatzes to models containing fermions and combined with the hopping expansion we could then investigate the phase diagramm of non-local Polyakov loop theories with heavy fermions and perform calculations at finite density. It would be also interesting to extend the used ansatzes and method to derive effective models for gauge theories with other gauge groups, such as G_2 and $SU(3)$, where results for an ansatz that assumes an exponential fall-off between the coupling might be especially interesting, as we know, we cannot include too many couplings in order to avoid instabilities of the IMC method and therefore have to reduce the number of couplings of non-local models by assuming some kind of analytical relationship between the couplings.

Appendix A

Represenations of Groups and Algebras

A.1 Gamma Matrices

The gamma matrices satisfy the Clifford algebra, whose defining property is the anti-commutation relation

$$\{\gamma^\mu, \gamma^\nu\} = \gamma^\mu\gamma^\nu + \gamma^\nu\gamma^\mu = 2\eta^{\mu\nu}\mathbb{1}_{4\times 4}. \tag{A.1}$$

where $\eta^{\mu\nu}$ is the Minkowski metric with signature $(+,-,-,-)$.

Furthermore

$$\gamma_\mu = \eta_{\mu\nu}\gamma^\nu = \left\{\gamma^0, -\gamma^1, -\gamma^2, -\gamma^3\right\}, \gamma^5 := \gamma^0\gamma^1\gamma^2\gamma^3 \tag{A.2}$$

The Dirac represenation of the gamma matrices is given by

$$\gamma^0 = \begin{pmatrix} 1 & 0 & 0 & 0 \\ 0 & 1 & 0 & 0 \\ 0 & 0 & -1 & 0 \\ 0 & 0 & 0 & -1 \end{pmatrix}, \qquad \gamma^1 = \begin{pmatrix} 0 & 0 & 0 & 1 \\ 0 & 0 & 1 & 0 \\ 0 & -1 & 0 & 0 \\ -1 & 0 & 0 & 0 \end{pmatrix}$$
$$\gamma^2 = \begin{pmatrix} 0 & 0 & 0 & -i \\ 0 & 0 & i & 0 \\ 0 & i & 0 & 0 \\ -i & 0 & 0 & 0 \end{pmatrix}, \qquad \gamma^3 = \begin{pmatrix} 0 & 0 & 1 & 0 \\ 0 & 0 & 0 & -1 \\ -1 & 0 & 0 & 0 \\ 0 & 1 & 0 & 0 \end{pmatrix}. \tag{A.3}$$

The Weyl or Chiral represenation is given by

$$\gamma^0 = \begin{pmatrix} & 1 \\ 1 & \end{pmatrix}, \quad \gamma^i = \begin{pmatrix} & \sigma^i \\ -\sigma^i & \end{pmatrix}, \quad \gamma^5 = \begin{pmatrix} -1 & \\ & 1 \end{pmatrix} \tag{A.4}$$

such that γ_5 and chiral projection operators are diagonal

$$\gamma^5 = \begin{pmatrix} -1 & \\ & 1 \end{pmatrix}, \quad P_L = \frac{1-\gamma^5}{2} = \begin{pmatrix} 1 & \\ & 0 \end{pmatrix}, \quad P_R = \frac{1+\gamma^5}{2} = \begin{pmatrix} 0 & \\ & 1 \end{pmatrix}. \tag{A.5}$$

A.2 The Lie Group SU(2)

The Lie group SU(2) can be parametrized in the defining represenation via

$$SU(2) = \left\{ \exp\left(-\tfrac{\mathrm{i}}{2}\vec{\alpha}\cdot\vec{\sigma}\right) \middle|\, \vec{\alpha} \in \mathbb{R}^3 \right\}, \tag{A.6}$$

where the matrices σ_i, $i = 1, 2, 3$ are a basis for the algebra, given by all traceless, hermitian (2×2)-matrices.

Its algebra is of dimension 3 and a possible choice are the Pauli matrices, defined by

$$\sigma_1 = \begin{pmatrix} 0 & 1 \\ 1 & 0 \end{pmatrix}, \quad \sigma_2 = \begin{pmatrix} 0 & -\mathrm{i} \\ \mathrm{i} & 0 \end{pmatrix}, \quad \sigma_3 = \begin{pmatrix} 1 & 0 \\ 0 & -1 \end{pmatrix}. \tag{A.7}$$

With

$$\sigma_0 := \begin{pmatrix} 1 & 0 \\ 0 & 1 \end{pmatrix} \tag{A.8}$$

they satisfy the relation

$$\sigma_1^2 = \sigma_2^2 = \sigma_3^2 = \sigma_0^2 = \sigma_0. \tag{A.9}$$

The values of their determinants and traces are

$$\begin{aligned} \det \sigma_i &= -1 \\ \operatorname{tr} \sigma_i &= 0 \end{aligned} \quad \text{for } i = 1, 2, 3, \tag{A.10}$$

which implies that the Pauli matrices σ_i have eigenvalues +1 und -1.
Furthermore they satisfy the relations

$$\sigma_1\, \sigma_2\, \sigma_3 = \mathrm{i}\, \sigma_0, \tag{A.11}$$

and

$$\sigma_i\, \sigma_j = \delta_{ij}\sigma_0 + \mathrm{i} \sum_{k=1}^{3} \epsilon_{ijk}\, \sigma_k \text{ for } i, j = 1, 2, 3, \tag{A.12}$$

$$\tag{A.13}$$

hence the angular momentum and Clifford algebras

$$[\sigma_i\,, \sigma_j] = \sigma_i\, \sigma_j - \sigma_j\, \sigma_i = 2\,\mathrm{i} \sum_{k=1}^{3} \epsilon_{ijk}\, \sigma_k \text{ for } i, j = 1, 2, 3, \tag{A.14}$$

$$\{\sigma_i\,, \sigma_j\} = \sigma_i\, \sigma_j + \sigma_j\, \sigma_i = 2\, \delta_{ij}\sigma_0 \text{ for } i, j = 1, 2, 3. \tag{A.15}$$

A.2.1 SU(2) Reduction Formulas

Using formula 2.48 we get

$$\begin{aligned} &[D(p)] = (p), \in \mathbb{N}_0, \\ &D(p) = p + 1 \end{aligned} \tag{A.16}$$

Dynkin labels vs. dimension of represenation. As known by Spin: $d_r = 2s + 1$, $(2s) = 1, 2, \ldots$ is the Dynkin label and d_r is the dimension of the represenation, i.e. the dimension of the multiplet with spin s.

$$\begin{aligned} &(0) = [1], && \text{(trivial represenation)} \\ &(1) = [2], && \text{(fundamental represenation)} \\ &(2) = [3], && \text{(adjoint represenation)} \\ &(3) = [4] \end{aligned} \tag{A.17}$$

Using formula 2.47 for the Reduction of products, as known by coupling of particles with spin $s = 1/2$

$$\begin{aligned} &[2] \otimes [2] = [3] \oplus [1] \\ &[2] \otimes [2] \otimes [2] = [4] \oplus [2] \oplus [2] \end{aligned} \tag{A.18}$$

and for the Characters $\chi_{(n_1,\ldots,n_{rk})} = \chi_{[d_r]}$. We will label the caracters by the dimension of its represenation insteaf of its Dynkin label and ommit the brackets.

$$\begin{aligned} &\chi_2 \\ &\chi_3 = \chi_2^2 - 1, \\ &\chi_4 = \chi_2(\chi_2^2 - 2). \end{aligned} \tag{A.19}$$

A.3 The Lie Group SU(3)

The Lie group SU(3) is of rank 2 and its algebra if of dimension 8. It can be parametrized in the defining represenation via

$$SU(3) = \left\{ \exp\left(-\mathrm{i}\vec{\alpha} \cdot \vec{T}\right) \middle| \, \vec{\alpha} \in \mathbb{R}^8 \right\}, \tag{A.20}$$

where the matrices α_i, $i = 1, \ldots, 8$ are a basis of the set of traceless, hermitian $(3x3)$-matrices.

The standard choise of generatros in the defining representation, are given by

$$T_a = \frac{\lambda_a}{2} \tag{A.21}$$

where the Gell-Mann matrices

$$\lambda_1 = \begin{pmatrix} 0 & 1 & 0 \\ 1 & 0 & 0 \\ 0 & 0 & 0 \end{pmatrix} \qquad \lambda_2 = \begin{pmatrix} 0 & -i & 0 \\ i & 0 & 0 \\ 0 & 0 & 0 \end{pmatrix}$$
$$\lambda_3 = \begin{pmatrix} 1 & 0 & 0 \\ 0 & -1 & 0 \\ 0 & 0 & 0 \end{pmatrix} \qquad \lambda_4 = \begin{pmatrix} 0 & 0 & 1 \\ 0 & 0 & 0 \\ 1 & 0 & 0 \end{pmatrix}$$
$$\lambda_5 = \begin{pmatrix} 0 & 0 & -i \\ 0 & 0 & 0 \\ i & 0 & 0 \end{pmatrix} \qquad \lambda_6 = \begin{pmatrix} 0 & 0 & 0 \\ 0 & 0 & 1 \\ 0 & 1 & 0 \end{pmatrix}$$
$$\lambda_7 = \begin{pmatrix} 0 & 0 & 0 \\ 0 & 0 & -i \\ 0 & i & 0 \end{pmatrix} \qquad \lambda_8 = \frac{1}{\sqrt{3}} \begin{pmatrix} 1 & 0 & 0 \\ 0 & 1 & 0 \\ 0 & 0 & -2 \end{pmatrix} \tag{A.22}$$

are the analog of the Pauli matrices in SU(2) and obtained by different embeddings of the subgroup SU(2).

The T- generators obey the relations

$$[T_a, T_b] = i \sum_{c=1}^{8} f_{abc} T_c \tag{A.23}$$

$$\{T_a, T_b\} = \frac{1}{3}\delta_{ab} + \sum_{c=1}^{8} d_{abc} T_c \tag{A.24}$$

or equivalently

$$\{\lambda_a, \lambda_b\} = \frac{4}{3}\delta_{ab} + 2 \sum_{c=1}^{8} d_{abc} \lambda_c, \tag{A.25}$$

with the structure constants

$$\begin{aligned} f_{123} &= 1 \\ f_{147} &= -f_{156} = f_{246} = f_{257} = f_{345} = -f_{367} = \frac{1}{2} \\ f_{458} &= f_{678} = \frac{\sqrt{3}}{2}, \end{aligned} \tag{A.26}$$

while the remaining structure constants, which are not related to these by permutation, are zero.

The symmetric coefficient d-coefficients take the values:

$$\begin{aligned} d_{118} &= d_{228} = d_{338} = -d_{888} = \frac{1}{\sqrt{3}} \\ d_{448} &= d_{558} = d_{668} = d_{778} = -\frac{1}{2\sqrt{3}} \\ d_{146} &= d_{157} = -d_{247} = d_{256} = d_{344} = d_{355} = -d_{366} = -d_{377} = \frac{1}{2} \ . \end{aligned} \tag{A.27}$$

As a topological space SU(3) is a non-trivial, locally trivial bundle of a 3-sphere over a 5-sphere.

Casimir operators and eigenvalues

SU(3) has two Casmimir operators. The squared sum of the Gell-Mann matrices gives the quadratic Casimir operator and yields for the defining represenation

$$C = \sum_{i=1}^{8} \lambda_i \lambda_i = 4/3. \tag{A.28}$$

The second Casimir operator is cubic and the both of them are given in terms of the generators via

$$\hat{C}_1 = \sum_k \hat{T}_k \hat{T}_k = (p^2 + q^2 + 3p + 3q + pq)/3, \tag{A.29}$$

$$\hat{C}_2 = \sum_{jkl} d_{jkl} \hat{T}_j \hat{T}_k \hat{T}_l = (p - q)(3 + p + 2q)(3 + q + 2p)/18. \tag{A.30}$$

Cartan generators and ladder operators

The standard choice of generators for the Cartan algebra is given by

$$\begin{aligned} T_3 &= F_3 \\ Y &= \frac{2}{\sqrt{3}} F_8 \end{aligned} \tag{A.31}$$

and the corresponding ladder operators are given by

$$\begin{aligned} T_\pm &= F_1 \pm i F_2 \\ V_\pm &= F_4 \pm i F_5 \\ U_\pm &= F_6 \pm i F_7 \end{aligned} \tag{A.32}$$

A.3.1 SU(3) Reduction Formulas

Dynkin labels vs. dimension of represenation

$$
\begin{array}{llll}
(0,0) = [1], & & & \text{(trivial represenation)},\\
(1,0) = [3], & (0,1) = [\bar{3}], & & \text{(fundamental represenations)}\\
(2,0) = [6], & (0,2) = [\bar{6}], & (1,1) = [8], & \\
(2,1) = [15], & (1,2) = [\bar{15}], & (3,0) = [10], \quad (0,3) = [\bar{10}] &
\end{array} \tag{A.33}
$$

$$
\begin{aligned}
&[D(p,q)] = (p,q) \in \mathbb{N}_0^2,\\
&D(p,q) = \frac{1}{2}(p+1)(q+1)(p+q+2),
\end{aligned} \tag{A.34}
$$

Reduction

$$
\begin{aligned}
&[3] \otimes [3] = [6] \oplus [\bar{3}]\\
&[3] \otimes [\bar{3}] = [8] \oplus [1]\\
&[3] \otimes [6] = [10] \oplus [8]\\
&[3] \otimes [\bar{6}] = [\bar{15}] \oplus [\bar{3}]\\
&[3] \otimes [8] = [15] \oplus [\bar{6}] \oplus [\bar{3}]
\end{aligned} \tag{A.35}
$$

Characters $\chi_{(n_1,\ldots,n_{rk})} = \chi_{[d_r]}$ (for SU(3) we can ommit the different kind of brackets, since it is clear if we using the Dynkin label or the dimension as an index)

$$
\begin{aligned}
&\chi_3, \quad \chi_{\bar{3}},\\
&\chi_6 = \chi_3^2 - \chi_{\bar{3}},\\
&\chi_8 = \chi_3\chi_{\bar{3}} - 1,\\
&\chi_{10} = \chi_3^3 - 2\chi_3\chi_{\bar{3}} + 1,\\
&\chi_{15} = \chi_3^2(\chi_{\bar{3}} - 1) - 2\chi_3 + \chi_{\bar{3}}
\end{aligned} \tag{A.36}
$$

the others are obtained by

$$
\chi_{\bar{i}} = \bar{\chi}_i \tag{A.37}
$$

Appendix B

Surface Integrals in Spatial Strong Coupling Expansion

B.1 Elementary Cube

We integrate over spatial links of an elementary cube, which can either enclose a spatial volume and hence contain not timelike links, or a spacetime-volume, in which case the time-like axis is set to be in horizontal direction.

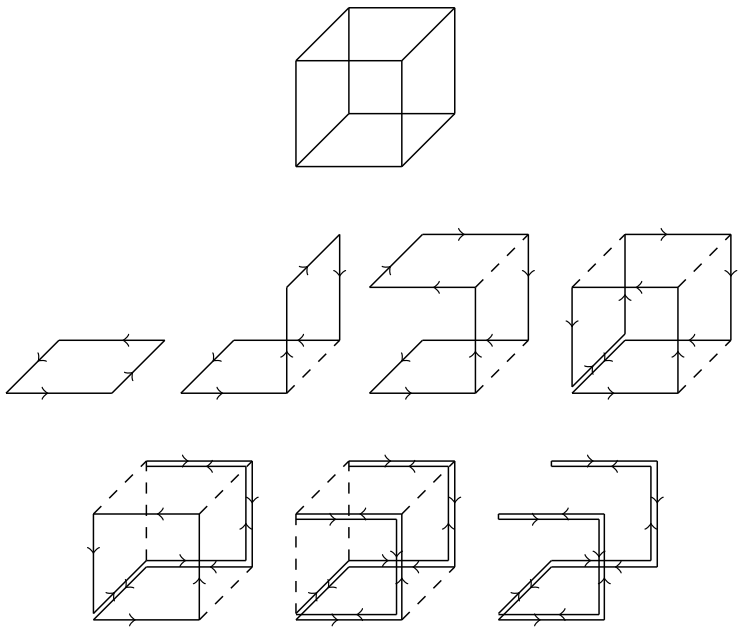

Figure B.1: Integration of Spatial Links of an Elementary Cube

We integrate step by step over spatial links, using integration rule 3.12, until all plaquettes are connected integration rule 3.12 is exhausted. For illustration purposes,

we start with one plaquette and gradually add the others plaquettes to the picture, such that the new plaquette is connected to the others via a spatial link, and immidiately integrate over a the common spatial link. We see that not all links will be integrated out before integration rule 3.12 is exhausted but the remaining links describe a path back and forth and yields a term of the form

$$\chi_r\left(\left(\prod_{i=1}^{7} U_i\right)\left(\prod_{i=1}^{7} U_i\right)^{-1}\right) = \chi_r(\mathbb{1}). \tag{B.1}$$

B.2 Two Timelike Connected Elementary Ladders

We integrate over the spatial links of two elementary ladders in timelike direction that are connected only via timelike links (fig. B.2 (top)).

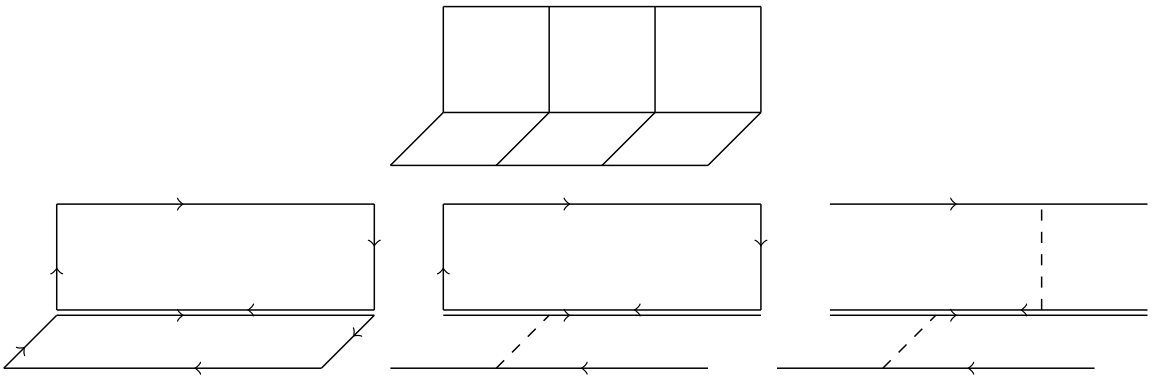

Figure B.2: Integration of spatial links for two by spatial links not connected elementary ladders

We us integration rule 3.12 to integrate in the first step over all inner spatial links (fig. B.2 (bottom, left)). In the second step we use the integration rule 3.13 to integrate over the spatial links on the left and right edge of the lower elementary ladder, which are identified via lattice periodicy and obtain an interaction pair (fig. B.2 (bottom,middle)). We do the same for the upper elementary ladder and obtain another elementary interaction pair (fig. B.2 (bottom, right)), leading to an overall interaction term of the form

$$\sim \bar{\chi}_r(P_i)\chi_r(P_j) \cdot \bar{\chi}_r(P_j)\chi_r(P_k), \qquad < i,k >= \sqrt{2}a. \tag{B.2}$$

B.3 Two Ladders Connected by spatial Decorations

We integrate over the spatial links of two elementary ladders in timelike direction that are connected only via additonal spatial decorations (fig. B.3).

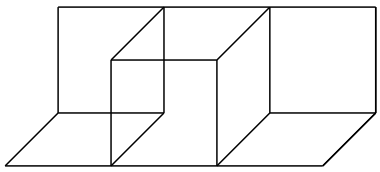

Figure B.3: Two elementary ladders connected via spatial decorations

We integrate step by step over the spatial links (fig B.4). We see that the whole surface can be joined by applying integration rule 3.12, yielding only one character function for the whole surface. In the last step we use integration rule 3.13, to integrate over the spatial links on the left and on the right edge of the surface, which are indentified by lattice periodicy, and obtain one interaction term of the form

$$\sim \chi_r(P_i)\bar{\chi}(P_j), \qquad < i,j >= \sqrt{2}a. \tag{B.3}$$

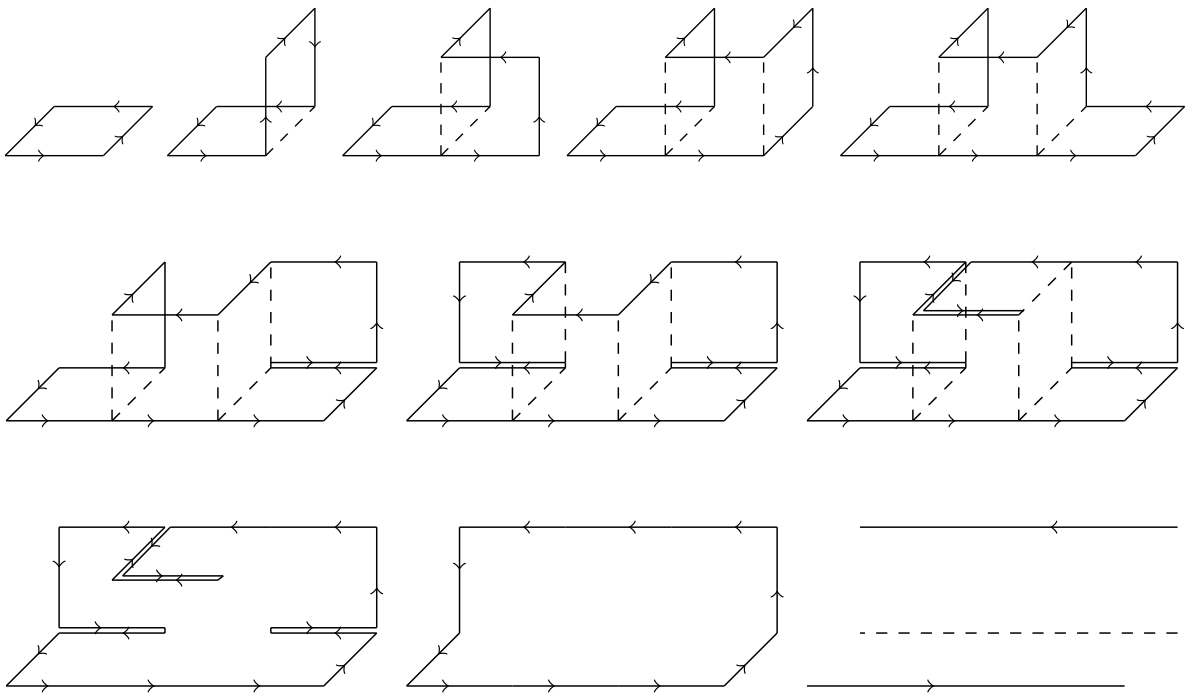

Figure B.4: Integration of spatial links for two by spatial links connected elementary ladders

Appendix C

IMC Method

C.1 Class Function Proof

Claim:

For class functions F and $\tilde{F}$

$$\vec{L} \cdot (F\vec{L}\tilde{F}) = F\vec{L}^2\tilde{F} + \vec{L}F \cdot \vec{L}\tilde{F}, \tag{C.1}$$

is again a class function itself.

Proof:

It can be easily shown by applying a character expansion to the functions F and $\tilde{F}$, which takes for $\tilde{F}$ (and similarly for F) to apply a sum over characters in all irreducible represenations χ_r of the form

$$\tilde{F}(g) = \sum_k a_k \chi_k(g). \tag{C.2}$$

which reduces all derivatives occuring in eq. C.1 to the derivatives

$$L_a\chi_p(g) = \lim_{t\to 0} \frac{\chi_p(\exp(t\,T_a)g - \chi_p(g))}{t} = \chi_p\left(\frac{(\exp(t\,T_a)-1)}{t}g\right)\Big|_{t=0} = \chi_p(T_a g), \tag{C.3}$$

$$L_a^2\chi_p(g) = \chi_p(T_a^2 g) \tag{C.4}$$

and one is therefore left with showing for eq. C.1 the invariance of the terms

$$\sum_a \chi_p(T_a^2 g), \qquad\qquad \sum_a \chi_p(T_a g)\chi_q(T_a g), \tag{C.5}$$

under the action $g \to hgh^{-1}$, for $h \in G$. Invariance of the first term is obvious since $\sum_a \chi_p(T_a^2 g) = \chi_p(\sum_a T_a^2 g)$ and $\sum_a T_a^2$ is the quadratic Casimir operator and commutating with all group elements. The latter statement can be seen by noticing that invariance

of the Killing metric $\mathrm{Tr}(T_a T_b)$ means that $h^{-1}T_a h$ is just a rotation of T_a with respect to this metric and can be expanded as $R_a^c T_c$ with an orthogonal matrix R. Therefore

$$\sum_a \chi_p(T_a hgh^{-1})\chi_q(T_a hgh^{-1}) = \sum_a \chi_p(h^{-1}T_a hg)\chi_q(h^{-1}T_a hg) =$$
$$\sum_a \chi_p(R_a^c T_c g)\chi_q(R_a^d T_d g) = \sum_{c,d} \delta^{cd}\chi_p(T_c g)\chi_q(T_d g) = \sum_a \chi_p(T_a g)\chi_q(T_a g), \tag{C.6}$$

proving alltogether the invariance of eq. C.1.

C.2 SU(3) IMC Method

For $SU(3)$ there are two fundamental represenation, complex conjugated to each other, hence $p, q = 1, 2$ The characters and the gemetric DSE will be complex.

$$\Pi_{lin} = \prod_{p=1}^{p_{max}} \prod_{r=1}^{r_{max}} \prod_{<i,j>=r} \exp\left(-\lambda_{p,r}(\chi_{p,i}\bar{\chi}_{p,j} + \bar{\chi}_{p,i}\chi_{p,j})\right) \tag{C.7}$$

We have two differnt geometric DSEs according to the two different values of p, hence

$$\sum_{i\in L} \left\langle \frac{1}{2}K_{p1,i}\left(\frac{\partial \vec{f}_i}{\partial \chi_i} + \vec{f}_i \frac{\partial ln\Pi_{1,i}(\vec{\lambda})}{\partial \chi_i}\right) + K_{p2,i}\left(\frac{\partial \vec{f}_i}{\partial \bar{\chi}_i} + \vec{f}_i \frac{\partial ln\Pi_{2,i}(\vec{\lambda})}{\partial \bar{\chi}_i}\right) - c_p\, \chi_{p,i}\, \vec{f}_i \right\rangle_{\text{full}} = \vec{0}, \tag{C.8}$$

with $p = 1, 2$.

The lowest Casimir eigenvalues are given by

$$\begin{aligned}
c_{[3]} &= c_{[\bar{3}]} = \frac{8}{3}, \\
c_{[8]} &= c_{(1,1)} = c_{[3]} + c_{[\bar{3}]} + 2\left(1 - \frac{2}{3}\right) = \frac{16}{3} + \frac{2}{3} = 6, \\
c_{[6]} &= c_{(2,0)} = c_{[3]} + c_{[3]} + 2\left(1 - \frac{1}{3}\right) = \frac{16}{3} + \frac{4}{3} = \frac{20}{3}, \\
c_{[\bar{6}]} &= c_{(0,2)} = c_{[\bar{3}]} + c_{[\bar{3}]} + 2\left(2 - \frac{4}{3}\right) = \frac{16}{3} + \frac{4}{3} = \frac{20}{3}.
\end{aligned} \tag{C.9}$$

From the reduction formulas we know that for a product of fundamental characters the reduction involves only the trival, the 6- and the 8 dimensional represenations and the only non-vanishing Glebsch-Gordon coefficients are all equal to one, hence

$$\begin{aligned}
C_{12}^{[8]} = C_{21}^{[8]} = C_{12}^{[1]} = C_{21}^{[1]} = 1, \\
C_{11}^{[6]} = C_{11}^{[\bar{3}]} = 1, \\
C_{22}^{[\bar{6}]} = C_{22}^{[3]} = 1.
\end{aligned} \tag{C.10}$$

Therefore we get for $K_{pq,i}$

$$\begin{aligned}
K_{11} &= \frac{16}{3}\chi^2 - \frac{20}{3}\chi_6 - \frac{8}{3}\chi_{\bar{3}} = \frac{16}{3}\chi^2 - \frac{20}{3}(\chi^2 - \bar{\chi}) - \frac{8}{3}\bar{\chi} = -\frac{4}{3}\chi^2 + 4\bar{\chi} \\
K_{12} &= K_{21} = \frac{16}{3}\chi\bar{\chi} - 6\chi_8 = \frac{16}{3}\chi\bar{\chi} - 6(\chi\bar{\chi} - 1) = -\frac{2}{3}\chi\bar{\chi} + 6 \\
K_{22} &= K_{11}^* = \frac{16}{3}\bar{\chi}^2 - \frac{20}{3}\chi_{\bar{6}} - \frac{8}{3}\chi_3 = \frac{16}{3}\chi^2 - \frac{20}{3}(\bar{\chi}^2 - \chi) - \frac{8}{3}\chi = -\frac{4}{3}\bar{\chi}^2 + 4\chi, \quad \text{(C.11)}
\end{aligned}$$

where have omitted the lattice index i and we have used for K_{12} that the Casimir eigenvalue of the trivial represenation is zero.

Since

$$\frac{\partial ln\Pi_{2,i}(\vec{\lambda})}{\partial\bar{\chi}_i} = \frac{\partial ln\Pi_{1,i}(\vec{\lambda})}{\partial\chi_i}^*, \tag{C.12}$$

if we set the functions f differently for each value $p = 1, 2$ according to

$$f^{(1)}_{l,d,i} = \frac{1}{\lambda_{l,d}}\frac{\partial \ln(\Pi_{l,d,i})}{\partial\chi_{1,i}}, \qquad \text{and} \qquad f^{(2)}_{l,d,i} = \frac{1}{\lambda_{l,d}}\frac{\partial \ln(\Pi_{l,d,i})}{\partial\bar{\chi}_{1,i}} = f^{(1)*}_{l,d,i}, \tag{C.13}$$

we get two complex conjugate equations

$$\sum_{i\in L}\left\langle \frac{1}{2}K_{p1,i}\left(\frac{\partial\vec{f}_i^{(p)}}{\partial\chi_i} + \vec{f}_i^{(p)}\frac{\partial ln\Pi_{1,i}(\vec{\lambda})}{\partial\chi_i}\right) + K_{p2,i}\left(\frac{\partial\vec{f}_i^{(p)}}{\partial\bar{\chi}_i} + \vec{f}_i^{(p)}\frac{\partial ln\Pi_{2,i}(\vec{\lambda})}{\partial\bar{\chi}_i}\right) - c_p\,\chi_{p,i}\,\vec{f}_i^{(p)}\right\rangle_{\text{full}} = \vec{0}, \tag{C.14}$$

with $p = 1, 2$.

For the linear systems we can write the equations as

$$\begin{aligned}
0 &= A\vec{\lambda} + \vec{v} = Re(A)\vec{\lambda} + iIm(A)\vec{\lambda} + \vec{v} + i\vec{v}, \\
A &= \sum_{i\in L}\left\langle \frac{1}{2}K_{p1,i}\left(\vec{f}_i^{(p)}\frac{\partial S_{1,i}(\vec{\lambda})}{\partial\chi_i}\right) + K_{p2,i}\left(\vec{f}_i^{(p)}\frac{\partial S_{2,i}(\vec{\lambda})}{\partial\bar{\chi}_i}\right)\right\rangle_{\text{full}}, \\
\vec{v} &= \sum_{i\in L}\left\langle \frac{1}{2}K_{p1,i}\left(\frac{\partial\vec{f}_i^{(p)}}{\partial\chi_i}\right) + K_{p2,i}\left(\frac{\partial\vec{f}_i^{(p)}}{\partial\bar{\chi}_i}\right) - c_p\,\chi_{p,i}\,\vec{f}_i^{(p)}\right\rangle_{\text{full}}. \qquad \text{(C.15)}
\end{aligned}$$

Bibliography

[1] S. I. Tomonaga and J. R. Oppenheimer, "On Infinite Field Reactions in Quantum Field Theory," Phys. Rev. **74**, 224 (1948).

[2] J. S. Schwinger, "On Quantum electrodynamics and the magnetic moment of the electron," Phys. Rev. **73**, 416 (1948).

[3] R. P. Feynman, "Space-time approach to non-relativistic quantum mechanics", Rev. Mod. Phys., **20(2)**, 367, (1948).

[4] G. 't Hooft and M. J. G. Veltman, "Regularization and Renormalization of Gauge Fields," Nucl. Phys. B **44**, 189 (1972).

[5] G. 't Hooft, "The Glorious days of physics: Renormalization of gauge theories," hep-th/9812203.

[6] S. L. Glashow, "Partial Symmetries of Weak Interactions," Nucl. Phys. **22**, 579 (1961).

[7] A. Salam and J. C. Ward, "Electromagnetic and weak interactions", Physics Letters, **13**, 168 November (1964).

[8] S. Weinberg, "A Model of Leptons," Phys. Rev. Lett. **19**, 1264 (1967).

[9] H. Fritzsch and M. Gell-Mann, "Current algebra: Quarks and what else?," eConf C **720906V2**, 135 (1972) [hep-ph/0208010].

[10] H. Fritzsch, M. Gell-Mann and H. Leutwyler, "Advantages of the Color Octet Gluon Picture," Phys. Lett. **47B**, 365 (1973).

[11] T. Aoyama, M. Hayakawa, T. Kinoshita and M. Nio, "Tenth-Order QED Contribution to the Electron g-2 and an Improved Value of the Fine Structure Constant," Phys. Rev. Lett. **109**, 111807 (2012) [arXiv:1205.5368 [hep-ph]].

[12] T. Aoyama, M. Hayakawa, T. Kinoshita and M. Nio, "Tenth-Order Electron Anomalous Magnetic Moment — Contribution of Diagrams without Closed Lepton Loops," Phys. Rev. D **91**, no. 3, 033006 (2015) [arXiv:1412.8284 [hep-ph]].

[13] M. Nio, "QED tenth-order contribution to the electron anomalous magnetic moment and a new value of the fine-structure constant" (PDF), Fundamental Constants Meeting 2015. Eltville, Germany, Jump up.

[14] D. Hanneke, S. F. Hoogerheide and G. Gabrielse, "Cavity Control of a Single-Electron Quantum Cyclotron: Measuring the Electron Magnetic Moment," Phys. Rev. A **83**, 052122 (2011) [arXiv:1009.4831 [physics.atom-ph]].

[15] P. M. Watkins, "Discovery Of The W And Z Bosons," Contemp. Phys. **27**, 291 (1986).

[16] G. Aad *et al.* [ATLAS Collaboration], "Observation of a new particle in the search for the Standard Model Higgs boson with the ATLAS detector at the LHC," Phys. Lett. B **716**, 1 (2012) [arXiv:1207.7214 [hep-ex]].

[17] S. Chatrchyan *et al.* [CMS Collaboration], "Observation of a new boson at a mass of 125 GeV with the CMS experiment at the LHC," Phys. Lett. B **716**, 30 (2012) [arXiv:1207.7235 [hep-ex]].

[18] W.F. Fry and D. Haidt, CERN Yellow Report, 75-01.

[19] D. Haidt, Contribution to the American Physical Society Conference at Washington, April 1974.

[20] F.J. Hasert et al, "Search for elastic muon-neutrino electron scattering", Phys. Lett. **46B** (1973) 121.

[21] F.J. Hasert et al, "Observation of neutrino-like interactions without muon or electron in the Gargamelle neutrino experiment", Phys. Lett. **46B** (1973) 138

[22] F.J. Hasert et al, "Observation of neutrino-like interactions without muon or electron in the Gargamelle neutrino experiment", Nucl. Phys. **B73** (1974) 1

[23] U. Amaldi, W. de Boer and H. Furstenau, "Comparison of grand unified theories with electroweak and strong coupling constants measured at LEP," Phys. Lett. B **260**, 447 (1991).

[24] F. Jegerlehner, "The hierarchy problem of the electroweak Standard Model revisited," arXiv:1305.6652 [hep-ph].

[25] R. D. Peccei and H. R. Quinn, "CP Conservation in the Presence of Instantons," Phys. Rev. Lett. **38**, 1440 (1977).

[26] R. D. Peccei, "The Strong CP problem and axions," Lect. Notes Phys. **741**, 3 (2008) [hep-ph/0607268].

[27] F. Capozzi, E. Lisi, A. Marrone, D. Montanino and A. Palazzo, "Neutrino masses and mixings: Status of known and unknown 3ν parameters," Nucl. Phys. B **908**, 218 (2016) [arXiv:1601.07777 [hep-ph]].

[28] M. E. Peskin, "Dark matter and particle physics," J. Phys. Soc. Jap. **76**, 111017 (2007) [arXiv:0707.1536 [hep-ph]].

[29] M. J. Mortonson, D. H. Weinberg and M. White, "Dark Energy: A Short Review," arXiv:1401.0046 [astro-ph.CO].

[30] D. Oriti, "Approaches to Quantum Gravity: Toward a New Understanding of Space, Time and Matter", Cambridge University Press

[31] D. J. Gross and F. Wilczek, "Ultraviolet Behavior of Nonabelian Gauge Theories," Phys. Rev. Lett. **30**, 1343 (1973).

[32] H. D. Politzer, "Reliable Perturbative Results for Strong Interactions?," Phys. Rev. Lett. **30**, 1346 (1973).

[33] P. Braun-Munzinger and J. Stachel, "The quest for the quark-gluon plasma," Nature **448**, 302 (2007).

[34] K. Adcox *et al.* [PHENIX Collaboration], "Suppression of hadrons with large transverse momentum in central Au+Au collisions at $\sqrt{s_{NN}}$ = 130-GeV," Phys. Rev. Lett. **88**, 022301 (2002) [nucl-ex/0109003].

[35] C. Adler *et al.* [STAR Collaboration], "Disappearance of back-to-back high p_T hadron correlations in central Au+Au collisions at $\sqrt{s_{NN}}$ = 200-GeV," Phys. Rev. Lett. **90**, 082302 (2003) [nucl-ex/0210033].

[36] G. Aad *et al.* [ATLAS Collaboration], "Observation of a Centrality-Dependent Dijet Asymmetry in Lead-Lead Collisions at $\sqrt{s_{NN}}$ = 2.77 TeV with the ATLAS Detector at the LHC," Phys. Rev. Lett. **105**, 252303 (2010) [arXiv:1011.6182 [hep-ex]].

[37] S. Necco and R. Sommer, "The N(f) = 0 heavy quark potential from short to intermediate distances," Nucl. Phys. B **622**, 328 (2002) [hep-lat/0108008].

[38] M. Cardoso, N. Cardoso and P. Bicudo, "Lattice QCD computation of the colour fields for the static hybrid quark-gluon-antiquark system, and microscopic study of the Casimir scaling," Phys. Rev. D **81**, 034504 (2010) [arXiv:0912.3181 [hep-lat]].

[39] bibitemSchwinger:1962tp J. S. Schwinger, "Gauge Invariance and Mass II.," Phys. Rev. **128**, 2425 (1962).

[40] K. G. Wilson, "Confinement of Quarks," Phys. Rev. D **10**, 2445 (1974).

[41] A. M. Polyakov, "Compact Gauge Fields and the Infrared Catastrophe," Phys. Lett. **59B**, 82 (1975).

[42] K. Holland, P. Minkowski, M. Pepe and U. J. Wiese, "Exceptional confinement in G(2) gauge theory," Nucl. Phys. B **668**, 207 (2003) [hep-lat/0302023].

[43] M. Pepe, "Confinement and the center of the gauge group," PoS LAT **2005**, 017 (2006) [Nucl. Phys. Proc. Suppl. **153**, 207 (2006)] [hep-lat/0510013].

[44] M. Pepe and U.-J. Wiese, "Exceptional Deconfinement in G(2) Gauge Theory," Nucl. Phys. B **768**, 21 (2007) [hep-lat/0610076].

[45] S. Gupta, "Lattice QCD with chemical potential: Evading the fermion-sign problem," Pramana **63**, 1211 (2004).

[46] L. Bongiovanni, "Numerical methods for the sign problem in Lattice Field Theory," arXiv:1603.06458 [hep-lat].

[47] S. Hands, S. Cotter, P. Giudice and J. I. Skullerud, "The Phase Diagram of Two Color QCD," J. Phys. Conf. Ser. **432**, 012020 (2013) [arXiv:1210.6559 [hep-lat]].

[48] P. Braun-Munzinger and J. Wambach, "The Phase Diagram of Strongly-Interacting Matter," Rev. Mod. Phys. **81**, 1031 (2009) [arXiv:0801.4256 [hep-ph]].

[49] M. A. Stephanov, "QCD phase diagram: An Overview," PoS LAT **2006**, 024 (2006) [hep-lat/0701002].

[50] B. J. Schaefer and M. Wagner, "On the QCD phase structure from effective models," Prog. Part. Nucl. Phys. **62**, 381 (2009) [arXiv:0812.2855 [hep-ph]].

[51] O. Kaczmarek *et al.*, "Phase boundary for the chiral transition in (2+1) -flavor QCD at small values of the chemical potential," Phys. Rev. D **83**, 014504 (2011) [arXiv:1011.3130 [hep-lat]].

[52] S. Borsanyi, G. Endrodi, Z. Fodor, S. D. Katz, S. Krieg, C. Ratti and K. K. Szabo, "QCD equation of state at nonzero chemical potential: continuum results with physical quark masses at order mu^2," JHEP **1208**, 053 (2012) [arXiv:1204.6710 [hep-lat]].

[53] P. de Forcrand and O. Philipsen, "QCD phase diagram at small densities from simulations with imaginary mu," hep-ph/0301209.

[54] P. de Forcrand and O. Philipsen, "Constraining the QCD phase diagram by tricritical lines at imaginary chemical potential," Phys. Rev. Lett. **105**, 152001 (2010) [arXiv:1004.3144 [hep-lat]].

[55] D. Sexty, "Simulating full QCD at nonzero density using the complex Langevin equation," Phys. Lett. B **729**, 108 (2014) [arXiv:1307.7748 [hep-lat]].

[56] G. Aarts, F. Attanasio, B. Jäger, E. Seiler, D. Sexty and I. O. Stamatescu, "QCD at nonzero chemical potential: recent progress on the lattice," AIP Conf. Proc. **1701**, 020001 (2016) [arXiv:1412.0847 [hep-lat]].

[57] G. Aarts, E. Seiler, D. Sexty and I. O. Stamatescu, "Simulating QCD at nonzero baryon density to all orders in the hopping parameter expansion," Phys. Rev. D **90**, no. 11, 114505 (2014) [arXiv:1408.3770 [hep-lat]].

[58] G. Aarts and I. O. Stamatescu, "Stochastic quantization at finite chemical potential," JHEP **0809**, 018 (2008) [arXiv:0807.1597 [hep-lat]].

[59] K. Langfeld and J. M. Pawlowski, "Two-color QCD with heavy quarks at finite densities," Phys. Rev. D **88**, no. 7, 071502 (2013) [arXiv:1307.0455 [hep-lat]].

[60] M. Cristoforetti, F. Di Renzo, G. Eruzzi, A. Mukherjee, C. Schmidt, L. Scorzato and C. Torrero, "An efficient method to compute the residual phase on a Lefschetz thimble," Phys. Rev. D **89**, no. 11, 114505 (2014) [arXiv:1403.5637 [hep-lat]].

[61] J. M. Pawlowski, "Aspects of the functional renormalisation group," Annals Phys. **322**, 2831 (2007) [hep-th/0512261].

[62] C. S. Fischer, "Infrared properties of QCD from Dyson-Schwinger equations," J. Phys. G **32**, R253 (2006) [hep-ph/0605173].

[63] C. D. Roberts and A. G. Williams, "Dyson-Schwinger equations and their application to hadronic physics," Prog. Part. Nucl. Phys. **33**, 477 (1994) [hep-ph/9403224].

[64] R. Alkofer and L. von Smekal, "The Infrared behavior of QCD Green's functions: Confinement dynamical symmetry breaking, and hadrons as relativistic bound states," Phys. Rept. **353**, 281 (2001) [hep-ph/0007355].

[65] S. P. Klevansky, "The Nambu-Jona-Lasinio model of quantum chromodynamics," Rev. Mod. Phys. **64**, 649 (1992).

[66] J. Morais, J. Moreira, B. Hiller, A. H. Blin and A. A. Osipov, "The T–μ Phase Diagram of the Nambu–Jona-Lasinio Model in the Presence of Explicit Symmetry-breaking Interactions," Acta Phys. Polon. Supp. **8**, no. 1, 199 (2015) [arXiv:1411.3203 [hep-ph]].

[67] B. J. Schaefer and J. Wambach, "The Phase diagram of the quark meson model," Nucl. Phys. A **757**, 479 (2005) [nucl-th/0403039].

[68] K. Fukushima, "Chiral effective model with the Polyakov loop," Phys. Lett. B **591**, 277 (2004) [hep-ph/0310121].

[69] E. Megias, E. Ruiz Arriola and L. L. Salcedo, "Polyakov loop in chiral quark models at finite temperature," Phys. Rev. D **74**, 065005 (2006) [hep-ph/0412308].

[70] C. Ratti, M. A. Thaler and W. Weise, "Phases of QCD: Lattice thermodynamics and a field theoretical model," Phys. Rev. D **73**, 014019 (2006) [hep-ph/0506234].

[71] M. Dutra, O. Lourenço, A. Delfino, T. Frederico and M. Malheiro, "Polyakov–Nambu–Jona-Lasinio phase diagrams and quarkyonic phase from order parameters," Phys. Rev. D **88**, no. 11, 114013 (2013) [arXiv:1312.1130 [hep-ph]].

[72] Z. f. Cui, C. Shi, W. m. Sun, Y. l. Wang and H. s. Zong, "The Wigner Solution and QCD Phase Transitions in a Modified PNJL Model," Eur. Phys. J. C **74**, 2782 (2014) [arXiv:1311.4014 [hep-ph]].

[73] B. J. Schaefer, J. M. Pawlowski and J. Wambach, "The Phase Structure of the Polyakov–Quark-Meson Model," Phys. Rev. D **76**, 074023 (2007) [arXiv:0704.3234 [hep-ph]].

[74] V. Skokov, B. Stokic, B. Friman and K. Redlich, "Meson fluctuations and thermodynamics of the Polyakov loop extended quark-meson model," Phys. Rev. C **82**, 015206 (2010) [arXiv:1004.2665 [hep-ph]].

[75] T. K. Herbst, J. M. Pawlowski and B. J. Schaefer, "The phase structure of the Polyakov–quark–meson model beyond mean field," Phys. Lett. B **696**, 58 (2011) [arXiv:1008.0081 [hep-ph]].

[76] J. B. Kogut, M. A. Stephanov, D. Toublan, J. J. M. Verbaarschot and A. Zhitnitsky, "QCD - like theories at finite baryon density," Nucl. Phys. B **582**, 477 (2000) [hep-ph/0001171].

[77] L. von Smekal, "Universal Aspects of QCD-like Theories," Nucl. Phys. Proc. Suppl. **228**, 179 (2012) [arXiv:1205.4205 [hep-ph]].

[78] F. Karsch and M. Lutgemeier, "Deconfinement and chiral symmetry restoration in an SU(3) gauge theory with adjoint fermions," Nucl. Phys. B **550**, 449 (1999) [hep-lat/9812023].

[79] J. B. Kogut, M. A. Stephanov and D. Toublan, "On two color QCD with baryon chemical potential," Phys. Lett. B **464**, 183 (1999) [hep-ph/9906346].

[80] J. B. Kogut, D. K. Sinclair, S. J. Hands and S. E. Morrison, "Two color QCD at nonzero quark number density," Phys. Rev. D **64**, 094505 (2001) [hep-lat/0105026].

[81] N. Strodthoff, B. J. Schaefer and L. von Smekal, "Quark-meson-diquark model for two-color QCD," Phys. Rev. D **85**, 074007 (2012) [arXiv:1112.5401 [hep-ph]].

[82] N. Strodthoff and L. von Smekal, "Polyakov-Quark-Meson-Diquark Model for two-color QCD," Phys. Lett. B **731**, 350 (2014) [arXiv:1306.2897 [hep-ph]].

[83] A. Maas and B. H. Wellegehausen, "G_2 gauge theories," PoS LATTICE **2012**, 080 (2012) [arXiv:1210.7950 [hep-lat]].

[84] B. H. Wellegehausen and L. von Smekal, "Lattice simulations of G_2-QCD at finite density," PoS LATTICE **2014** (2015) 177 [arXiv:1501.06706 [hep-lat]].

[85] B. H. Wellegehausen, A. Maas, A. Wipf and L. von Smekal, "Hadron masses and baryonic scales in G_2-QCD at finite density," Phys. Rev. D **89**, no. 5, 056007 (2014) [arXiv:1312.5579 [hep-lat]].

[86] . Aoki, G. Endrodi, Z. Fodor, S. D. Katz and K. K. Szabo, "The Order of the quantum chromodynamics transition predicted by the standard model of particle physics," Nature **443**, 675 (2006) [hep-lat/0611014].

[87] S. Borsanyi *et al.* [Wuppertal-Budapest Collaboration], "Is there still any T_c mystery in lattice QCD? Results with physical masses in the continuum limit III," JHEP **1009**, 073 (2010) [arXiv:1005.3508 [hep-lat]].

[88] A. Bazavov *et al.* [HotQCD Collaboration], "Equation of state in (2+1)-flavor QCD," Phys. Rev. D **90**, 094503 (2014) [arXiv:1407.6387 [hep-lat]].

[89] C. S. Fischer, J. Luecker and C. A. Welzbacher, "Locating the critical end point of QCD," Nucl. Phys. A **931**, 774 (2014) [arXiv:1410.0124 [hep-ph]].

[90] G. Eichmann, C. S. Fischer and C. A. Welzbacher, "Baryon effects on the location of QCD's critical end point," Phys. Rev. D **93**, no. 3, 034013 (2016) [arXiv:1509.02082 [hep-ph]].

[91] B. Friman, C. Hohne, J. Knoll, S. Leupold, J. Randrup, R. Rapp and P. Senger, "The CBM physics book: Compressed baryonic matter in laboratory experiments," Lect. Notes Phys. **814**, pp.1 (2011).

[92] L. McLerran and R. D. Pisarski, "Phases of cold, dense quarks at large N(c)," Nucl. Phys. A **796**, 83 (2007) [arXiv:0706.2191 [hep-ph]].

[93] M. G. Alford, A. Schmitt, K. Rajagopal and T. Schäfer, "Color superconductivity in dense quark matter," Rev. Mod. Phys. **80**, 1455 (2008) [arXiv:0709.4635 [hep-ph]].

[94] M. G. Alford, K. Rajagopal and F. Wilczek, "Color flavor locking and chiral symmetry breaking in high density QCD," Nucl. Phys. B **537**, 443 (1999) [hep-ph/9804403].

[95] C. Gattringer, "Flux representation of an effective Polyakov loop model for QCD thermodynamics," Nucl. Phys. B **850**, 242 (2011) [arXiv:1104.2503 [hep-lat]].

[96] Y. Delgado Mercado and C. Gattringer, "Monte Carlo simulation of the SU(3) spin model with chemical potential in a flux representation," Nucl. Phys. B **862**, 737 (2012) [arXiv:1204.6074 [hep-lat]].

[97] M. Fromm, J. Langelage, S. Lottini and O. Philipsen, "The QCD deconfinement transition for heavy quarks and all baryon chemical potentials," JHEP **1201**, 042 (2012) [arXiv:1111.4953 [hep-lat]].

[98] M. Fromm, J. Langelage, S. Lottini, M. Neuman and O. Philipsen, "Onset Transition to Cold Nuclear Matter from Lattice QCD with Heavy Quarks," Phys. Rev. Lett. **110**, no. 12, 122001 (2013) [arXiv:1207.3005 [hep-lat]].

[99] G. Aarts and F. A. James, "Complex Langevin dynamics in the SU(3) spin model at nonzero chemical potential revisited," JHEP **1201**, 118 (2012) [arXiv:1112.4655 [hep-lat]].

[100] J. Greensite and K. Splittorff, "Mean field theory of effective spin models as a baryon fugacity expansion," Phys. Rev. D **86**, 074501 (2012) [arXiv:1206.1159 [hep-lat]].

[101] C. Wozar, T. Kaestner, A. Wipf, T. Heinzl and B. Pozsgay, "Phase structure of Z(3)-Polyakov-loop models," Phys. Rev. D **74**, 114501 (2006) [hep-lat/0605012].

[102] C. Wozar, T. Kaestner, A. Wipf and T. Heinzl, "Inverse Monte-Carlo determination of effective lattice models for SU(3) Yang-Mills theory at finite temperature," Phys. Rev. D **76**, 085004 (2007) [arXiv:0704.2570 [hep-lat]].

[103] T. Heinzl, T. Kaestner and A. Wipf, "Effective actions for the SU(2) confinement-deconfinement phase transition," *Phys. Rev. D* **72**, *065005 (2005)* [arXiv:hep-lat/0502013].

[104] C. Gattringer, C.B. Lang, "Quantum Chromodynamics on the Lattice", Springer Verlag, 2009.

[105] J. Greensite, "An Introduction to the Confinement Problem", Springer Verlag, 2011.

[106] A. Wipf, "Statistical Approach to Quantum Field Theory: An Introduction", Springer Verlag, 2012.

[107] M. Nakahara, "Geometry, Topology and Physics", Institute of Physics Publishing, 2003

[108] N. Nakanishi, I. Ojima, "Covariant Operator Formalism Of Gauge Theories And Quantum Gravity", World Scientific Lecture Notes in Physics, 1990.

[109] C. D. Roberts and S. M. Schmidt, "Dyson-Schwinger equations: Density, temperature and continuum strong QCD," Prog. Part. Nucl. Phys. **45**, S1 (2000) [nucl-th/0005064].

[110] R. Haag, "Local Quantum Physics: Fields, Particles, Algebras", Springer Verlag, 2013

[111] R. Sommer, "A New way to set the energy scale in lattice gauge theories and its applications to the static force and alpha-s in SU(2) Yang-Mills theory," Nucl. Phys. B **411**, 839 (1994) [hep-lat/9310022].

[112] C. G. Callan, Jr., "Broken scale invariance in scalar field theory," Phys. Rev. D **2**, 1541 (1970).

[113] K. Symanzik, "Small distance behavior in field theory and power counting," Commun. Math. Phys. **18**, 227 (1970).

[114] A. Petermann and E. C. G. Stueckelberg, "Restriction of possible interactions in quantum electrodynamics", Phys. Rev., **82**, 548 (1951).

[115] K. G. Wilson, "The Renormalization Group: Critical Phenomena and the Kondo Problem," Rev. Mod. Phys. **47**, 773 (1975).

[116] L. H. Ryder, "Quantum Field Theory". Cambridge University Press, Cambridge, UK, 1985.

[117] R. N. Cahn, "Semi-Simple Lie Algebras and Their Representations", Benjamin-Cummings, 1984.

[118] Marina von Steinkirch, "Introduction to Group Theory for Physicists", Lectures at State University of New York, 2011.

[119] W. Greiner, B. Müller, "Quantum Mehcanics: Symmetries", Springer Verlag, 1994

[120] A. M. Polyakov, "Thermal Properties of Gauge Fields and Quark Liberation," Phys. Lett. **72B**, 477 (1978).

[121] L. Susskind, "Lattice Models of Quark Confinement at High Temperature," Phys. Rev. D **20**, 2610 (1979).

[122] B. Svetitsky and L. G. Yaffe, "Critical Behavior at Finite Temperature Confinement Transitions," Nucl. Phys. B **210**, 423 (1982).

[123] L. G. Yaffe and B. Svetitsky, "First Order Phase Transition in the SU(3) Gauge Theory at Finite Temperature," *Phys. Rev. D* **26***, 963 (1982).*

[124] J. Greensite and K. Langfeld, "Effective Polyakov line action from the relative weights method," Phys. Rev. D **87**, 094501 (2013) [arXiv:1301.4977 [hep-lat]].

[125] J. Greensite and K. Langfeld, "Effective Polyakov line action from strong lattice couplings to the deconfinement transition," Phys. Rev. D **88**, 074503 (2013) [arXiv:1305.0048 [hep-lat]].

[126] Guy Buss, "Analytische Aspekte effektiver SU(N)-Gittereichtheorien", Diplomarbeit, FSU Jena, 2004.

[127] B. H. Wellegehausen, "Effektive Polyakov-Loop-Modelle für SU(N)- und G2-Eichtheorien", Diploma thesis, 2008.

[128] I. Montvay and G. Münster, "Quantum Fields on a Lattice". Cambridge University Press, Cambridge, UK, 1994.

[129] J. M. Drouffe and J. B. Zuber, "Strong Coupling and Mean Field Methods in Lattice Gauge Theories," Phys. Rept. **102**, 1 (1983).

[130] J. Langelage, S. Lottini and O. Philipsen, "Centre symmetric 3d effective actions for thermal SU(N) Yang-Mills from strong coupling series," JHEP **1102**, 057 (2011) Erratum: [JHEP **1107**, 014 (2011)] [arXiv:1010.0951 [hep-lat]].

[131] J. Langelage, S. Lottini and O. Philipsen, "Effective Polyakov-loop theory for pure Yang-Mills from strong coupling expansion," PoS LATTICE **2010**, 196 (2010) [arXiv:1011.0095 [hep-lat]].

[132] A. Dumitru, Y. Hatta, J. Lenaghan, K. Orginos and R. D. Pisarski, "Deconfining phase transition as a matrix model of renormalized Polyakov loops," Phys. Rev. D **70**, 034511 (2004) [hep-th/0311223].

[133] M. Billo, M. Caselle, A. D'Adda and S. Panzeri, "Toward an analytic determination of the deconfinement temperature in SU(2) LGT," Nucl. Phys. B **472**, 163 (1996) [hep-lat/9601020].

[134] S. Uhlmann, R. Meinel and A. Wipf, "Ward identities for invariant group integrals," J. Phys. A **40**, 4367 (2007) [hep-th/0611170].

[135] D. Smith, A. Dumitru, R. Pisarski and L. von Smekal, "Effective potential for SU(2) Polyakov loops and Wilson loop eigenvalues," Phys. Rev. D **88**, no. 5, 054020 (2013) [arXiv:1307.6339 [hep-lat]].

[136] P. Scior, D. Scheffler, D. Smith and L. von Smekal, "Effective SU(2) Polyakov Loop Theories with Heavy Quarks on the Lattice," PoS LATTICE **2014**, 173 (2015) [arXiv:1412.7089 [hep-lat]].

Acknowledgment

First of all I would like to thank Prof. Lorenz von Smekal for giving me the opportunity and support to do my PhD in his research group. Furthermore, I would like to thank Prof. Christian Fischer for his feedback during the PhD committee meetings and for taking his to be the second examiner of this thesis. Next, I would like to thank the members of the research group and those who have supported and helped me over the past few years. I am grateful to Lukas Holicki, who was always willing to give programming related advice, to Eduard Seifert for his helpful feedback and to my parents and uncle who were always supportive. A special thanks goes to Björn Wellegehausen who mentored me over the past three and a half years and without whose advice, not only regarding the physics but also the programming methods involved, this thesis would not have been possible.

Erklärung

Ich erkläre: Ich habe die vorgelegte Dissertation selbstständig und ohne unerlaubte fremde Hilfe und nur mit den Hilfen angefertigt, die ich in der Dissertation angegeben habe. Alle Textstellen, die wörtlich oder sinngemäß aus veröffentlichten Schriften entnommen sind, und alle Angaben, die auf mündlichen Auskünften beruhen, sind als solche kenntlich gemacht. Ich stimme einer evtl. Überprüfung meiner Dissertation durch eine Antiplagiat-Software zu. Bei den von mir durchgeführten und in der Dissertation erwähnten Untersuchungen habe ich die Grundsätze guter wissenschaftlicher Praxis, wie sie in der *Satzung der Justus-Liebig-Universität Gießen zur Sicherung guter wissenschaftlicher Praxis* niedergelegt sind, eingehalten.

Gießen, den 13.07.2017

Bardiya Bahrampour